Automated Hippocampal Location and Extraction

Heidi M. Bonnici

B.Sc (hons) M.Sc.

A thesis submitted in fulfilment of requirements for the degree of Doctor of Philosophy

To

Department of Psychiatry

School of Medicine and Veterinary Medicine

University of Edinburgh

2009

Abstract

The hippocampus is a complex brain structure that has been studied extensively and is subject to abnormal structural change in various neuropsychiatric disorders. The highest definition *in vivo* method of visualizing the anatomy of this structure is structural Magnetic Resonance Imaging (MRI). Gross structure can be assessed by the naked eye inspection of MRI scans but measurement is required to compare scans from individuals within normal ranges, and to assess change over time in individuals. The gold standard of such measurement is manual tracing of the boundaries of the hippocampus on scans. This is known as a Region Of Interest (ROI) approach. ROI is laborious and there are difficulties with test-retest and inter-rater reliability. These difficulties are primarily due to uncertainty in designation of the hippocampus boundary. An improved, less labour intensive and more reliable method is clearly desirable.

This thesis describes a fully automated hybrid methodology that is able to first locate and then extract hippocampal volumes from 3D 1.5T MRI T1 brain scans automatically. The hybrid algorithm uses brain atlas mappings and fuzzy inference to locate hippocampal areas and create initial hippocampal boundaries. This initial location is used to seed a deformable manifold algorithm. Rule based deformations are then applied to refine the estimate of the hippocampus locations. Finally, the hippocampus boundaries are corrected through an inference process that assures adherence to an expected hippocampus volume.

The ICC values of this methodology when compared to the manual segmentation of the same hippocampi result in a 0.73 for the left and 0.81 for the right hippocampi. These values both fall within the range of reliability testing according to the manual 'gold standard' technique. Thus, this thesis describes the development and validation of a genuinely automated approach to hippocampal volume extraction of potential utility in studies of a range of neuropsychiatric disorders and could eventually find clinical applications.

Acknowledgments

My most special thanks go to my supervisor, Bill Moorhead, for making my PhD studies such a pleasant experience. It was through him that I was able to embark into the area of brain imaging that I am enjoying so much. He helped me to find my own niche in such a vast area, and always encouraged my ideas as well as guiding me through all the obstacles. I would also like to thank him for allowing me to use part of his code in my methodology, namely the sulcal ridge algorithm.

I would also like to thank Stephen Lawrie, my second supervisor, for his feedback and encouragement on my work, and always keeping an eye out on my progress. It was a pleasure to have my work reviewed by Eve Johnstone and would like to thank her for her advice on the detailed comments that led to an improved final version.

I would like to thank Bill Moorhead, Stephen Lawrie and Eve Johnstone for allowing and encouraging me to attend several international conferences, allowing me the opportunity to network with several international scientists and to present my work. I am indebted to the Principal scholarship for providing financial support during my studies.

My special thanks go to my colleagues Ruth Philip and Liana Romaniuk, whose friendship and company meant so much to me during my PhD time. With them my time at the Kennedy Tower will be remembered with many a fond memory. Thanks

also go to all my colleagues at the Kennedy Tower for their support, interest and advice in my work.

Finally, I would like to thank my parents for their continuing love and support. It is through them that I have been able to continue my studies and their support is priceless.

Declaration

I declare that this thesis was composed by myself, that the work contained herein is my own excerpt where explicitly stated otherwise in the text, and that this work has not been submitted for any other degree or professional qualification except as specified.

(Heidi Bonnici)

Chapter 1 - Introduction

This chapter provides a general overview of the issues in the field of structural MRI image segmentation as well as the relevance of the hippocampus and its change in shape and volume. A brief account of research into these fields has also been presented and discussed, looking at different approaches to segmenting the hippocampus, from manual to automated techniques. Chapter 1 also demonstrates the relevance of the motivation and aims that this study offers.

1.1 Motivation and Aims

The Hippocampus is a sub-cortical brain structure lying in the inferior medial part of the temporal lobe. It has been known to be clearly involved in memory function for more than 50 years (Scoville WB 1957). It is subject to abnormal structural change in various psychiatric disorders. The best *in vivo* method of visualizing the anatomy of this structure is structural Magnetic Resonance Imaging (MRI).

Gross structure can be assessed by naked eye inspection of MRI scans but measurement is required to compare scans from individuals with normal ranges, and to assess change over time in individuals. The gold standard of such measurement is manual tracing of the boundaries of the hippocampus on scans. This so-called Region Of Interest (ROI) approach is a long and laborious task and there may be difficulties in test-retest and inter-rater reliability, partly due to the relatively small size of the hippocampus and the variability in its boundary presentation. Using ROI methods, tracing a pair of hippocampi of a subject could take anywhere from two to four hours. An improved, quicker and more reliable method is clearly desirable. The main motivation for this work has been to develop an automated hippocampus tracing methodology using artificial intelligence techniques and to assess its performance in comparison to the gold standard technique of manual tracing. A secondary motivation has been to apply this methodology to a cohort of psychiatric subjects and controls, with a view to analysing the results of the volumetric assessments of the hippocampi serial scans in this sample. This would allow the possibility of assessing

hippocampal structural change over time and in different subject groups, and to compare possibly different rates of change.

1.2 The Hippocampus

1.2.1 The Hippocampal Structure

The hippocampus may be the one of the most studied structures in the brain. It forms part of the Limbic System, along with the amygdala, cingulate gyrus, fornix, hypothalamus and thalamus. The hippocampus is made up of five subfields, the three Cornu Ammonis sections (CA1, CA2 and CA3), the dentate gyrus, and the subiculum (Amaral & Witter 1989, Amaral 1999, Amaral and Lavenex 2006). A band of white matter runs along the medial side of the hippocampus, known as the fimbria. Another band of white matter known as the alveus borders the wall of the hippocampus adjacent to the lateral ventricle. It is these 5 subfields, the alveus and the fimbria that constitute the region of the hippocampus.

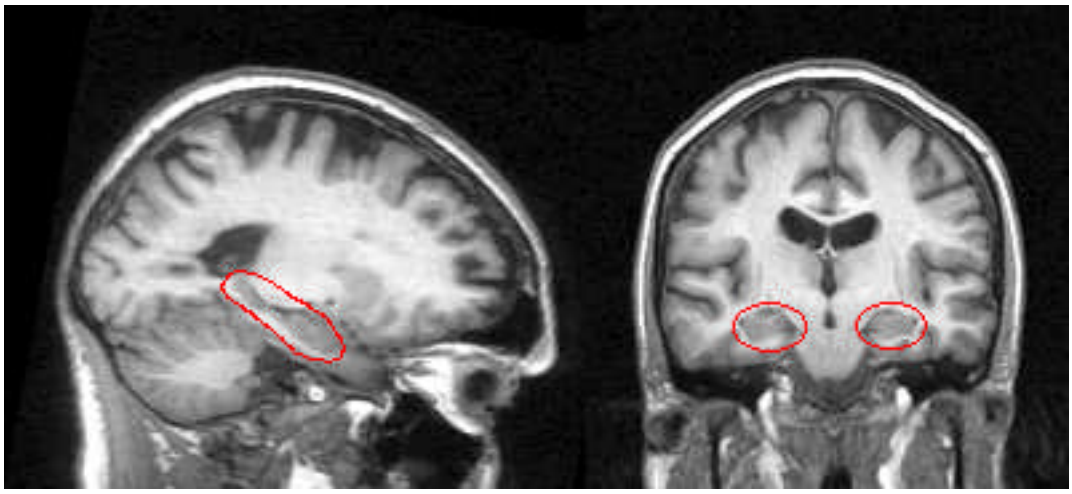

Figure 1.1 Sagittal and coronal MRI views of the hippocampus. The hippocampal region is circled in red

The information flow through the hippocampal structure can be viewed as flowing through a loop of the structure, commencing from the entorhinal cortex to the dentate gyrus. The first step in the flow loop is the passage of information passing to the dentate gyrus from the entorhinal cortex along what is known as the Perforant path. Axons called mossy fibres, pass impulses from the dentate gyrus to CA3, and then to the CA2 and CA1 regions through the Schaeffer collaterals. Finally, the information is sent from the CA1 subfield to the subiculum, which outputs the information from the hippocampus to the entorhinal cortex, or to other sub-cortical regions ((McNaughton, Barnes et al. 1989), (Hasselmo and McClelland 1999), (Duvernoy 2004) and (Lavenex, Amaral et al. 2006)).

1.2.2 The Hippocampal Functions

The hippocampus plays an important role in the encoding and retrieval of long-term memories, but not in memory storage itself (Eichenbaum 1999). Damage to the hippocampus results in difficulties in creating new memories, but storage and retrieval of old memories is not affected. Similarly, the learning of new abilities is not affected if the hippocampus is damaged in any way. There is evidence for the theory that two types of memory exist, declarative and non-declarative, where the hippocampus has a direct impact on declarative memory (consciously learning) but not non-declarative memory (such as learning a new musical instrument) ((Eichenbaum 1999), (Addis, Moscovitch et al. 2004)).

The hippocampus also has a main role in spatial navigation functions. A study on London taxi drivers ((Maguire, Burgess et al. 1998), (Maguire, Gadian et al. 2000), (Maguire, Spiers et al. 2003; Maguire, Valentine et al. 2003)) showed that the posterior hippocampus was larger in taxi drivers than in a control group. The anterior hippocampus, however, was larger in controls. These volume changes correlated, positively and negatively respectively, with amount of time the person worked as a taxi driver. This gives further evidence to the theory that spatial navigation functions are carried out in the posterior hippocampus and that this volume can increase if the skill is increased.

1.2.3 The hippocampal structure in Schizophrenia

Hippocampal volume reduction may be said to have now become one of the most consistent structural abnormalities found in schizophrenia (Heckers 2001). The first report of abnormalities in the hippocampal volume in schizophrenia is found in Bogerts in 1985 (Bogerts, Meertz et al. 1985) where post-mortem analysis of 13 brains of schizophrenic patients and 9 controls showed a significant reduction in hippocampal volume. Most manual segmentation studies show some significant reduction in volume in the left hippocampus. A review of structural MRI studies in schizophrenia from 1987 to 1998 can be found in McCarley (McCarley, Wible et al. 1999). From the 118 studies reviewed, 30 focused on the medial temporal lobe structures, 77% of which reported volume reduction in one or more of its structures.

Results reported by Lawrie et al. suggest that people with a high risk of developing schizophrenia have a more likely chance of developing the illness if they have a particularly small amygdala-hippocampal complex, and that this abnormality is largely genetically mediated (Lawrie, Whalley et al. 2002).

Velakoulis et al. (Velakoulis, Pantelis et al. 1999; Velakoulis, Wood et al. 2006) looked at a population of 140 controls, 46 patients with chronic schizophrenia and 32 patients with first episode psychosis. After manually segmenting the hippocampus, both patient groups were found to have a significantly smaller volume of the left hippocampus, and the chronic schizophrenia patients had smaller right hippocampal volumes, which were associated with greater age and longer duration of illness. This association was not found in first episode patients, perhaps due to the smaller number of patients in this group.

Not all studies have similar findings – for example ((Shenton, Gerig et al. 2002); (Tanskanen, Veijola et al. 2005); (Lopez-Garcia, Aizenstein et al. 2006)) all found no significant change in volume in the hippocampi of patients of schizophrenia when compared to healthy controls. However, Shenton (Shenton, Gerig et al. 2002) observed that the asymmetry between the left and right hippocampi was greater in the schizophrenic group, and the right hippocampus volume was found to be larger than the left in all groups in the study by Tanskanen (Tanskanen, Veijola et al. 2005). Other volumetric tracing studies ((Narr, Thompson et al. 2004); (Lee, Kim et al. 2004); (Weiss, Dewitt et al. 2005); (Chakos, Schobel et al. 2005); (Exner, Nehrkorn et al. 2008)) report significant bilateral reductions of hippocampal volume in their

schizophrenic populations when compared to their healthy controls. However, two of these studies contain only male subjects and controls ((Weiss, Dewitt et al. 2005); (Chakos, Schobel et al. 2005)), and a third reports the reduction only in males and not in females (Exner, Nehrkorn et al. 2008). Meta-analysis has however demonstrated clear reductions of about 4% in the hippocampus (and amygdala) on ROI studies as a whole.

Voxel Based Morphometry (VBM), an automated process, has been used in recent studies to evaluate volume and density changes in grey matter in schizophrenic subjects. Most studies tend to report significant volume and/or structure change of the hippocampus ((Rametti, Segarra et al. 2007); (Honea 2008)) although density changes are reported (Rametti, Segarra et al. 2007). Other studies report group volume differences in the left hippocampus ((Kubicki 2002); (Job, Whalley et al. 2005; Moorhead, Harris et al. 2006)).

In conclusion, although it is clear that volume reductions of the hippocampus seem to be a consistent finding in schizophrenia (when volume changes are reported), such results are not invariably found. Methodologies that are able to calculate structural volumes for larger cohorts more accurately may be a key component to clarifying the relationship between the hippocampus and schizophrenia, and possibly determining the time of change from hippocampal volume when a patient develops schizophrenia ((Moorhead, Job et al. 2004); (Job, Whalley et al. 2002); (Lawrie, Whalley et al. 2002)).

1.2.4 The hippocampal structure in Bipolar Disorder

In Bipolar Disorder the reported studies of hippocampal volume changes are not consistent in their findings. The inconsistencies may be due to a number of factors such as age of onset, psychotic symptoms or the use of medications or phase of illness (Frey, Andreazza et al. 2007). Houser et al (Hauser, Matochik et al. 2000) report no volume differences in the hippocampi of 25 patients with bipolar disorder type I and 22 patients with bipolar disorder type II when compared with 19 healthy controls. It is important to note, however, that the hippocampus was manually traced on relatively thick 5mm coronal slices in this study, a method known to be less accurate than the use of finer slices, as slices that are 5mm thick creates a larger noise component and thus diminishes the analysis sensitivity.

Some studies report volume reduction in the hippocampus. Blumberg et al (Blumberg, Kaufman et al. 2003) looked at a cohort of 36 bipolar disorder type I patients and 56 controls. This cohort included adolescents, and the authors report a trend in the reduction of hippocampal volume in the patient group. Frazier et al (Frazier, Chiu et al. 2005) looked exclusively at youths and reported significant hippocampal volume decreases between a control group and a subject cohort with bipolar disorder type I. Interestingly, they noted that females in the cohort seemed to drive the effect. Another study reporting results from adolescents with bipolar disorder also reported smaller hippocampus volumes in the bipolar group (Bearden, Soares et al. 2008). The study also reports a significant positive correlation between the size of the hippocampus and the age in patients, in contrast to the healthy controls

who showed an inverse relation. Frey et al. (Frey, Andreazza et al. 2007) have suggested that early onset bipolar disorder in adolescents might result in smaller hippocampi sizes since age of onset could impact the structural development that would be occurring at that time.

In contrast, other studies report enlarged hippocampal volumes, such as Beyer et al. (Beyer, Kuchibhatla et al. 2004) who found the left hippocampus was enlarged in older subjects. They suggest that the volume increase that they report may be associated with lithium medication. This finding is supported in other studies. For example, Yucel et al (Yucel, McKinnon et al. 2007), measured the hippocampi of 12 patients with bipolar disorder longitudinally over a 2 to 4 year period and found bilateral increases in the hippocampal volume of the patients over time. Bilateral hippocampal volume increase due to lithium has also been reported in contrast to patients who have not been treated with lithium ((Yucel, Taylor et al. 2008); (Foland, Altshuler et al. 2008); (Bearden, Thompson et al. 2008)). Besides this, Bearden et al. (Bearden, Thompson et al. 2008) also compare lithium treated patients with healthy controls, and as with unmedicated bipolar patients, a significant hippocampal volume increase is observed.

Overall, it may be particularly important to consider the age of the patients in the bipolar group as well as their medication history when looking at their hippocampi as this may affect results. A question to ask is why various studies looking at the same illness and same region can produce different findings. There are a number of possible reasons for this. McCarley et al. (McCarley, Wible et al. 1999) suggest that

not only could there be a variation of subject populations between studies, but also different ROI definitions in the studies could lead to studies differing in their results. Other possible reasons could range from the resolution (i.e. the voxel size) to the use of different scanners and their protocols, as well as other post processing methods. These can all be varied and could influence results in some way. In schizophrenia, therefore, there is strong evidence to support reduced hippocampal volume. This is not so in bipolar disorder, although further study is necessary.

1.3 Image Segmentation

Structural image segmentation in brain MRI results in a corresponding image map showing the various structures and substructures of the brain, generally by locating the boundaries of the structures. Segmenting subcortical brain structures from MRI scans is one of the most important and necessary processes in brain analysis as it provides a valuable tool for assessing anatomy. With the increase of subjects in cohorts and sensitivity remaining a requirement in segmentation of subcortical structures, a critical look at the benefits and limitations of current segmentation tools are discussed. Segmentation procedures come in three types. The original method of segmentation is manual segmentation, manually going through the MRI scan slice by slice and tracing the required brain structure boundaries. Semi-automated techniques have become more popular in recent times. They substantially reduce the procedural time, but still involve human users to guide the process, which may include having to manually edit the delineations of the region segmented. The last type of segmentation is fully automated segmentation in which the entire segmentation procedure is able to progress automatically with no human involvement in the process. Automated procedures are not as common or popular as semi-automated procedures, perhaps proof of the complexity and uncertainty of segmenting an MR image, and perhaps due to the strong feeling that exists of the necessity that human operator input is required, even if it is just to analyse the results. The following sections describe the three segmentation techniques in more detail and give studies as examples of each case.

1.3.1 Manual Segmentation

The gold standard of segmentation methods is manual segmentation. There are many studies which report results based on manual segmentation of subcortical structures in the brain, such as Pruessner et al (Pruessner, Li et al. 2000), Pantel et al (Pantel, O'Leary et al. 2000), Barnes et al. (Barnes, Whitwell et al. 2006), Tisserand et al. (Tisserand, Visser et al. 2000), Frazier et al. (Frazier, Hodge et al. 2008) and Strasser et al. (Strasser, Lilyestrom et al. 2005). The manual segmentation process is very time consuming and prone to subjective errors ((Pruessner, Li et al. 2000); (Chupin, Mukuna-Bantumbakulu et al. 2007)). There is also a question of inter-observer and intra-observer variability, which may limit how possible it could be to detect differences when comparing various subcortical structures (Chupin, Hammers et al. 2007).

It has increasingly become apparent that studies of small numbers of subjects do not provide clear-cut results to relevant questions because of individual variability and multiple confounders that then create problems for analysis when manual tracing is used because of the time required to produce a manually traced map in an adequate number of scans (Morey, Petty et al. 2009). Although manual segmentation provides accurate measures of hippocampal volume, automated processes would reduce the subjectivity of the segmentation process and would of course provide a considerable saving of time. Using computer techniques to help with segmentation process has therefore become an essential part of the analysis of structural scans.

1.3.2 Semi-Automated Segmentation

A number of semi-automated segmentation methods have appeared in the last ten years. Although manual segmentation remains the gold standard, Semi-automated techniques are by far the most common used. These methodologies have gained popularity as they decrease the processing time of segmentation, although they still involve manual intervention, such as seeding before segmentation (stating where the regions of interest are in a scan) or editing the resultant segmentation (such as editing after thresholding). Various types of processing techniques have been explored.

Chupin et al. (Chupin, Hammers et al. 2007; Chupin, Mukunabantumbakulu et al. 2007) used a Markovian deformation process with a deformable constraint based on prior knowledge, which is calculated with manual intervention. A user must manually define bounding boxes and seed points in order for the methodology to work, making the entire process semi-automated. A study by Ashton et al. (Ashton, Parker et al. 1997)) also use deformable models, the elastic deformable model, used with seed points and constraints to segment the hippocampus. The seed points and the constraint were all produced from boundaries that had previously been traced manually.

These methodologies speed up processing time of segmentation considerably compared to manual segmentation, allowing them to process a greater quantity of scans. The necessity of including human involvement still increases processing time,

and it provides a subjective element to segmentation as is present in manual segmentation.

1.3.3 Automated Segmentation

One group, who state that their method is fully automated uses a Bayesian approach (Fischl, Salat et al. 2002), where the results of 42 manually labelled data sets are used to derive a probabilistic prior atlas map using linear registration to the atlas. Segmentation is then performed using Maximum A Posteriori (MAP) estimation. The resulting segmentation is highly dependant on the probabilistic atlas and hence the 42 labelled data sets used to create the atlas. It also requires some human intervention, which means that the procedure of segmentation cannot be considered to be fully automated.

Barnes et al. (Barnes, Foster et al. 2008) compare three different automated methods of calculating rates of atrophy within the hippocampal region. They look at fluid change that is calculated by the three methods, Jacobian change, region propagation or boundary shift. They found that the boundary shift integral's results were the closest to the manual results. The method however, can only be used for longitudinal studies, to assess the change from one hippocampus to another.

A combination of prior knowledge and deformable models was developed by Kelemen et al. (Kelemen, Szekely et al. 1999). The authors use brain atlases to help identify brain structures for the deformable model, removing the need for users to

guide the deformable registration, but the registration depends substantially on the prior knowledge that is derived from the brain atlases used.

Zhou and Rajapakse (Zhou and Rajapakse 2005) propose segmenting subcortical brain structures using fuzzy templates. These templates are based on structural features such as intensity values and location, plus the location relationship of structures with each other. Although the method removes the need of expert users to manually define the various structures, making the method fully automated, it still requires a learning process where the fuzzy membership functions are derived from a set of training images. The fuzzy membership functions will also depend heavily on the types of images used during training and the training images still need to be segmented manually.

Morra et al (Morra, Tu et al. 2008), like the above study, also report that their method is fully automated, whilst requiring 21 hand-labelled scans to allow the AdaBoost algorithm to learn classification rules that will enable it to segment hippocampi in unseen scans. This hand-labelling has the disadvantage of possibly making the method cohort or study specific.

Information fusion is a methodology created by Barra and Boire (Barra and Boire 2001) that also involves fuzzy logic. Fuzzy logic is used to merge various data about the structures. Another way of looking at segmentation is by using shape descriptors: Mangin et al. (Mangin, Riviere et al. 2004) take on this approach by using moments of 3D coordinates to describe brain structure changes.

Some studies have created hybrid techniques, merging various procedures and algorithms to create a result of all the results. Yang et al (Yang and Duncan 2004) for example, used Maximum A Posterior (MAP) estimation with level set prior information. Another case of hybrid algorithms is that of Amini et al (Amini, Soltanian-Zadeh et al. 2004), which used fuzzy clustering along with a deformable modelling algorithm in order to segment the thalamus.

Automated segmentation techniques are not relied upon in research as much as semi-automated techniques are. However, as various methodologies emerge, the quality of the automated segmentation is increasing, especially with the emergence of hybrid techniques. The ability to combine results from different algorithms to produce one result increases the reliability of findings in noisy and ambiguous territory such as the analysis of structural MRI scans of the brain. Hybrid methodologies allow this, enabling separated algorithms to process specific functionalities and then using the results together to decide on a final result.

Table 1 presents a table comparing the three main types of methods.

	Manual	**Semi-Automated**	**Automated**
Input required	yes	yes	yes
Time taken (approx)	Hours	30 minutes	2 minutes
ICC	0.9	0.85	0.85
Subjectivity	yes	no	no
Editing	yes	yes	yes

Table 1: Table comparing the 3 method types

The methodology described in this thesis is a fully automated hybrid hippocampal segmentation algorithm. Unlike the other methodologies described above, no human involvement is required in any part of the process and no training data is required to be produced beforehand in order to allow a model to learn. The methodology applies a novel technique that mimics the procedure performed by a human tracer to produce hippocampus segmentations from MRI scans. The hybrid approach is applied so as to cater for different requirements that are a necessary component when addressing the hippocampus since it is such an adaptable structure in a noisy environment. The methodology is fast, reliable and the results are comparable to human segmentations.

1.4 Overview of Chapters

This chapter has provided a general overview of the issues in the field of structural MRI image segmentation as well as the relevance of the hippocampus and its change in shape and volume. A brief account of research into these fields has also been presented and discussed. Chapter 1 demonstrates the relevance of the motivation and aims that this study offers. The remaining chapters of this thesis are organized as follows:

Chapter 2: Image Processing Algorithms

This chapter provides detailed explanations of the methods and algorithms that are used in the Automated Hippocampus Location and Extraction (AHLE) methodology developed in this thesis. A range of image processing techniques is discussed here, from how the image is managed and manipulated to give access to the range of measurements necessary to replicate human tracing, to Gaussian smoothing, mathematical morphology and edge detection. These are the fundamental processing techniques on which the algorithms presented in later chapters are built upon.

Chapter 3: Artificial Intelligence Algorithms

Having discussed the standard image processing methods from chapter 2, chapter 3 discusses the artificial intelligence algorithms that can be used in image processing for image segmentation that is more accurate than the standard image processing algorithms that do not involve any learning. Two methods are discussed, Fuzzy logic and image processing and Deformable manifold modelling.

Chapter 4: The Hippocampus Location and Extraction Methodology

Chapter 4 presents the main aspect of this study, discussing how the algorithms presented in chapters 2 and 3 are used to develop the hybrid methodology. The chapter examines how these algorithms are modified and implemented to create the methodology that first locates and then extracts the boundary trace of each hippocampus.

Chapter 5: Reliability Testing

In order to assess the quality of the hippocampal traces that the methodology produces, the traces need to be compared to the gold standard of hippocampal tracing, manual tracing. An explanation of the cohort used, the methods performed to assess automated tracing to manual tracing and the results is given in this chapter.

Chapter 6: Performance of the Methodology on a Cohort

Chapter 5 provides results of the quality of the performance of the methodology, now chapter 6 applies the methodology to a cohort of over 185 brain scans and 7 subject groups including schizophrenia and bipolar I patients. The results show sex and group differences and this is presented and discussed in this chapter.

Chapter 7: Conclusions

The final chapter discusses the outcomes of this thesis, and the importance this research presents as an example of automated image segmentation methods. The limitations of the current algorithm are discussed as well as possible solutions for

further optimization such a Genetic Algorithms to search for the best combination of variables used throughout the hybrid algorithm.

Chapter 2 - Image Processing Algorithms

This chapter provides detailed explanations of the base methods and algorithms that are used in the AHLE methodology. A range of image processing techniques is discussed. These include how the image is stored and manipulated, processed to obtain Gaussian smoothing and low level feature detection. These functions deal with image management, and are in essence 2D image functions that are being extended to the 3D MRI space. The functions are of limited use to MRI processing in their raw form, and need to be integrated with intelligent algorithms in order to gain the power necessary for this methodology. The functions created for this methodology are designed to be reusable, meaning that the code can be used again for modified functions. This is an important aspect to software engineering.

2.1 Image Analysis in MRI

This section looks at two different methodologies that are at the base of our MRI processing and analysis. The structure of the MRI scan is first discussed, and the techniques involved in processing and manipulating it in a programming environment. Also we present procedures for handling the pre-processing of an MRI scan. The methodology discussed here is the procedure adopted at the Imaging Lab at the Department of Psychiatry, University of Edinburgh.

2.1.1 The structural MR image format

The first element that needs to be considered in image processing is the data structure. Structural MRI provides a 3 dimensional (3D) image. The scans used in this project consist of 218 X 182 X 182 voxels. The image is stored as a structure and this structure will need to be managed in order to manipulate the image. The structure used is a 3D vector array. Each position in the array represents a voxel in the image, and will contain the intensity value of that specific voxel. This is depicted in figure 2.1:

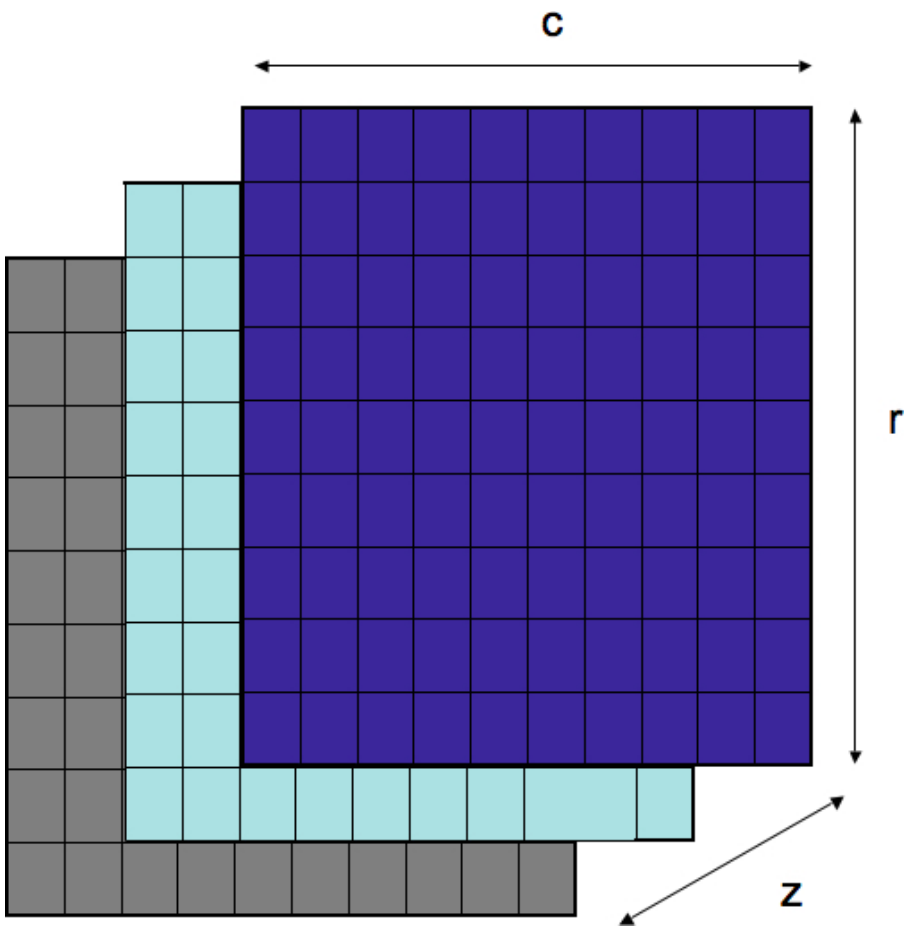

Figure 2.1: The MRI scan as a 3D array. Each position represents a voxel.

The total number of rows, columns and slices are NR, NC and NZ respectively. Therefore, for axial view NR = 218, NC = 182 and NZ = 182, whilst for coronal and sagittal views NR = 182, NC = 182 and NZ = 218.

An important aspect to processing the image is the selection of a position within the image array. To do this the following equation is used:

```
pos = (z*NCNR)+(r*NC) + c;
```

Where NCNR is the product of NC and NR. Standard 2D image processing uses a 4-point or 8-point neighbourhood. Figure 2.2 depicts the 8-point neighbourhood:

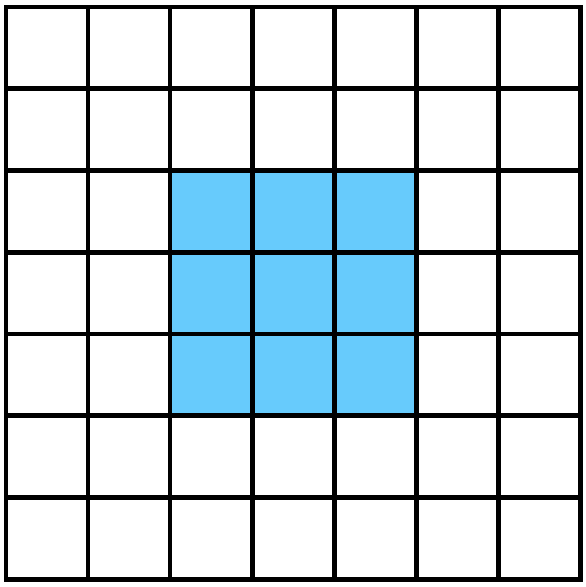

Figure 2.2: An 8-point neighbourhood in a 2D image

If the position value of the current voxel x is known, then moving around its neighbouring voxels is as follows:

- Right or left: x is incremented by 1 to move right and decremented by 1 to move left `x = (z*NCNR) +(r*NC) ± c; left = x – 1; right = x + 1.`
- Up or down: To move up or down you need to increment or decrement by NCNR from x respectively: up = x + NCNR. Down = x – NCNR.
- Up and right or up and left (upper diagonals): Using the two previous points, moving up involves incrementing the x value by NCNR, and left or right is achieved by decrementing or incrementing that value by 1 respectively. Therefore, up and right = x + NCNR + 1; up and left = x + NCNR -1.

- Down and right or down and left (lower diagonals): As previous step, however this time decrement x by NCNR to lower the row by one. Therefore, down and right = x – NCNR + 1; down and left = x – NCNR – 1.

Figure 2.3 shows a descriptive version of these manipulations.

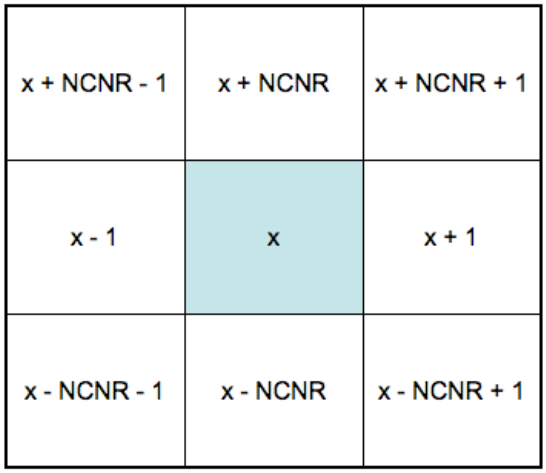

Figure 2.3: Moving around the 8-point neighbourhood

In this 3D environment, the 8-point neighbourhood is extended into a 3D neighbourhood. This increases the neighbourhood size to 26 and is represented in figure 2.4, where the dark blue squares represent the neighbours of the central pink voxel.

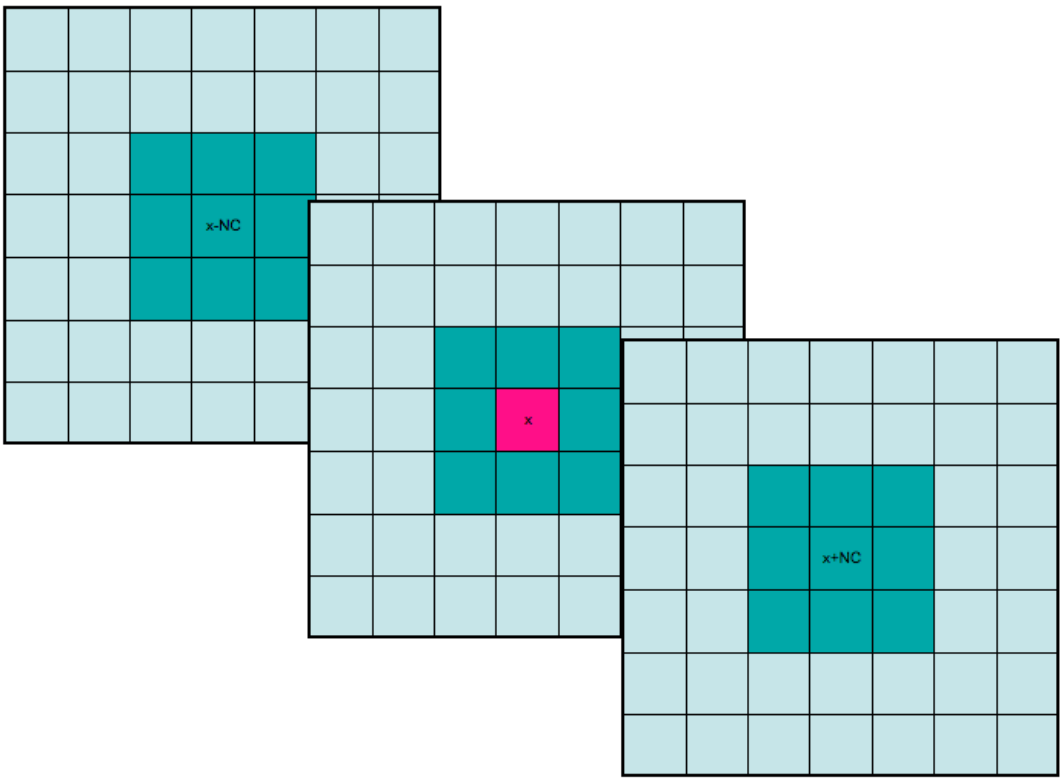

Figure 2.4: a 26-point neighbourhood in a 3D image

Moving forward and backwards in this neighbourhood is possible by incrementing or decrementing the current voxel x by NC. The other movements (up, down, left, right etc…) use the same equations as before with the addition of + NC or – NC.

This mathematical base provides the foundations on which functions can be applied to in order to replicate the human procedure of hippocampal tracing. By using this approach of traversing a 3D image, one is able to control how to manipulate the data, whether it is in sagittal or coronal view. This allows the algorithm to mimic the steps a hand tracer takes to perform the task. This approach also facilitates the separation of structure from noise by observing the continuity of the structure in three dimensions, and checks for local connectivity.

2.1.2 Image Pre-processing.

This section gives a description of the procedure used to reorient, extract and warp the brain scans at the Imaging Lab, Department of Psychiatry, University of Edinburgh. This procedure is performed in order to bring all the scans in a cohort in a uniform coordinate space, and is done using the SPM 2 package (http://www.fil.ion.ucl.ac.uk/spm/ (Ashburner, Andersson et al. 2000; Ashburner and Friston 2000)). The procedure was applied to 1.5T images and is as follows:

1. If the scan is in coronal format, then the scan is first reoriented into an axial format. This is done using the MRICRO software package (http://www.mricro.com).
2. Continuing in SPM, the T1 brain scan is segmented in native space using the functions SPM_segment.
3. Next the brain tissue voxels are extracted to create a second image using SPM_xbrain, effectively removing non-brain tissue. This results in two images both in native space. Image 1 is the extracted brain image and image 2 is the full brain image produced in step 2.
4. A 9-point affine transformation is performed. This co-registers the extracted brain with standard Montreal Neurological Institute (MNI) space.
5. Re-slice the images to 1 X 1 X 1 mm resolution. This results the extracted brain and whole head scan being ACPC aligned. Thus all study images are aligned on the Anterior Commissure Posterior Commissure (ACPC) axis.

6. The next step is to obtain a high quality extracted brain image. To do this the extracted brain image is warped into MNI space. The brain is expanded to fit onto the MNI template. The new T1 image produces a set of warp parameters. These parameters are used warp the whole brain image into MNI space.
7. We apply masks to remove non-brain tissue and run dilation and erosion processes to obtain our high quality brain extraction in MNI space.
8. This procedure works on about 75% of the scans. 15 % of the remaining scans produce a good quality image by repeating the procedure. The remaining 10% require manual handling to remove eye sockets and other non-brain tissue image residue, to produce an acceptable image.
9. The next step is to bring this improved extracted brain back into native space (AC-PC registered). The whole brain image is needed to do this, in a reverse procedure to step 6. This is used to produce a set of warp parameters that are then used to convert extracted brain back into the AC-PC space.
10. Grey and white segmentations are now performed in the Montreal Neurological Institute (MNI) space. Once this is complete, the segmentations are warped back into native space using the whole brain warp.
11. Also in MNI space the mapping to generate warped images is performed. This is done using the Center of Cardiovascular Bioinformatics and Modeling (**CCBM**) template (which has an intensity value for each brain structure). The result is warped into native space. This is a repeat usage of the warp derived in step 9.

2.2 Image Processing Techniques

2.2.1 Mathematical Morphology

Morphology is the form and structure of an object (Parker 1997). Morphological operators use set theory and geometry in order to analyze and manipulate image structures. The functions explained in this section are of limited use to MRI processing in their raw form, and need to be integrated with intelligent algorithms in order to gain the power necessary for this methodology.

In a morphological function the image is used as input, and each resulting voxel value will depend on the values of the neighbouring voxels. This is done with the means of a "structuring element". There are different possible methods of implementing a structuring element; in this case a 3X3 matrix is used (this can be thought of as a kernel such as that found in smoothing algorithms). This matrix contains a specific pattern to be applied to a structure found in the image.

The structuring element is then superimposed on the image. The centre voxel is considered the main voxel, and has a position value of (0, 0) in the matrix (see figure 2.5). The neighbouring voxels' positions will differ from this centre voxel by ±1 position on either axis. This structuring element is able to "see" the pattern around the centre voxel.

(1,-1)	(1,0)	(1,1)
(0,-1)	(0,0)	(0,1)
(-1,-1)	(-1,0)	(-1,1)

Figure 2.5: The structuring element used in mathematical morphology. The centre voxel is the main voxel being considered. All neighbouring voxel positions vary by a value of +/-1.

Various manipulations can then be performed on the pattern the structuring element is superimposing according to what is needed. The two most elementary operators are Erosion and Dilation.

Erosion

In Erosion, voxels around the boundary of a structure are deleted from the image.

Formally, erosion of an image *I* by a structuring element *S* is given by

$$I \ominus S = \{x | (S)_x \subseteq I\}$$

Where the result is the translation of S given by the vector x. This means that for every target voxel, if the structuring element is completely inside the object, then the

voxel is kept in the object, otherwise it is removed, thus eroding (or shrinking) the object.

Dilation

Dilation is used to grow a region of an image by increasing the voxels at the boundary of the region.

The formal description of dilation of an image *I* by a structuring element *S* is given by

$$I \oplus S = \{x | (\hat{S})_x \cap I \neq \emptyset\}$$

This means that for every target voxel if the majority of the structuring element is in the object, then that target voxel is added to the object, thus dilating (increasing) the object.

Morphological Opening and Closing

The erosion and dilation operators can be combined to create a combined function that successively opens and closes giving incremental boundary changes with reduced susceptibility to noise in the raw data. Opening removes jagged edges and allows spaces between objects to increase, an ‘opening up’ of space. Closing helps to complete an object by ‘closing up’ gaps and breaks.

These morphological operators used iteratively are able to refine a boundary in a similar manner to a hand tracer iteratively adjusting their tracing.

2.2.2 Image Smoothing

Image smoothing is a key procedure in image processing. It is used to reduce the noise of the image. This results in a blurred image. Doing so removes noise and generates clearer boundaries. Smoothing is generally the first step in most image processing methodologies such as edge detection. Figure 2.6 depicts the difference between an original image and a smoothed image.

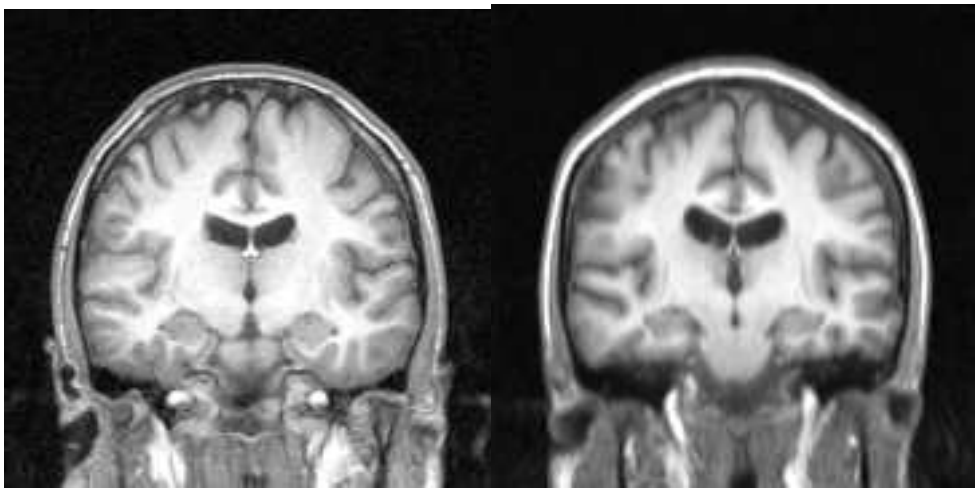

Figure 2.6: Original and smoothed MRI images; left image is the original image, whilst the right image is the smoothed image.

The smoothing algorithm used in this method is known as Gaussian smoothing. A 2D convolution operator is used with a Gaussian kernel. Convolution is a procedure where an array called a ‘kernel’ is passed over the image array. At each voxel, which overlaps with the kernel, the current kernel value and the voxel value are multiplied together. Finally, the multiplied values are added together to generate the result value of the target voxel. The general equation for the target voxel value is:

$$O(i,j) = \sum_{k=1}^{m} \sum_{l=1}^{n} I(i+k-1, j+l-1) K(k,l)$$

The Gaussian kernel has its values set to reproduce a Gaussian with a standard deviation of 1.0, as can be seen in figure 2.7. Since the image is in 3D, this 1D kernel is passed over the image in all 3 directions. The target voxel is always the voxel that overlaps with the 3rd kernel value.

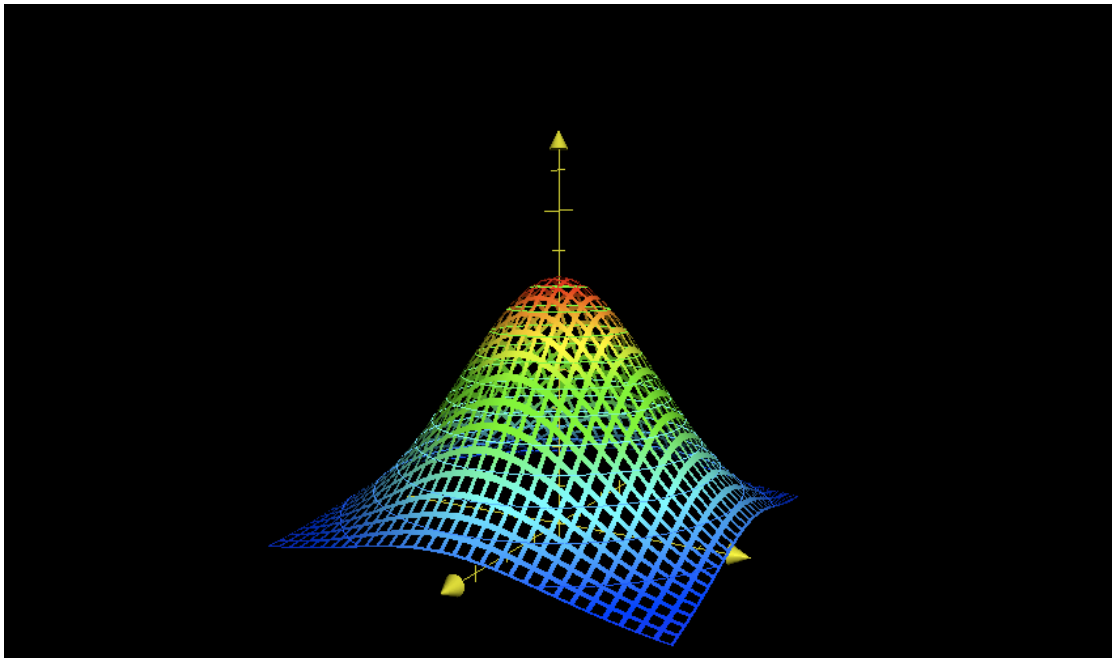

Figure 2.7: The Gaussian distribution

The algorithm is as follows:

Algorithm 1 The Gaussian Smoothing Algorithm

1. Set gaussian kernel
2. Blur:
   2a. Blur in the r direction
   2b. Blur in the c direction
   2c. Blur in the z direction
3. Return the blurred image.

2.2.3 Image Thresholding

Once the image is smoothed to reduce noise, it is then used to produce a threshold version of the scan. This version of the smoothed scan is a binary image of voxel values either 0 or 255 (black or white). In many cases thresholding is used to label objects in the image to the background (background would be labelled 0 and the object labelled 255). In this implementation, however, thresholding is used to roughly segment the white and grey matter in the image.

Thresholding is not an accurate function to segment an image into grey and white matter. The best results of thresholding come from images with modal intensity distributions. In these cases the intensity values of the image produce a distribution with distinct peaks, allowing the possibility of segmenting at a threshold value or values. The images used in this project do not give distinct peaks and so it is not as easy or possible to cleanly segment the image according to the intensity values.

However, it helps to give an initial estimate on where in the image the boundaries between the grey and white matter may be found.

Each scan is threshold by a different value. Some scans may be darker than others (lower intensity values) so it is important to recognize this when segmenting. A too high threshold value and the algorithm will label too much white matter as grey. To overcome this, the threshold algorithm identifies the average intensity value of the scan, and uses this as the threshold value of the scan. Any voxel with an intensity value higher than the threshold value is labelled potential white matter (value 255), whilst any voxel with intensity value lower than the threshold value is labelled as grey matter (value 0). This thresholding is only a rough estimate and is intended for use in tandem with other maps as will be discussed shortly.

Algorithm 2 The Image Thresholding Algorithm

1. Calculate average intensity value using $A = \sum i(x)/X$
2. $\forall x \in X$:
    3. if $i(x) > A$ then $x = white$
    4. if $i(x) < A$ then $x = grey$

2.2.4 Edge Detection

Edge detection is another way of locating boundaries between grey and white matter besides thresholding. These algorithms are intensity-based algorithms, like thresholding, however they tend to be more sensitive to the varying values. The

reason for this is that they focus on calculating gradients of changing intensity values of voxels near each other. A steeper gradient will show a greater difference between intensity values, and this alerts the algorithm of a potential boundary (or *edge*). There are a number of algorithms around, most differ on the initial smoothing filter and the way the gradient is calculated. The algorithm implemented in this project uses the Canny Edge Detector, which is the best performing and popular of the algorithms available to date (Heath, Sarkar et al. 1997), even though it was developed in the late 1980s (Canny 1986). There have been variations of this detector implemented; however it is the standard edge detector that we considered for this study. This implementation looks at each slice as a 2D image, which is then collected together to form a complete 3D output.

The Canny Edge Detector

Algorithm 3 The Canny Edge Detection Algorithm

1. Gaussian smooth image

For every slice in the scan:

2. Find the gradient in the x direction $-> G_x$
3. Find the gradient in the y direction $-> G_y$
4. Find the magnitudes of the gradients G_v using $G_v = \sqrt{G_x^2 + G_y^2}$
5. Find the directions of the magnitudes θusing the equation $\theta_v = \arctan[\frac{G_y}{G_x}]$
6. Convert directions from radians to degrees D_v with $D_v = \theta \times \frac{180}{\pi}$
7. Perform Non-Maximal Suppression on each voxel
8. Perform Hysteresis on each voxel

A detailed explanation of his methods can be found in Canny's paper (Canny 1986). The algorithm can be split into four main steps:

- Gaussian Smoothing

  Smoothing is the first step in the procedure to reduce noise in the image. The Gaussian smoothing algorithm explained earlier is used to do this.

- Calculating the edge magnitudes and directions

  Once the image is smoothed, it is moved on to the next step, which is to calculate the derivatives of the intensity values. This needs to be done in each direction, hence the derivatives in x and y directions are computed. Therefore the gradient magnitude at each voxel is calculated using the equation:

$$G_v = \sqrt{G_x^2 + G_y^2}$$

  The direction of the gradient at that voxel is given by:

$$\theta_v = \arctan[\frac{G_y}{G_x}]$$

  θ being in radians must then be converted into degrees using:

$$D_v = \theta \times \frac{180}{\pi}$$

  This equation gives a degrees value between 0 and 360. This must then be approximated to the 8 possible directions a line can take on the image grid. These 8 directions can be sub-grouped into 4 directions (0, 45, 90, 135) as can be seen in figure 2.8:

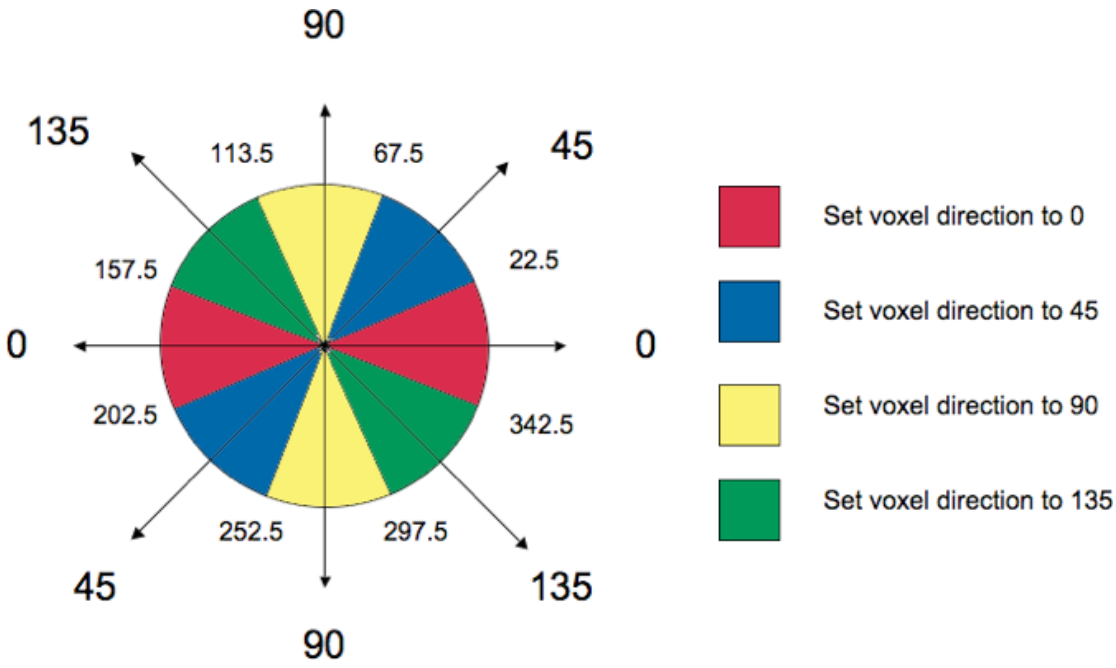

Figure 2.8: Gradient Directions

- Perform Non-Maximal Suppression

  The resulting image from step 2 will result in thick edges. This next function suppresses any voxels that are not considered to be part of the edge it is tracing, to create an edge that is only 1 voxel wide. If a voxel has an intensity value greater than 0, then its neighbours along the direction it is marked at are considered. If the voxel has a greater intensity value than these two neighbours then it is kept as an edge, otherwise its value is set to 0. Figure 2.9 depicts the difference before and after non-maximal suppression. (A) is the upper manifold of the hippocampus before non-maximal suppression, whilst (B) is the same section after the function is run.

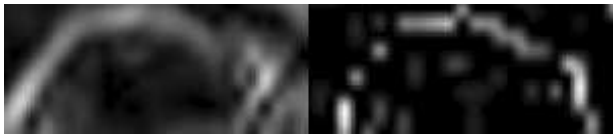

Figure 2.9: Non-Maximal suppression of the upper hippocampus boundary; left image is before function is run; right image is the same boundary after function is run.

- Perform Hysteresis

  The final function of the algorithm ensures that all edges are of the same value. Two threshold values are used, T2 being a higher value than T1. Any value greater than T2 is considered to definitely be an edge voxel and is marked as such. Its neighbours are then looked at and if any of them have a higher value than T1 they are also marked as part of the edge. If a voxel is below the T1 value then it is ignored.

Edge Detection Results

The entire Canny process is viewed in figure 2.10:

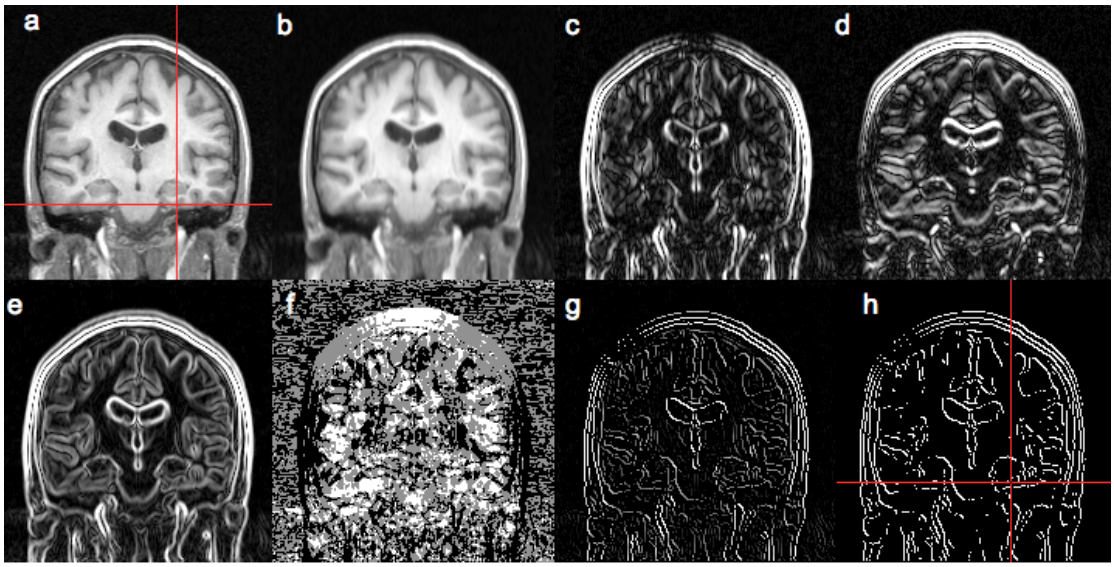

Figure 2.10: The Canny edge detection process: (a) the original image, (b) smoothed image, (c) change of gradient along the x direction, (d) change of gradient along the y direction, (e) gradient magnitudes, (f) directions of gradients, (g) maximal suppression, (h) final result after hysteresis is performed.

As can be seen from the figure, the canny edge detector is able to detect strong boundaries in an MR image. The results, however, become limited for the hippocampus boundary, as can be seen in figure 2.11:

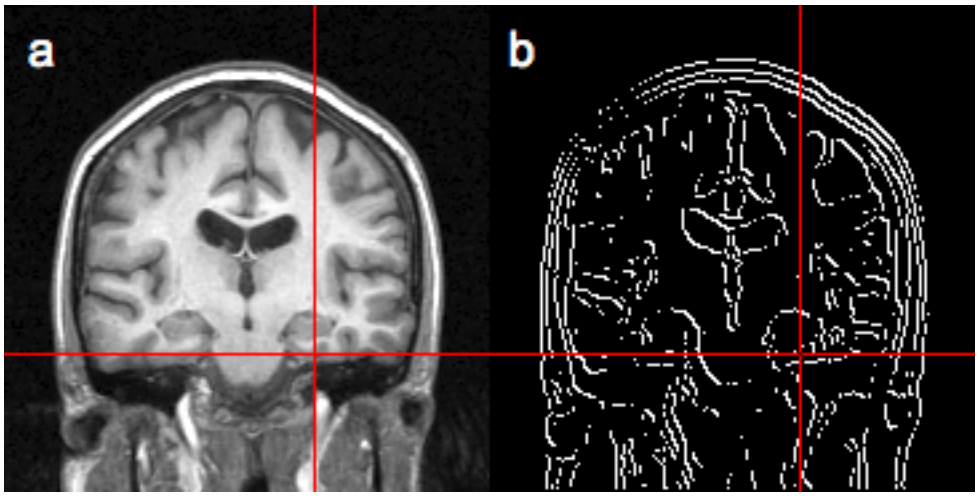

Figure 2.11: The Canny edge detector results: The hippocampus lower boundary is not found as can be seen by the cross bars in (a) the original image and (b) the final result image.

Edge detection is able to give a good approximation of the upper but not the lower hippocampal manifold. In the case of the lower hippocampal manifold, the algorithm detects the parahippocampal gyrus boundary rather than the actual hippocampal boundary. Thus canny edge detection cannot locate the complete hippocampus boundary.

2.3 Conclusion

This chapter has described various image processing techniques, including MR image manipulation and the standard morphological and edge detection processes. It is clear that although these functions and methodologies are useful and may even be necessary, they are not enough to locate the hippocampi in an MR image. These techniques therefore need to be used along with other algorithms in order to produce the desired result of automated hippocampal volume extraction.

Chapter 3 - Artificial Intelligence Algorithms

Having applied standard image processing methods in chapter 2, this chapter considers two artificial intelligence algorithms that can be used in hippocampal extraction. These are Fuzzy Image Processing and Deformable Manifold Modelling.

3.1 Fuzzy Image Processing

3.1.1 Overview

The idea of a ‘fuzzy concept’ or ‘fuzzy perception’ is one that implies vague concepts, concepts which do not have an exact meaning and which may need further description in order for the meaning to become clearer. The concept or perception cannot be precisely measured and therefore is designated a value which is intuitive to the human user. One example of this can be the concept of height (as a category rather than as a measurable dimension). The idea of being tall is relative and a person could be very tall, not so tall, or short, compared to someone else. Since it is not a specific meaning, one would describe these values, which are intuitive to us, as being fuzzy. In this section, an explanation into fuzzy logic and fuzzy sets is given, and then how this is implemented into image processing is discussed.

3.1.2 Fuzzy Sets and Fuzzy Logic

Zadeh (Zadeh 1965) first introduced fuzzy sets to model ambiguity. A fuzzy set consists of elements that cannot be described in precise terms. These elements will possess degrees of membership for each set, describing how likely it is that the element in question is part of that set. The idea is to be able to form some sort of model on the ambiguity of complex systems where membership is not black and

white, but consist of various types of grey as well. This allows the possibility to process human knowledge using fuzzy logic. This type of logic uses if-then rules in order to determine the fuzzy set in which an element belongs. These elements used as input are generally non-fuzzy datasets, that is, data that has been measured and collected in some form.

3.1.3 Fuzzy Image Processing

In the previous section, the concept of fuzzy membership was explained by referring to a set where it is not always possible to describe an element as being black or white, but rather that there exists many shades of grey. This is an ideal explanation when applying fuzzy logic to image processing, since in most cases (and an MRI scan is one of them) the objects in an image are not portrayed with just black or white pixels or voxels, but in various grey intensity values. Trying to deduce boundaries from these grey intensities values is a difficult task. In order to do this a method must be found that mimics the judgements made in hand tracing. This means that the judgement made on whether a voxel is in the hippocampus or not is dependent upon context information. Fuzzy processing allows context information of the voxels to be gathered and manages the vagueness of this decision. This allows the fuzzy approach to be a more suitable method to manage imperfect boundaries between two segments.

Fuzzy inference can also be used in image processing as a way of fusing different segmentation algorithms in order to produce a convergent optimal result from the

results of the many different algorithms. This can be encoded using if-then rules that help to decide on the best label for a voxel or pixel. Fuzzy processing is used in this methodology in order to locate the initial hippocampal seed points and the procedure is discussed in detail in the next chapter.

The next section presents another method that involves fuzzy inference and is another example of how fuzzy processing can be applied to image processing. Briefly, fuzzy processing is used to grade how likely a voxel is to be at the centre of a sulcal ridge or not in a 3D MRI scan, and the result of this method is a sulcal ridge brain map.

3.1.4 The Sulcal Ridge Finder Algorithm

The sulcal ridge finder algorithm is an example of applying fuzzy processing to the image-processing domain, and is used in the methodology as is described in the next chapter. The function was created by Dr. Bill Moorhead at the Imaging Lab, Department of Psychiatry, University of Edinburgh. It is part of another methodology used to calculate the Gyrification Index of the prefrontal lobe (Bonnici, William et al. 2007). Its purpose can also be used for this project as it aims to produce a brain map of the strongest white matter ridges from an extracted brain scan input. This brain map will be able to help locate the lower boundary of the hippocampus later on in the process. Algorithm 4 gives a representation of the Sulcal Ridge finder function:

Algorithm 4 The Sulcal Ridge Finder Algorithm

1. Smooth Image
2. For every coronal slice:
    a. Set scope variable
    b. Find intensity threshold value
    c. For every voxel in slice:
        i. If voxel intensity is greater than threshold then
            1. For every direction:
                a. Calculate left average intensity value
                b. Calculate right average intensity value
                c. If voxel intensity greater than left AND right then
                    i. Increment voxel accumulator
                d. End if
            2. End for
        ii. End if
    d. End for
3. End for

The function begins by smoothing the input scan using an averaging function. Once this is completed, the process proceeds slice by slice from a coronal view. For each slice, a variable is set to determine the scope of the ridge (width) and a threshold is found (which was set to 0.8 times the average intensity value of the grey tissue. This was associated with the minimal intensity value for white matter presentation. This value was determined from qualitative assessments from a number of processed scans). The procedure then moves voxel by voxel in the slice. For each voxel, if the voxel's intensity value is above the threshold, then it is considered to potentially be

in a ridge and the ridge characteristics for that voxel must be determined. This is done by assessing where on the ridge the voxel is positioned. The voxel's neighbourhood is used to obtain this information. The averages from opposite directions are compared to populate a fuzzy space. It is an iterative process, done in the 8 principal directions within the slice, where an intensity average value on either side of the voxel is calculated. The scale of the directional average is varied; the scope term in the algorithm sets the maximum scale that the average is allowed to vary up to. In the ridge detector the scope is set to 5. This means that the directional average value is allowed to vary from 1 up to 5. This process results in two intensity values. A depiction of this is given in figure 3.1.

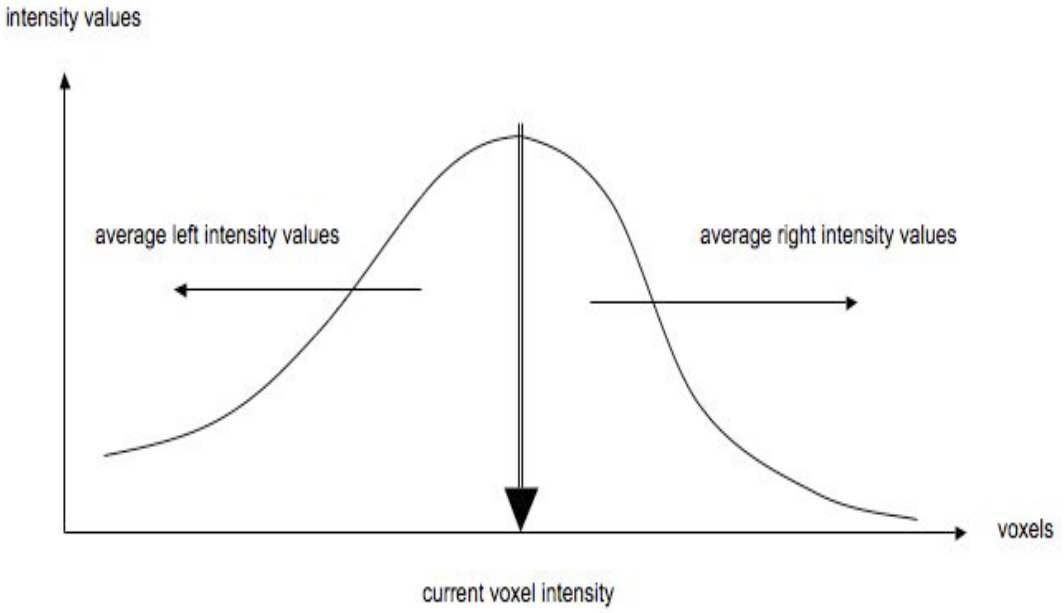

Figure 3.1: Calculating the ridge characteristics of a voxel

If the current voxel's intensity value is larger than both the averaged values on either side, then the voxel's accumulator is incremented. The resulting output scan from

this function is an image of the accumulator values, showing the voxels with the strongest sulcal ridge characteristics as perceived from every direction.

3.1.5 Conclusions of Fuzzy Image Processing

This section has introduced and explained the fuzzy processing technique, the logic behind it and how it can be applied to image processing. A discussion of the sulcal ridge finder algorithm has also presented an algorithm that uses the fuzzy processing technique to detect the sulcal ridges in a structural MRI. The fuzzy processing makes this procedure robust to noise and variability of ridge presentation; a necessary component for a function interacting with a noisy environment such as 3D MRI scans.

3.2 Deformable models

3.2.1 Overview

Deformable models are physics-based models that deform under the laws of Newton mechanics, in particular, by the theory of elasticity expressed in the Lagrange dynamics (Terzopoulos and McInerney 1997; He, Peng et al. 2008). These models are active models that represent a powerful tool to treat physical objects in images. A manifold is a 3D deformable model that potentially is able to deform towards the object's boundary.

Two types of methodologies exist to perform manifold deformation ((He, Peng et al. 2008)). The two variations are:

1. **Snakes** (Kass, Witkin et al. 1988), where the manifold deforms according to an energy equation who's change needs to be minimized. The equation includes internal manifold energy and external image energy.
2. **Level Set Methods** (Malladi and Sethian 1995) deform the manifold at a speed F. F is based on the curvature of the manifold as well as the features derived from the image

According to He et al. (He, Peng et al. 2008), to date eight variations of deformable model methods have been applied to medical image segmentation. A review of these methods is found in (He, Peng et al. 2008). Briefly, the eight methods are:

1. **Classic "Balloon" snakes**. This is the original snake introduced by Kass et al. in 1988 (Kass, Witkin et al. 1988). This snake is a type of contour that is based on minimizing an energy functional. This energy functional is derived from the boundary in the image itself**.** This process deforms the contour towards the boundary.
2. **Topology snakes.** To overcome topological inflexibility of the classic snake, McInerney et al (McInerney and Terzopoulos 2000) adapt the classic snake methodology to allow for topological changes that need to be managed by the deforming snake. The adaptation also makes it possible to discover the boundary of an object that is embedded with smaller object boundaries. They do this by using an affine cell 'image decomposition' framework that allows the snake to adapt to the topology of the snake object through splitting and merging.
3. **Distance snakes**. Developed by Cohen & Cohen (Cohen and Cohen 1993). This modification to the classic snake allows the manifold to be a distance away from the object of interest, to allow the snake to be initialized when the location of the object is not known. This is done by using a different external energy by including the distance of each pixel to its closest edge pixel from the edge image.
4. **Gradient vector flow snakes**. Developed by Xu and Prince (Prince and Xu 1996; Prince 1997; Xu 2000; Xu, Valentino et al. 2008). The main difference of this method to others is the use of a new kind of external force field called *gradient vector flow*. They state that this field is "a spatial diffusion of the

gradient an edge map derived from the image." Due to this new external force the manifold can start at a distance from the boundary and still locate it.

5. **Original level set**. As explained earlier, level set methods focus on the speed that the manifold expands at. In this case, the manifold is initialized inside the object of interest and iteratively expands at a speed F. F is usually a fast speed, and when the manifold hits a boundary, the speed decreases or even stops if the boundary gradient is strong enough.
6. **Geodesic active contour.** This methodology was developed as an extension to the level set (Caselles, Kimmel et al. 1997). They extended the classical energy minimization procedures found in the classic snake with the way the curve evolves in a level set.
7. **Area and length active contour.** An add-on to the geodesic active contour by Siddiqi (Siddiqi, Lauziere et al. 1998). In order to increase the attraction of the manifold to the boundary of interest, a weighted area function is included. The main benefit of this is faster computational time.
8. **Constrained optimization.** Deforms the manifold using a velocity function. Constrains the deformation process with a use of an energy function.

The methodology described in this thesis is based on the classic deformable methodology. The classic balloon methodology is used to deform 2D lines. In this study, the 2D lines are modified into 3D manifolds and therefore the procedure is modified accordingly to deform the manifolds. Being part of a larger methodology and to accommodate the noisy environment of MRI scans, the classic balloon methodology was the procedure of choice, since it is the ideal candidate as there is

no need for speedy deformations or having the manifolds initialize at a distance of the boundary. The MRI environment is so noisy that doing so will hinder the deformation process.

3.2.2 Deforming the Manifold

The manifold begins as an initial smooth plane close to the boundary. Using local energies the manifold is able to deform in such a way as to take on the shape of the boundary. The energies used are internal and external energies. The objective of the manifold deformation process is to minimize the total energy value, and once this is achieved a stable manifold is formed which would infer that the required boundary is located by the manifold, as can be seen in figure 3.2.

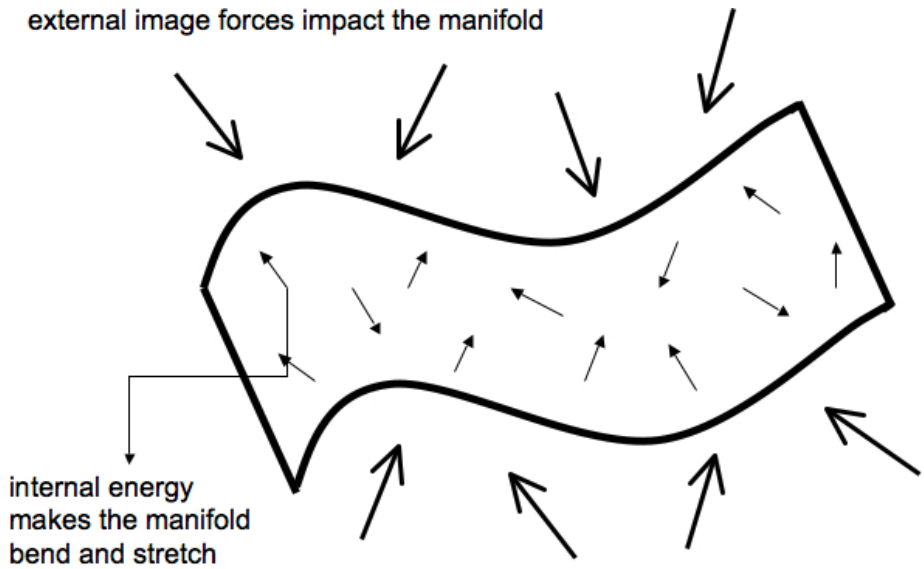

Figure 3.2: A graphic description of the manifold deforming under internal and external energies.

The manifold is processed iteratively and is manipulated slice by slice. Since it is manipulated in 2D, the 2D name of the manifold is the snake. The contour for each slice is represented as

$$c(s) = (x(s), y(s))$$

where x(s) and y(s) are the contour coordinates on the slice and s E [0,1], stating whether that coordinate is part of the contour or not (0 not in contour, 1 in contour). The equation for the energy of the snake is:

$$E_s = \int E_{int}[x(s), y(s)] + E_{ext}[x(s), y(s)]ds$$

Where E_{int} represents the internal energy and E_{ext} represents the external energy of the snake. In order for the procedure to be coded, the equations need to be discretized. Therefore N samples of the contour are taken, known as vertices $\mathbf{v_i}$ such that $v_i = v(s)_s = ih$ and $h = 1/N$. This means that each vertex position is spaced equally.

3.2.4 Internal Energy

Internal energy is derived from forces at work in the plane, and is usually generated by simulating physical properties such as elasticity and rigidity of the plane (Terzopoulos and McInerney 1997). Therefore, the internal energy equation is a summation of two parts, elastic energy ad rigidity energy.

$$E_{int} = \frac{1}{2}(\alpha(s)E_e + \beta(s)E_r)$$

The coefficients $\alpha(s)$ and $\beta(s)$ are terms that manipulate the strength of elasticity and rigidity forces found in the snake. If $\alpha(s)$ is small then the snake is encouraged to expand. The larger this value is assigned the more the snake will shrink. One can compare this term as to how much a rubber band can be pulled. The coefficient mimics the elastic band's ability to be stretched. Rigidity is a measure of the snake's 'bendiness'. The $\beta(s)$ coefficient therefore regulates how much the snake is allowed to bend during deformation. The larger the value of $\beta(s)$, the more rigid and stiff the snake becomes, the smaller the value and the snake becomes more bendable and is able to bend around contours more.

The equation to calculate elastic energy E_e is done by calculating the first derivative and is as follows:

$$E_e = d - \| \mathbf{v}_i - \mathbf{v}_{i-1} \|$$

This can be expanded to

$$E_e = d - \sqrt{(x_i - x_{i-1})^2 + (y_i - y_{i-1})^2}$$

Where d is the average between the vertices of the snake. This will help to keep the vertices at equal distances. The rest of the equation works at attempting to minimize the vertex distances, giving the snake the elastic property to stretch or shrink

The second derivative provides the equation for rigid energy E_r and is:

$$E_r = \| \mathbf{v}_{i-1} - 2\mathbf{v}_i + \mathbf{v}_{i+1} \|$$

That can be expanded to

$$E_r = \sqrt{(x_{i-1} -2 x_i + x_{i+1})^2 + (y_{i-1} -2 y_i + y_{i+1})^2}$$

This equation is able to approximate the snake's curvature.

3.2.5 External Energy

In contrast to internal energy, external energy is derived from the external environment of the manifold, the image, and is used to attract the snake towards the contour. This energy value is calculated through the intensity gradient changes found in the image. The equation for this value is

$$E_{ext} = k_{ext} \sum_{i=1}^{N} g(x_i, y_i)$$

As the snake vertices approach an edge in the intensity profile, this external energy value will become maximal.

3.2.6 Minimizing Energy Potential

The goal of deformable models is to minimize the energy functional

$$\sum_{i=1}^{N}(\alpha(i)E_e + \beta(i)E_r + E_{ext})$$

Therefore, for each iteration, every vertex in the snake moves within a 3 X 3 framework to the voxel in which the energy functional value is minimal compared to the other voxels in the neighbourhood. For implementation, each energy value must be normalized. For the internal energy, dividing E_e and E_r by the largest value in the voxel neighbourhood does this. The external energy is normalized using the following equation

$$\overline{E_{ext}} = \frac{E_{ext} - min}{max - min}$$

Where min is the minimum gradient value in the neighbourhood and max is the maximum gradient value in the same neighbourhood.

3.2.7 Turning a snake into a manifold

The image in question is a 3D image. This means that the snakes in every 2D slice must be connected with the neighbouring slices in order to provide continuity. Doing so converts the snake into a manifold. To do this the algorithm is extended to include a simple function where each vertex in the current snake checks to make sure it is connected to the previous slice's vertex that is at the same location on the snake. It does this when it is checking its neighbourhood for the minimal energy functional. Therefore, the vertex will move to the neighbour on the basis of not only the energy

functional but also on the connection of the vertex with the previous slice. If moving to the voxel with the minimal energy functional will disconnect the vertices, then it is not chosen and the voxel in the neighbourhood with the next minimal energy function is considered.

3.2.8 The Algorithm

Algorithm 5 outlines the main steps of the deformable manifold implementation in pseudo code.

Algorithm 5 The Deformable Manifold Algorithm

1. Repeat until only a small amount of vertices move
in an iteration or until an iteration limit is reached
2. For each vertex v_i $i = 1, \ldots, N$ where $N = totalnumberofvertices$
   a. Find neighbour voxel in $3X3$ vicinity with
   minimal energy functional
   3. If slice is not first slice then
      a. Confirm that selected voxel is linked to previous vertex
      b. If linked then assign $\mathbf{v}_i$ to that voxel
      Else repeat with next voxel with minimal energy functional
   Else assign vi to that voxel
4. Again for each vertex $\mathbf{v}_j$
   a. Calculate E_r
5. For local maxima vertices
   a. If threshold is exceeded then Set β to 0
6. Update value of d

3.3 Conclusions

Deformable modelling is a very popular methodology to use in image processing when boundary identification in images with too much noise or irregularity is required. If placed close to the required boundary area the manifold is able to locate and deform into the boundary shape, making it possible to analyze the shape and volume of the object that the boundary is encapsulating.

Since the classic deformable manifold is sensitive to energy minima, and could potentially locate unwanted boundaries, many extensions and modifications of the classic methodology have been developed, such as gradient vector flow and constrained optimization (Cohen and Cohen 1993), (McInerney and Terzopoulos 2000), (Xu 2000), (Caselles, Kimmel et al. 1997) and (Siddiqi, Lauziere et al. 1998). However, to locate the hippocampi boundaries in this project, what is needed to be found is not always the strong boundary, since the hippocampus is sometimes ill defined and hardly ever consistent for each scan.

Limitations of deformable manifolds

One significant issue with deformable manifolds is that the deformation process is not object specific. The algorithm is also very sensitive to the initial location of the manifold. If the manifold is initialized in a wrong location on the image, the manifold will deform to the closest object it finds, which might not be the target object. The algorithm therefore requires prior information on the location of the

object it is supposed to locate in the image. Finally, solutions are not intuitive and are computationally heavy.

Chapter 4 - The Automated Hippocampus Location and Extraction Methodology

Chapter 2 provided information on base morphological image processing, and chapter 3 considered the artificial intelligence methods of fuzzy inference and deformable modelling. This chapter explains how the algorithms described and explained in chapters 2 and 3 are used together to create a hybrid algorithm that is able to automatically locate and then extract the hippocampi from an MRI scan.

Scans are a noisy environment and each hippocampus is unique. The methodology discussed in this chapter aims to mimic the functionality of a hand tracer to enable the hippocampal volume extraction. An outline of the methodology and its algorithm is first given and explained. Then each section is discussed.

4.1 Methodology Outline

The Automated Hippocampus Location and Extraction (AHLE) methodology is a hybrid algorithm that requires the user to input the original 3D MRI scans of each subject for processing. Using a template, the AHLE algorithm generates the extracted hippocampus. Thus, no manual intervention is necessary in the AHLE process. The algorithm outputs three files. The original image superimposed with the hippocampal boundary traces is the first output and two files text files that contain volume data output. One text file reports the volume of each hippocampus slice by slice. This means that for each coronal slice the volume of each hippocampus (left and right) are recorded. The second text file reports in summary the total hippocampal volume for each hippocampus (left and right) for each scan.

The hybrid algorithm consists of two processing steps to produce the required output. This can be seen in the flow chart in figure 4.1.

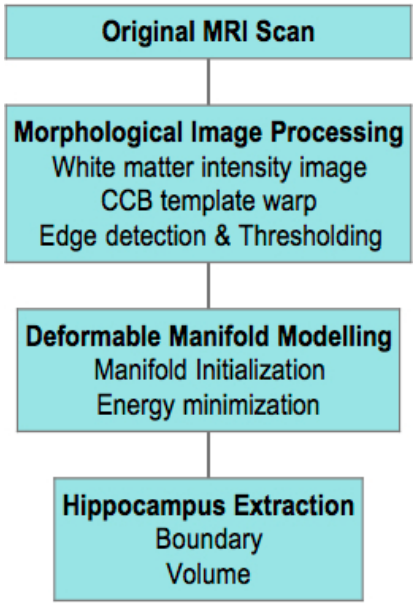

Figure 4.1: A flow chart representing the main processes of the methodology. Each section contains a collection of functions and algorithms that are all used to create a correct result. This makes the methodology a hybrid algorithm.

The first part is entitled *Morphological Image Processing*, and this consists of standard morphological image processing techniques that must be applied to the input image in order to generate brain maps that will be used in the second main processing step. These techniques are warping, thresholding, white matter ridge detection and edge detection. This first processing step is discussed in further detail in the next section of this chapter.

The second processing step is entitled *Deformable Manifold Modelling*, and it is through this step that the hippocampus is located and extracted. This is split into two functions. First, the hippocampi must be located and an initial manifold created close to the hippocampi seeds. This involves calculating the centroid positions for each

hippocampus in each slice. After this step is complete, the manifold is initialized and the second part can be started. This part performs the boundary extraction where deformable modelling is run to allow the initial manifold to locate the hippocampal boundary through energy minimization. This design is seen in figure 4.2

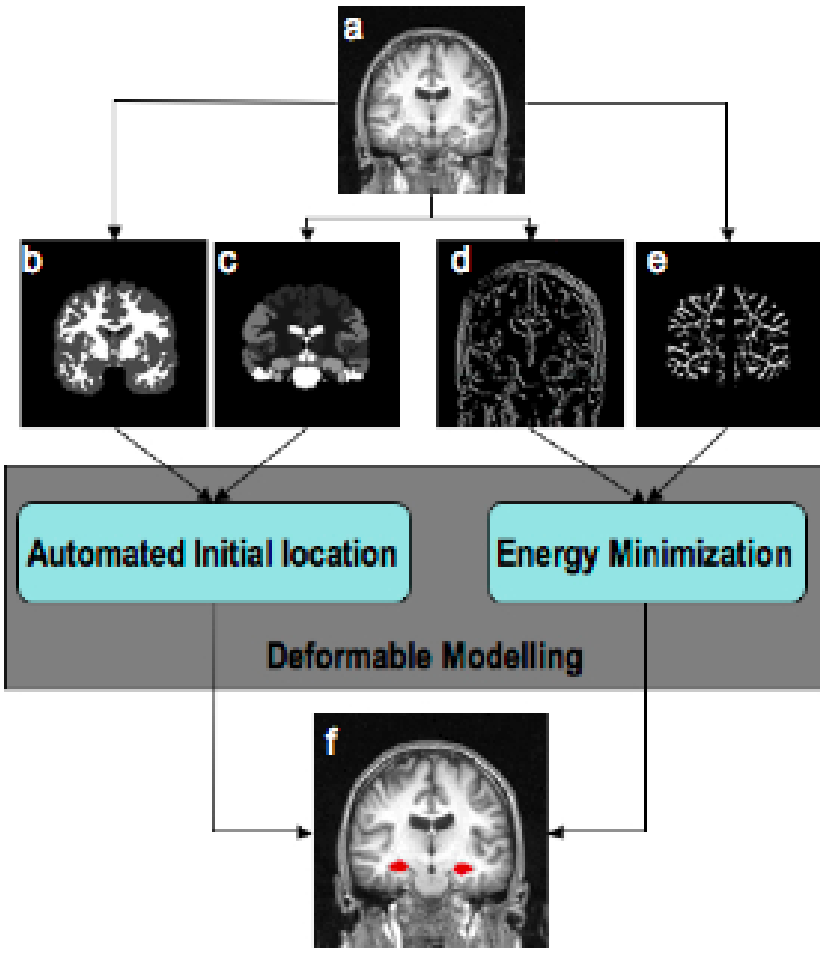

Figure 4.2: A graphical representation of the input required at each stage of the methodology. (a) is the original MRI scan, (b) is the threshold map, (c) is the warp map, (d) is the edge map , (e) is the sulcal ridge map and (f) is the final resultant map with the segmented hippocampi represented in red.

Finally, the manifold is corrected for inconsistencies through the slices using fuzzy inference. Algorithm 6 shows the Automated Hippocampus Location and Extraction (AHLE) process.

Algorithm 6 The Automated-HLE algorithm

For every scan in cohort

1. Perform Image processing functions
   a. Generate threshold map
   b. Generate warp scan
   c. Generate edge detection map
   d. Generate white matter ridge map
2. For each slice in scan
   a. Locate centre hippocampus seeds
   b. Create initial manifolds
   c. Deform manifolds
   d. Correct using fuzzy inference
   e. Calculate slice volumes
3. Calculate Hippocampal volumes
4. Output the traces and volume data

4.2 Morphological Image Processing

The first aspect of the methodology is to create image maps from the original input scan. These maps will be used in different aspects of the location and extraction processing in the second phase of the methodology. Four types of image processing functions are performed. These methods and functions are all discussed in detail in chapter 2 and descriptions follow shortly. In this section, focus is given to the implementation and adaptation of these methods for the purpose of the AHLE methodology. The four maps to be created are:

1) Image thresholding map

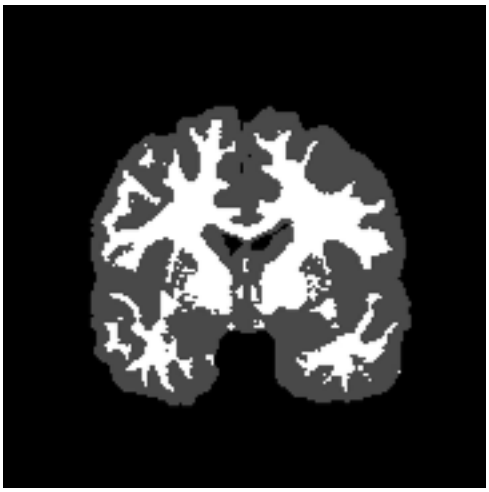

Figure 4.3: The threshold map of a subject

The map in figure 4.3 is created using the image thresholding algorithm. The version implemented for this methodology is standard as is described in chapter 2. The

function finds the average intensity value of the original scan and then splits the scan into grey or white matter voxel by voxel. The main use of this map is to gather information on definite grey matter areas that can be used later on in the methodology to deduce core hippocampal areas. This type of thresholding is commonly referred to as a set level approach, and for the core of the hippocampus this approach is a reasonable one to take.

2) *Individual atlas map*

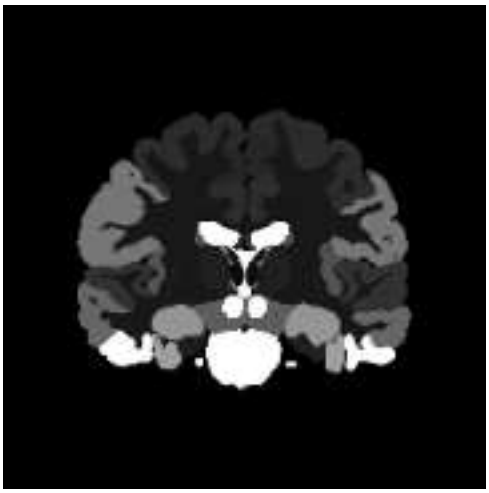

Figure4.4: An example of a subject's warp map

Figure 4.4 is produced using the warping functions provided by SPM. This atlas map is unique to every scan processed and is used to give a general idea of where the hippocampi are located throughout the 3D image of the brain. The CCB T1 image is warped onto the subject image. This warp is then used to superimpose the CCB atlas image onto the subject image.

3) *Edge detection map*

Figure 4.5: the edge detection map

The edge detection map depicted in figure 4.5 will be needed to locate edges in the original scan. The map is created using the Canny Edge Detector algorithm as explained in chapter 2, where the original scan is first smoothed with a Gaussian kernel, then the change in gradients and their directions are found, and finally non-maximal voxels are suppressed. Hysteresis is not included here as it ignores weaker edges and the hippocampus tends to produce weak edges in an edge map if it produces edges at all. This map is used to detect the upper boundary of the hippocampus.

4) *White matter ridge map*

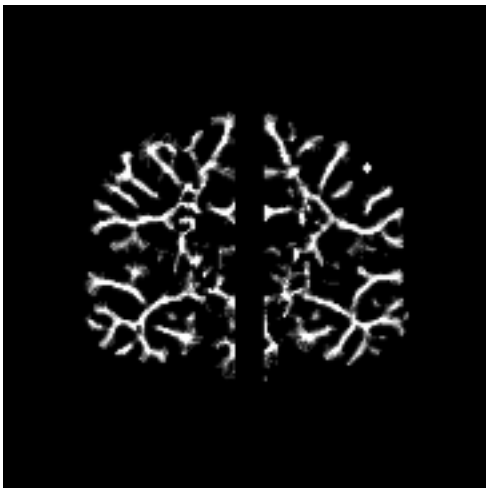

Figure 4.6: The white matter ridge map

This map is also used for edge detection, to detect the lower boundary of the hippocampus. This is because the lower boundary is marked for most of its course by a sheet of white matter. The thickness of this sheet varies in both coronal and sagittal directions. At some points this sheet thickness is reduced to a faint white trace, but is always detectable in this map, thus allowing the lower boundary of the hippocampus to be recognized.

4.3 Manifold Initialization

The manifold initialization process in itself can be split into two parts. Firstly, it is important that seed points can be found. This helps to secure a location spot on the scan to give a guide as to where the hippocampi can be found on the scan. Once seed points have been established for the hippocampus in every slice, the boundary can be initialized.

4.3.1 Finding the hippocampal seed point

By using the information from the individual atlas map and threshold map, it is possible to determine an area in the scan that could potentially contain the hippocampus. The generality of both maps means that it would not be possible to extract the boundary of the hippocampus at this stage; however, the central part of this area is certain to be contained within the hippocampus. This suggests that by calculating the centroid of each hippocampus, one would be able to have a number of seed points from which the manifold processing could then start from. These maps identify the central area of the hippocampus but do not provide sufficient estimates that will allow a reliable measure of the boundary.

Calculating Centroids

Finding the central voxel of the hippocampus means that a voxel is found that is guaranteed to be in the hippocampal area. This can then be used as a seed point for

the boundary initialization process. Algorithm 7 is the centroid algorithm. This algorithm is seeded with the CCBM warp estimate of the location of the hippocampus.

Algorithm 7 The Centroid Algorithm

1.For every coronal slice:
  a. Split image in two
  b. For each half of image:
    i. if voxel marked as hipp then
      1. increment rowcount, columncount, areacount
      2. increment row value by current r
      3. increment col value by current c
    ii. End if
    iii. divide rowval by rowcount to get avg row value for each hipp
    iv. divide colval by colcount to get avg column value for each hipp
    v. find new positions using new row and col value. this position is centroid
  c. End for
2. End for

The algorithm finds the centre voxel of each hippocampus for every coronal slice by finding the middle row and middle column of those voxels marked as possibly being in the hippocampal area. The resulting voxel is then marked as the centroid voxel.

4.3.2 Manifold Initialization

With a seed point map giving the seed point for each hippocampus in every coronal slice, it is now possible to calculate the initial position of the manifold. Before proceeding to deforming this manifold towards the boundary, one final map needs to be created to aid with the initialization and other fuzzy processes. This map is the Euclidean distance map, and is created using the centroid map.

Calculating Euclidian Distances

Having found the central voxel for each hippocampus in every coronal slice, it is now possible to create a Euclidean distance map. Every voxel's distance with the central voxel is calculated in this map. A Euclidean distance map can be used to grade voxels in a fuzzy membership procedure, the further away from the central voxel a voxel is, the less value it will have in a fuzzy membership function. The Euclidean distance map generating algorithm can be found in algorithm 8.

Algorithm 8 The Euclidean Distance Algorithm

1. For every coronal slice
   a. Split image in half vertically
   b. For each half of image:
   c. Locate hippocampal centroid
      i. For each voxel in that half
         1. Calculate col and row differences between current position and centroid
         2. using differences calulate euclidian distance using $D = \sqrt{r^2 + c^2}$
         3. store result in same position value in a different image
      ii. End for
   d. End for
2. End for

The output of this algorithm is a map of the distances of each hippocampus voxel from the centroid voxel. In keeping with the centroid finding algorithm, the Euclidean distance algorithm works using coronal slices. The algorithm first splits the image in half vertically along the inter-hemisphere fissure, the left side becoming the distance map for the left hippocampus and the right half the map for the right hippocampus. The centroid voxel in the current slice for each hippocampus is found, and then, for every voxel, the column and row differences between that voxel and the centroid voxel are calculated. Once these differences are obtained, they can be used in the Euclidean equation to create a single distance value between the two voxels. These results create the Euclidean map as can be seen in figure 4.7.

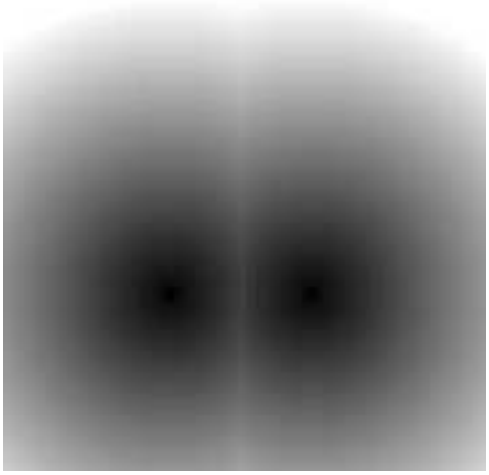

Figure 4.7: The Euclidean distance map of a subject showing the distance of each voxel in the image from the centre of each hippocampus.

Creating the Boundary

The hippocampal boundary separating the hippocampus from the amygdala is determined by the individual atlas map. This is not modified throughout the methodology. For each individual the placement of this hippocampus/amygdala boundary will be different and the methodology determines this with the individual atlas map. The posterior extent of the hippocampus for the algorithm is designated manually and is standard for all scans. The rest of the boundaries are then created using individual atlas, threshold, and distance maps. The information from these maps are used in a fuzzy inference process which grades a voxel as being in hippocampus space or not, and then the voxels with the strongest fuzzy membership are chosen and their edges become the boundary. The algorithm is found in Algorithm 9.

Algorithm 9 The Boundary Initialization Algorithm

1. For every coronal slice
   a. For every voxel in slice
      i. If voxel labelled hipp in warp map then
         1. If voxel marked as grey in threshold then
            a.If distance ¡ limit then
               i.Label voxel as hippocampus
            b. End if
         2. End if
      ii. End for
   b. End for
   c. Extract hippocampus edges
2. End for

The algorithm is a grading process. If a voxel is marked as being hippocampus in the warp map, then it is a potential hippocampal voxel. If the threshold map states that the voxel is grey matter, its grading increases, and the voxel is labelled as hippocampus if it is within a determined range of the centroid, given by the distance map. This means that the voxels that are labelled as hippocampus must fulfil three criteria (1.if the voxel is marked as in the hippocampus in the individual atlas map, 2.is a grey voxel in threshold map, and finally 3.is within a certain range of the centroid voxel), increasing the possibility that the voxel is actual hippocampus. The edges are then extracted, and with this final step, the initial hippocampal boundary is determined. This gives the methodology all the necessary components to run the manifold deformation process.

4.4 Adapting the Deformable Model

The deformable manifold process in this methodology is an adaptation of the theory that has been explained in chapter 3. This adaptation of the standard implementation is necessary in order for the manifolds to successfully deform to the correct hippocampal boundaries, due to the noisy environment that the algorithm is working in (the MRI scan), as well as the high variability of the hippocampal shape across subjects. The boundary created at initialization is now converted to the manifold that is to be deformed in this algorithm. The three key adaptations are discussed first and then the algorithm is given and explained.

4.4.1 Splitting the manifolds

One of the adaptations to the deformable manifold algorithm applied to this methodology is that of splitting the manifolds in half. This means that for the entire deformable process, the manifold representing the upper hippocampal boundary and the manifold representing the lower hippocampal boundary are considered and processed separately. It is a necessary adaptation as the hippocampus can be highly variable from scan to scan, and considering its boundary in this way helps to overcome some of this variability. In addition, as will be discussed shortly in the external energy of the boundary manifolds section, different external energies are required for the different type of boundary being considered (the upper boundary of

the hippocampus and the lower boundary of the hippocampus), and having separate boundary types. Once the manifold procedure is completed and corrected, the boundaries are linked together again using a line drawing algorithm. Upper and lower manifold examples can be seen in figure 4.8:

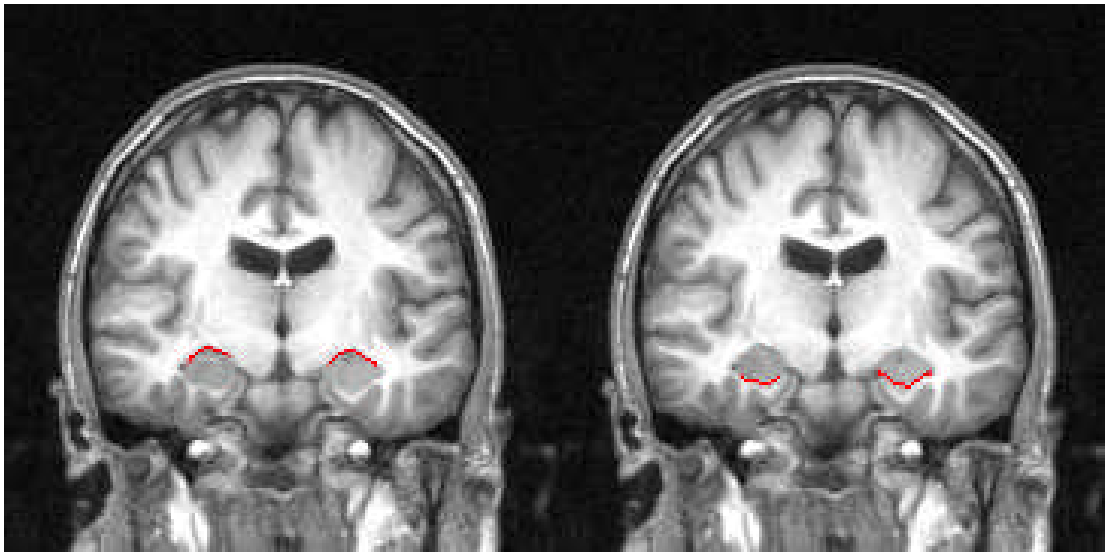

Figure 4.8: the upper (left) and lower (right) manifolds in coronal view

4.4.2 Deformation process

The deformation process for the methodology has also been adapted and is unique for this procedure. A seed slice is designated that is mid way between the amygdala cleave and the posterior extent of the hippocampus, more or less in the middle of the length of the hippocampus. This is a constant slice for all scans and is standard to the methodology. The deformation of the hippocampal boundaries starts from this slice,

and is chosen as is has a strong presentation of the hippocampal boundaries. This is the case for all scans and is therefore standard across all subjects and the middle hippocampus slice is always chosen, since it is probabilistically the slice with the clearest representation of the hippocampus boundaries. The deformation of the hippocampal boundaries begins on this slice and then moves forwards and backwards through the slices that neighbour it, until the whole hippocampus boundary has been deformed as required. This process is explained graphically in figure 4.9:

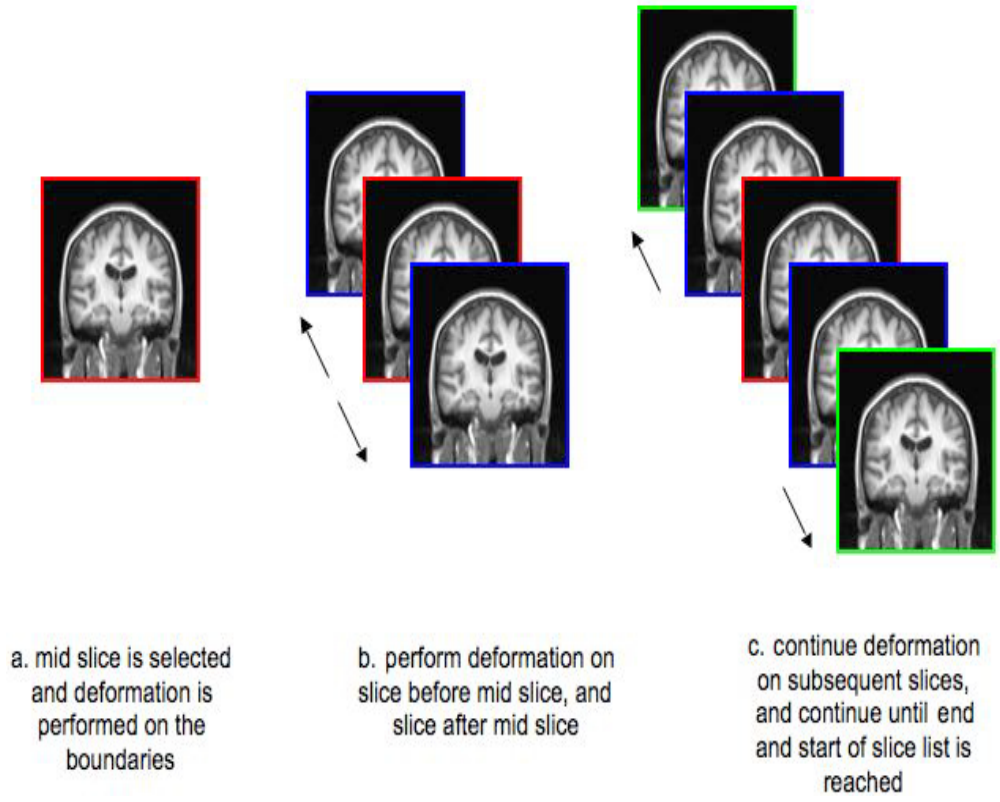

Figure 4.9: An illustration of the deformation process

Processing the slices in this way to deform the boundaries means that it is possible to pass on information of the neighbouring slices to the current slice, so that the

resulting boundaries can be as continuous as possible along the length of the hippocampus.

4.4.3 External energy of the boundary manifolds

The completion of the hippocampal extraction process is achieved with the final adaptation of the deformable manifold processing in which the external energy of the image is calculated for the different manifolds. The upper boundary of the hippocampus is more clearly defined than the lower, and the edge detection map is enough to be able to calculate the external energy when minimizing the energy functional. The lower boundary, however, is much more ill defined and hence requires additional information to calculate the external energy. In this case, two maps are used, the edge detection map (like the upper manifold) and the white matter ridge map.

4.5 The Algorithm

Algorithm 10 describes the main loops of the deformation process. The actual deformable manifold algorithm that is used to deform the manifolds is the algorithm explained in algorithm 5.

Algorithm 10 The Main Loop Algorithm

1.For centre slice:

a. For upper manifold

i. Perform deformation using algorithm 5

ii. Use edge map for external energy

b. End for

c. Repeat loop (a) for lower manifold

3. Repeat from centre slice to 1st slice

a. For upper manifold

i. Use information of previous slice manifold position

ii. Perform deformation using algorithm 5

iii.Use edge map for external energy

b. End for

c. For lower manifold

i. Use information of previous slice manifold position

ii. Perform deformation using algorithm 5

iii.Use edge map for external energy

d. End for

4. End repeat 5. Repeat step 3 from centre slice to last slice

6. End repeat

There are three main steps that are all performed in coronal view, the deformation process of the manifolds for the centre slice, a loop to deform the manifolds of the slices before the centre slice in succession, and a loop to deform the manifolds of the slices after the centre slice, also performed in succession. As explained earlier, upper and lower manifolds are processed separately, and different maps are used for the calculation of the external energy of the two manifolds. The edge map is used to calculate the external energy for the upper manifold, whilst both edge and ridge maps are required to calculate the external energy of the lower manifold correctly. The resulting output of this algorithm is two manifolds that have deformed to the upper and lower boundaries of the hippocampus. These boundaries are then corrected in sagittal view for any anomalies that may have occurred during processing using fuzzy inference. With these components in place, the processing phase that connects the upper and lower manifolds can be run.

4.6 The Boundary Correction Algorithm

Once the manifolds have located the hippocampal boundaries, one more function is left to complete the process. In order to provide continuity of the slices, a correction algorithm is run in sagittal view, correcting for any anomalies that may have occurred whilst the processing was performed in coronal view. In this way, the methodology mimics the process that a hand tracer would take to trace the hippocampus manually, needing information from both coronal and sagittal views in order to produce a correct manual trace of the hippocampus. The algorithm is seen in Algorithm 11:

Algorithm 11 The Boundary Correction Algorithm

1.For every sagittal slice:

  a. For upper manifold

    i. For each upper manifold voxel

      1. Perform fuzzy membership on neighbour voxels

      2. Adjust manifold position according to fuzzy membership

    ii. End for

  b. End for

  c. For lower manifold

    i. For each lower manifold voxel

      1. Perform fuzzy membership on neighbour voxels

      2. Adjust manifold position according to fuzzy membership

    ii. End for

  d. End for

2. End for

3. For every coronal slice

  a. Link start of manifolds

  b. Link end of manifolds

4. End for

This algorithm applies fuzzy inference to correct any anomalies of the hippocampal boundaries in sagittal view. Correction on the boundaries is performed on each manifold separately for each sagittal slice. In both cases, for each manifold voxel, the vertical neighbours are considered for fuzzy membership. Membership is decided using the neighbourhood manifold voxel information, the edge map in the case of the upper manifold and the sulcal ridge map for the lower manifold. Different maps are

used for the different manifolds since each map provides better information for its respective manifold. This means that the edge map is more effective at determining the upper boundary than the lower boundary, and the sulcal ridge map provides increased reliability in detecting the lower boundary of the hippocampus and it is this information instead of the edge map data that is used to detect the lower boundary. The manifold label is then moved to the voxel with the strongest fuzzy membership, if the value is stronger than that of the current voxel. This allows the sagittal information to be considered and added to the solution if needed.

Once this has been completed, the final stage of the algorithm and of the methodology is to link the two manifolds together to create one complete manifold. This is done in coronal view using a line drawing algorithm to join the starting points of the two manifolds and another line is drawn to join the two ends of the manifolds. The line drawing algorithm used for this purpose is the standard Bresenham (Bresenham 1965) line drawing algorithm (algorithms 12 and 13). This algorithm is the standard line drawing algorithm that is used in computer graphics, and therefore the standard algorithm to use in this kind of task.

Algorithm 12 The Bresenham Line Drawing Algorithm - Initialization

1.Calculate $deltax$ and $deltay$

2. Initialize line at starting point voxel

3. If end x larger than start x then x values are increasing

   a. $xinc1 = 1$ and $xinc2 = 1$

4. Else x values are decreasing

   a. $xinc1 = -1$ and $xinc2 = -1$

5. If end y larger than start y then y values are increasing

   a. $yinc1 = 1$ and $yinc2 = 1$

6. Else y values are decreasing

   a. $yinc = -1$ and $yinc = -1$

7. If $deltax >= deltay$ then there is at least 1 x value for every y value

   a.$xinc1 = 0$ (do not change x when $numerator >= denominator$)

   b. $yinc2 = 0$ (do not change y for every iteration)

   c. $denominator = deltax$

   d. $numerator = deltax/2$

   e. $toadd = deltay$

   f. $numpixels = deltax$ (since there are more x values)

8. Else

   a. $xinc2 = 0$ (do not change x for every iteration)

   b. $yinc1 = 0$ (do not change y when $numerator >= denominator$)

   c. $denominator = deltay$

   d. $numerator = deltay/2$

   e. $toadd = deltax$

   f. $numpixels = deltay$ (since there are more y values)

When drawing a line between two points on a computer screen, the line has to be approximated. The Bresenham algorithm is able to select the pixels required to

approximate the line correctly using integer math, making it an efficient line drawing process. The first two parts of the algorithm, from step 1 to step 8, certain variables are set. Step 9 in algorithm 13 is the actual loop where the line is drawn on the image.

Algorithm 13 The Bresenham Line Drawing Algorithm - Main Loop

9. For the number of pixels in *numpixels*
   a. mark current pixel as line
   b. increase *numerator* by *toadd* value
   c. if *numerator* >= *denominator* then
      i. calculate the new *numerator* (subtract *denominator*)
      ii. increment x by $xinc1$
      iii. increment y by $yinc1$
   d. increment x by $xinc2$
   e. increment y by $yinc2$
10. End for

Deltax and deltay values are determined by subtracting the end point x and y values from the starting point x and y values. The first voxel in the line is the starting point voxel. Next, it is important to know if the line's values are increasing or decreasing. This is done by comparing the starting x and y values to the end x and y values. If the end x is greater than the start x then x increases, and x decreases if the starting x value is greater. The rest of the variables are set according to whether deltax or deltay is larger, as this determines the line's length.

The main drawing loop of this algorithm beginning at step 10 starts by marking the current voxel as part of the line. It then needs to decide on whether to move to the voxel on the right, or to move to the voxel on the up-right diagonal of the current voxel. The decision is made by looking at the gradient value required and on the variables that were set prior to the loop initializing as explained earlier. If the value is less then half, then the right voxel is chosen, else the up-right diagonal voxel is chosen. This continues until the target voxel, the end voxel is reached, and once this has happened, the line has been formed.

The whole process of the AHLE methodology takes approximately two minutes per scan. Comparing it with the couple of hours it takes for manual segmentation of one hippocampus (therefore one scan would take around four hours), one can acknowledge that the speed of the process is an advantage of this methodology.

4.7 Conclusion

This chapter brings together the image processing and artificial intelligence techniques discussed in chapters 2 and 3 to reveal the methodology used to locate and extract hippocampal boundaries in 3D MRI scans. This hybrid algorithm uses brain maps and fuzzy inference to locate the hippocampal areas and create initial hippocampal boundaries, and then uses the brain maps to deform the boundaries until the correct boundaries are found. Finally, the boundaries are corrected for any anomalies through fuzzy inference in a sagittal view. The ability of this methodology to extract information from the scans in both coronal and sagittal views is a necessary technique in order to successfully locate and trace hippocampal boundaries, and as such, mimics the procedure a hand tracer takes in tracing the boundaries manually. Another aspect that mimics the hand tracer's ability of manual tracing hippocampal boundaries is that of creating an initial boundary around the hippocampus and then adjusting it until the tracer is satisfied that the trace represents the true hippocampal boundary. This technique is also successfully adopted by this hybrid methodology.

Results of the methodology are reported in chapters 5 and 6. Chapter 5 reports and discusses the reliability of the technique when compared to the results produced by a manual tracer. Chapter 6 reports the results produced when the methodology is applied to a large cohort, and compares these results to the ones published using Voxel Based Morphometry on the same cohort.

Chapter 5 - Reliability Testing

In order to assess the quality of the hippocampal traces that the methodology produces, the traces need to be compared to the gold standard of hippocampal tracing, manual tracing. An explanation of the scans used, the methods performed to compare automated tracing to manual tracing and the results and conclusions are given in this chapter.

5.1 Methods

Twenty subject scans were used for this testing, from the bipolar subject group. Details of the cohort are given in the next chapter. All scans were chosen blind to diagnosis, age and gender.

5.1.1 Manual tracing

The hippocampi were manually traced on coronal brain scan slices using the ANALYZE software version 4. The tracing was performed by one individual (HB) who was blind to diagnosis, age and gender, and followed a standardized protocol. The hippocampus was defined anatomically as the main hippocampal region, referring to the Cornu Ammonis sections, the Dentate Gyrus and the Subiculum. The hippocampus head was separated from the amygdala by looking for the alveus. This can be seen looking at the hippocampus from a sagittal view and looks like a narrow band of lighter grey intensity values separating the amygdala from the hippocampus. Consultation was provided by Dr. Heather Whalley and Dr. Andrew Stanfield. This procedure of manual tracing was performed on all twenty scans.

5.1.2 Automated tracing

Automated hippocampal tracing and volume extraction was performed on the same twenty scans by the automated hippocampal location and extraction methodology described in chapter 4. In brief, for every scan, the algorithm creates four brain maps, a warp map, a white matter ridge map, an edge detection map and a threshold map. The threshold and warp maps are used to locate central hippocampal seeds and create initial manifolds. The edge detection and white matter ridge maps are used to deform the manifold. Once the manifold deformation reaches an equilibrium state, the algorithm moves on to the next step, correcting the manifolds using fuzzy inference in sagittal view. Finally, the hippocampal volumes are calculated and the traces and volume data are output.

5.1.3 Comparison methodology

To evaluate the algorithm's performance in segmenting the hippocampi from the MRI brain scans, the Intraclass Correlation Coefficient (ICC) is calculated. This coefficient measures the consistency or correlation between two members of the same group. In this case, the group is the brain scan and the two members are the manual and automated tracing output. The SPSS software package is used to derive the ICC results. The implementation of the ICC variable in the reliability section of SPSS is aimed at estimating the inter-rater reliability, between manual and auto tracings.

5.2 Results

Figure 5.1 shows some of the hippocampal volume result slices for a control subject scan. Figures 5.2 and 5.3 depict the resulting slices for a schizophrenia subject slice and a bipolar subject slice respectively.

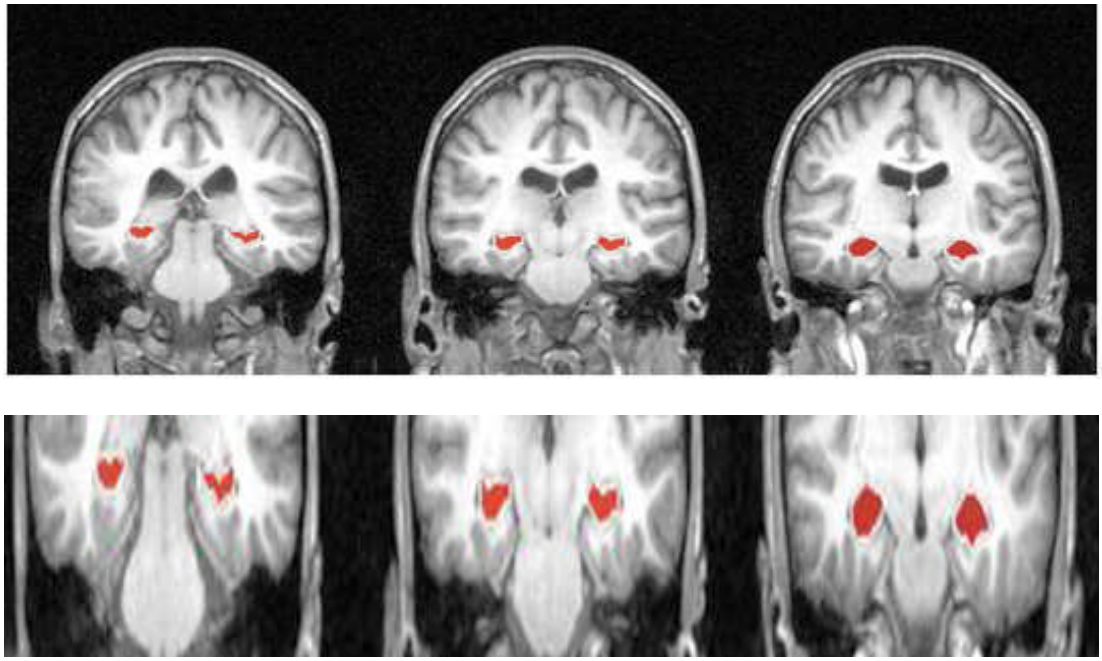

Figure 5.1: Three coronal slices from a control subject scan. The hippocampus is delineated in red. Hippocampus outline is delineated in white. The lower image is a magnification of the upper image.

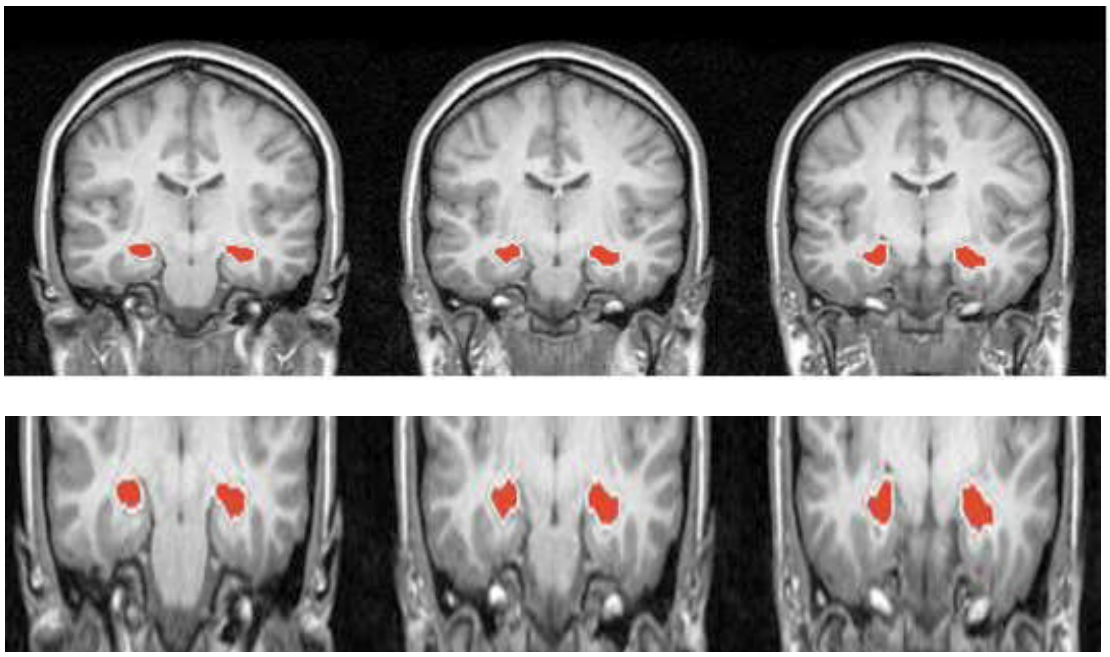

Figure 5.2: Three coronal slices from a schizophrenia subject scan. The hippocampus is delineated in red. Hippocampus outline is delineated in white. The lower image is a magnification of the upper image.

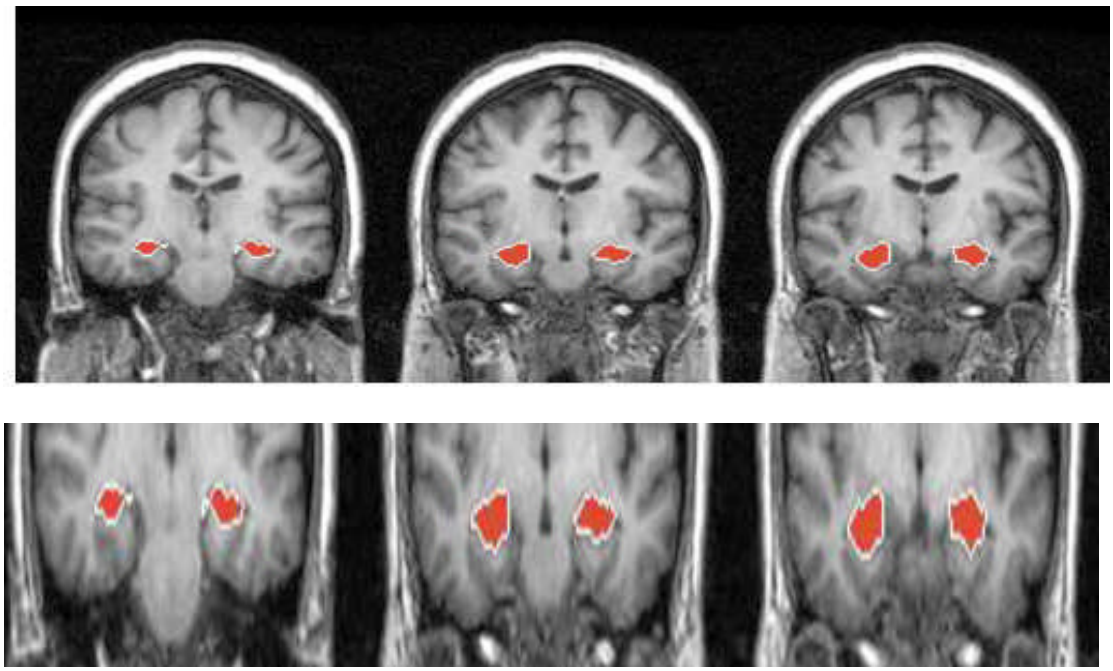

Figure 5.3: Three coronal slices from a bipolar subject scan. The hippocampus is delineated in red. Hippocampus outline is delineated in white. The lower image is a magnification of the upper image.

Figure 5.4 depicts a sequence of coronal slices of a healthy subject with the hippocampus delineated by the extraction algorithm and highlighted to clarify the hippocampus location in the scan.

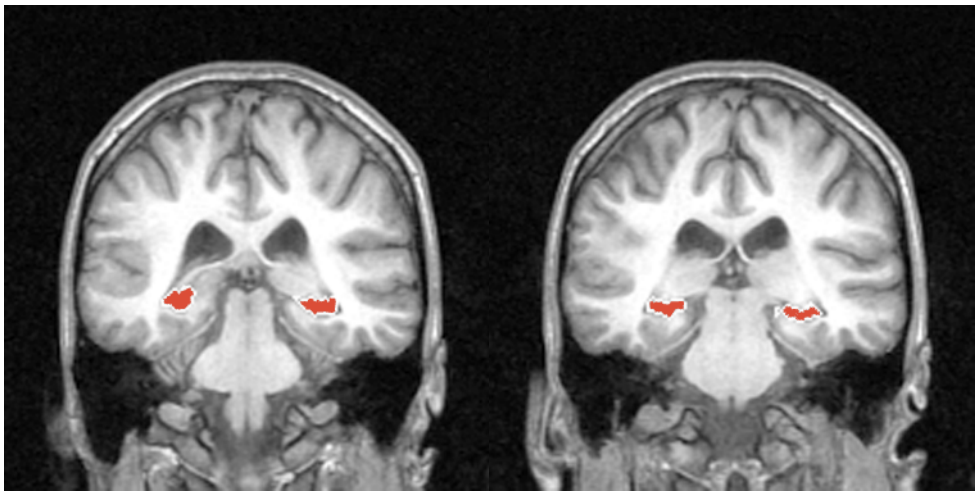

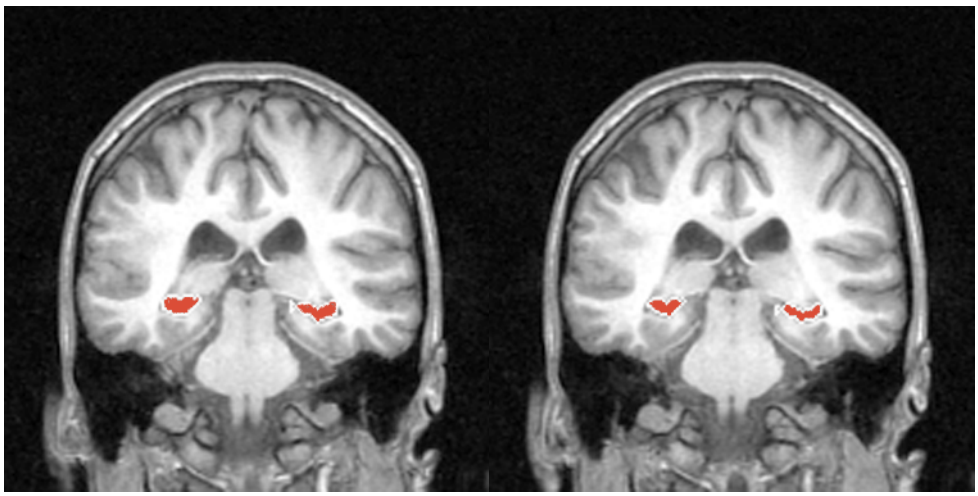

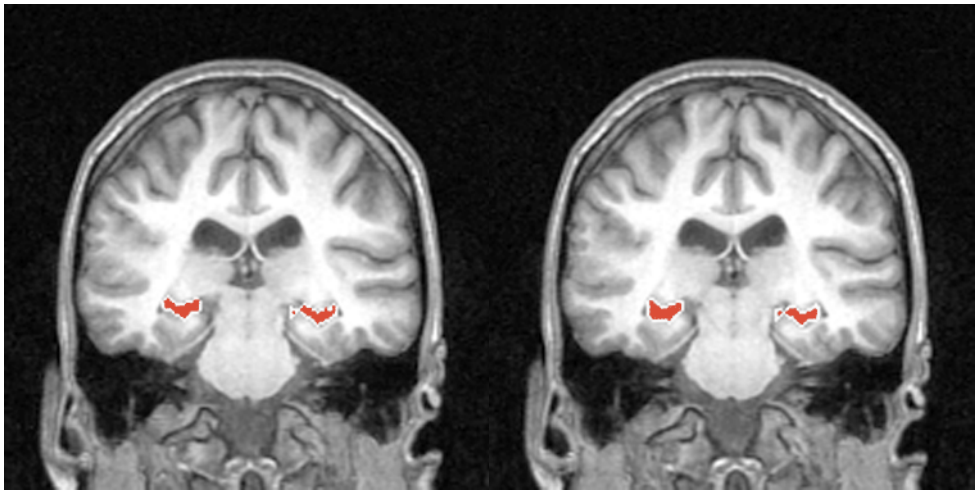

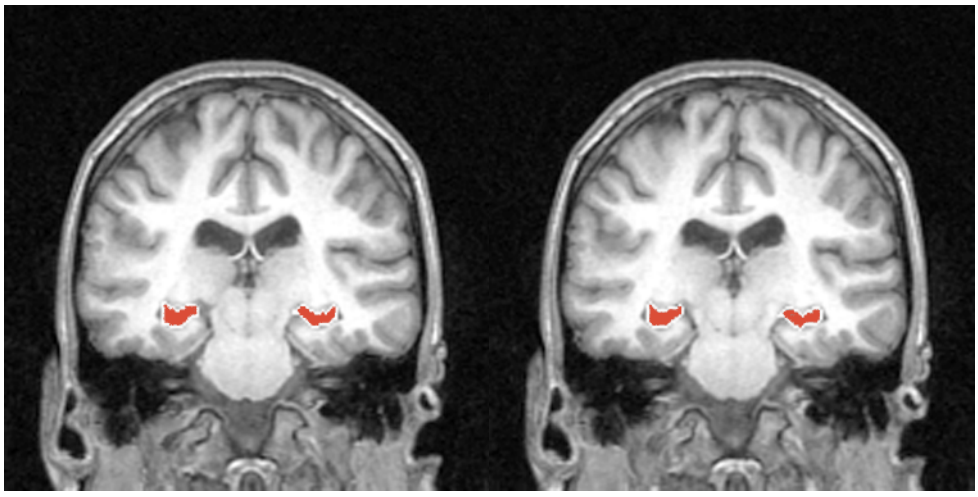

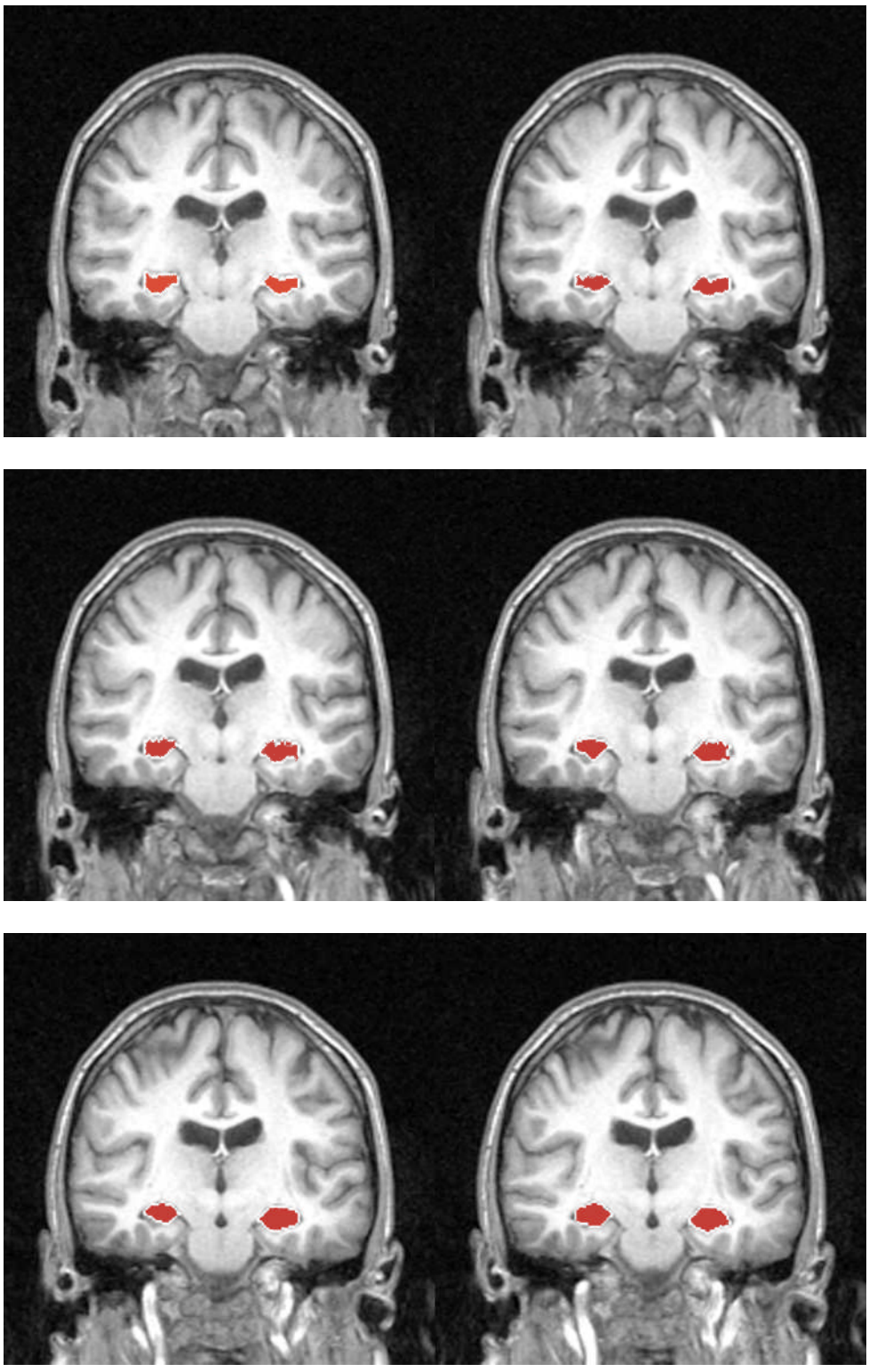

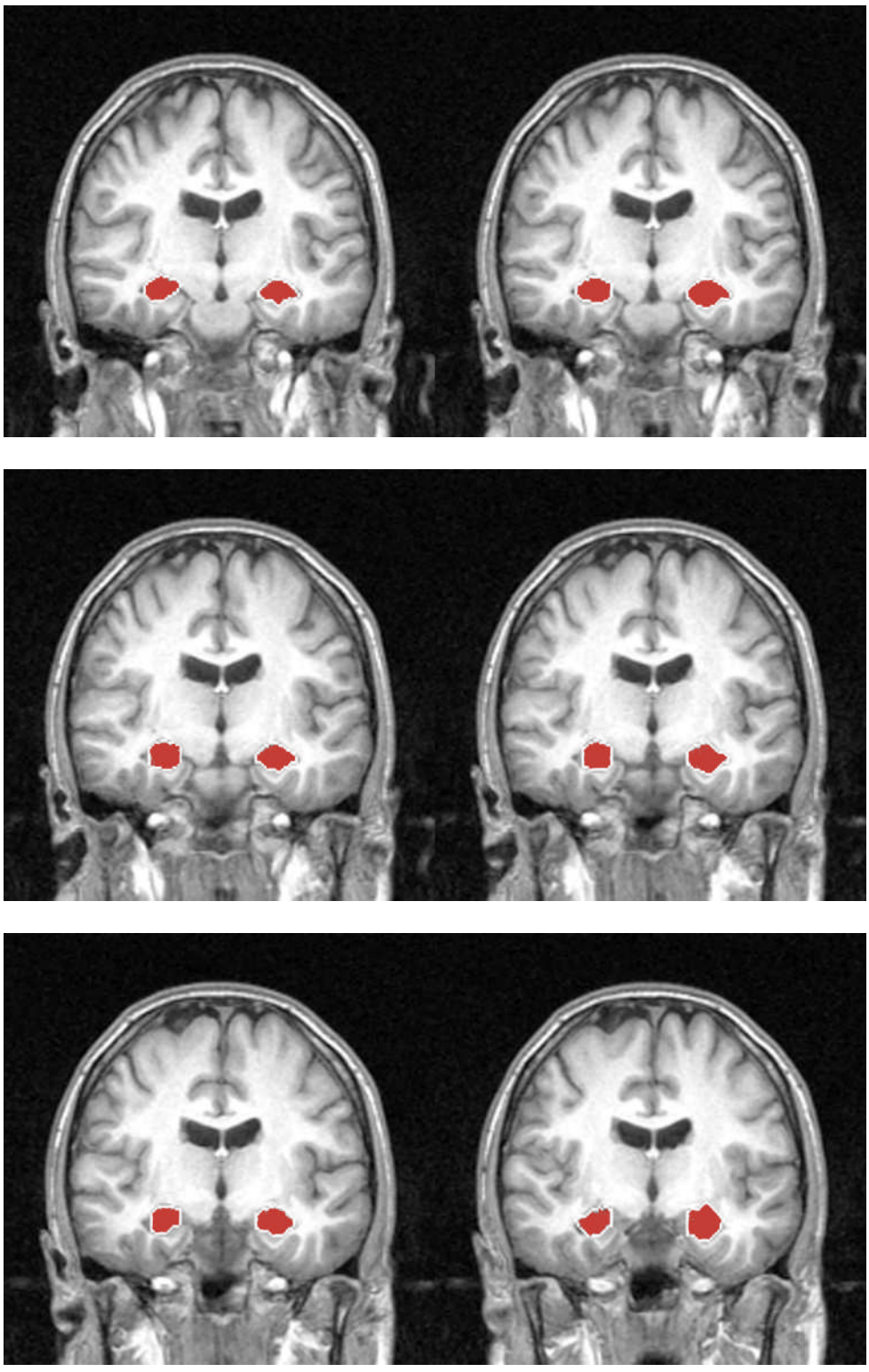

Figure 5.4: Coronal slices of a control subject with the hippocampus traced automatically

The Intraclass Correlation Coefficient (ICC) value for right hippocampal volumes of automated against manual segmentation is 0.81, and the left hippocampal volume ICC value of automated against manual segmentation is 0.73. Figure 5.6 and figure 5.7 show the correlations graph of left manual vs. automated hippocampal extraction volumes and right manual vs. automated hippocampal extraction volumes respectively.

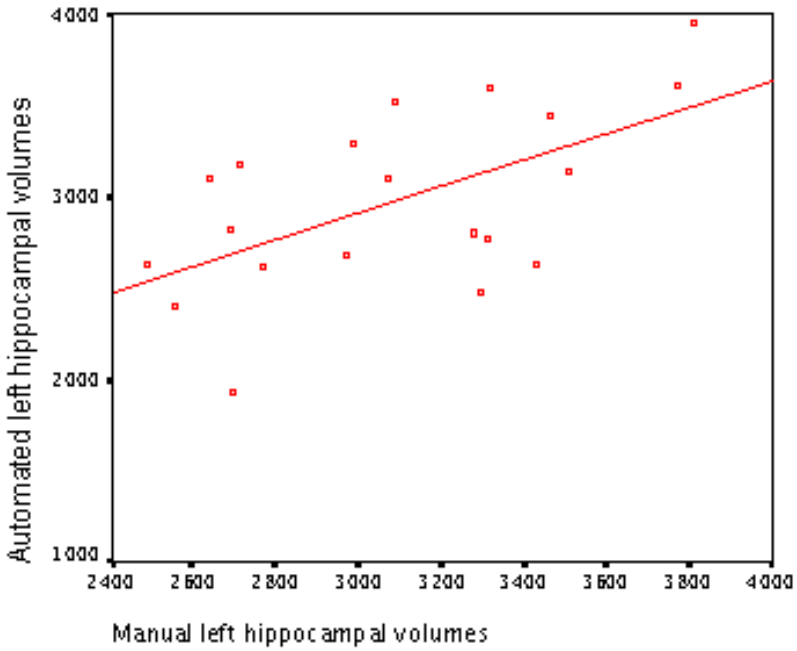

Figure 5.6: Left hippocampal correlation graph of manual vs. automated volume extractions

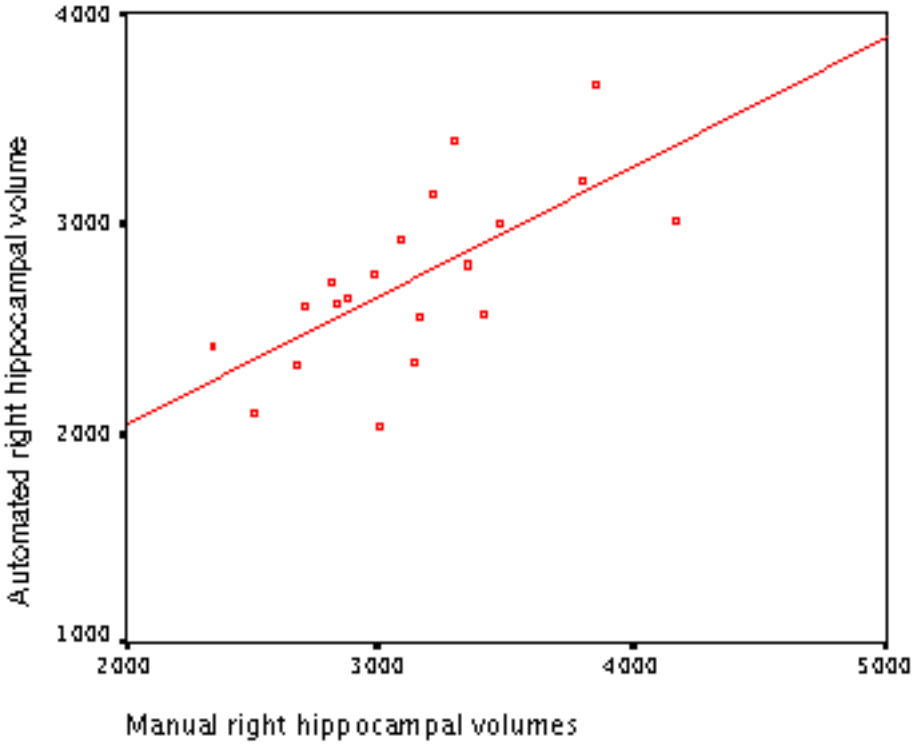

Figure 5.7: Right hippocampal correlation graph of manual vs. automated volume extractions

Comparing this methodology to other automated or semi-automated hippocampus segmentation extraction techniques. In this case, volume overlap error is taken into account (most of the time). The overlap error rate compares the overlap between the two segmentations (manual and automated) and the percentage result reflects the error rate between the overlap. These values generally range from 6% to 15%. This methodology gives a volume overlap error rate of 15%, which falls at the higher error percentage end of the scale.

5.3 Conclusion

Reliability results reported in hippocampal manual segmentation studies usually give ICC values between two raters. Frazier et al. (Frazier, Hodge et al. 2008) report ICC values of 0.96 and 0.92 for left and right hippocampal segmentations respectively, based on ten scans. Strasser et al. (Strasser, Lilyestrom et al. 2005) report an ICC value of 0.97 and Tisserand et al. (Tisserand, Visser et al. 2000) report that of 0.91. Pantel et al. (Pantel, O'Leary et al. 2000) report a value of 0.83 and 0.86 for the left hippocampus and 0.76 and 0.73 for the right hippocampus. These ICC values were based on comparing raters 2 and 3 from the gold standard tracer 1. The measures of these three raters were derived from hippocampal tracings of 15 scans. Pruessner et al. (Pruessner, Li et al. 2000) used five subjects to calculate their ICC values, with a result of 0.94 for the right and 0.86 for the left hippocampus. Finally, for manual segmentation results, Whalley et al (Whalley and Wardlaw 2001) report an ICC value of 0.82 for the amygdalo-hippocampal complex, whilst Barnes et al (Barnes, Whitwell et al. 2006) report an ICC result of 0.98 from one rater segmenting 20 scans twice. For a brain shape with a high surface area to volume such as the hippocampus, it must be noted that an ICC value of 0.98 is exceptionally high.

Reliability results from automated segmentation techniques are more vague and variable when relating the automated results to manual results, using voxel overlap and volume difference calculations rather than ICC values. Fischl et al (Fischl, Salat et al. 2002) report volume differences of left and right hippocampi when comparing their automated technique to manual labelling as being indistinguishable. However,

they do not report ICC values, the standard reliability measure for these methods. They do state that they use five expert tracers to manually label one scan for their manual labelling, and report a volume difference of 10% when comparing their automated segmentation results to manual segmentation. Chupin et al (Chupin, Hammers et al. 2007) state that their automated segmentation generally slightly over-estimated the hippocampal volume in comparison to manual segmentation and that the main differences were found in the tail of the hippocampus. They report a volume difference of 7% when comparing their automated process to the manual segmentation in 16 healthy control scans, and a volume difference of 9% for six Alzheimer patient scans. Zhou and Rajapakse (Zhou and Rajapakse 2005) report volume differences of 11% over 17 subjects. Our ICC results of 0.73 and 0.81 for left and right hippocampi respectively show that the technique is comparable to the gold standard of manual tracing.

A limitation of this reliability testing is that there is no intra-rater or inter-rater reliability testing for manual segmentations. This would have made the analysis more reliable, but was not possible due to time limitations. It would also have been beneficial to have the demographics of the 20 scans used for comparing the manual segmentation to the automated segmentation. Unfortunately this data has been lost.

This chapter provides evidence of the validity and quality of the hippocampal traces produced by the automated hippocampal location and extraction methodology by comparing the results given by this method with those of manual tracing, the gold standard. Examples of output slices from the automated procedure are also given in

this chapter, with slices taken from three subject groups, schizophrenia, bipolar and control. The ICC results given in the results section of this chapter show that there is correlation between the two methodologies, and therefore the automated process can be considered to be validated against the gold standard.

Chapter 6 - Performance of the Method on a Cohort

Chapter 5 provides results of the quality of the performance of the methodology in comparison to manual segmentation. In this chapter we apply the methodology to a cohort of 182 brain scans and 7 subject groups including schizophrenia and bipolar I patients. The results show sex and group differences and these are presented and discussed in this chapter.

6.1 The Cohort and Image Acquisition

Detailed information regarding recruitment procedures and patient characteristics of the cohort can be found in McIntosh et al (Mcintosh, Job et al. 2004) but an overview of the cohort groups is given here. Hospital notes were used to identify patients with a clinical diagnosis of bipolar disorder or schizophrenia. If patients had at least one first or second-degree family member with schizophrenia or bipolar disorder, they were then asked if any of their well relatives would take part in the study. Control subjects were recruited through social contacts and non-relatives of patients.

Subjects were recruited into one of the following seven groups:

1. *Controls* – People with no personal or family history of bipolar disorder or schizophrenia.
2. *Schizophrenic subjects from schizophrenic families* – Patients with schizophrenia who had at least one close relative with schizophrenia.
3. *Unaffected subjects from schizophrenic families* – Healthy subjects with at least two close relatives with schizophrenia.
4. *Bipolar subjects from bipolar families* – Patients with bipolar I disorder with at least one close relative with bipolar disorder.
5. *Unaffected subjects from bipolar families* – Healthy subjects with at least two close relatives with bipolar disorder.
6. *Bipolar subjects from mixed families* – Patients with bipolar I disorder with at least one close relative with schizophrenia.

7. *Unaffected subjects from mixed families* – Healthy subjects with at least one close relative with bipolar disorder and one close relative with schizophrenia.

Group Number	Group Name	N	Mean Age	Male
1	Control	49	35	23
2	SCZ from SCZ family	26	37	13
3	UA from SCZ family	24	39	11
4	BPD from BPD family	25	41	14
5	UA from BPD family	22	35	9
6	BPD from MIX family	19	40	7
7	UA from MIX family	26	34	14

Table 6.1: Characteristics of subject groups where SCZ = schizophrenia, BPD = Bipolar disorder, MIX = mixed family history, UA = unaffected.

Details of image acquisition are also given in McIntosh et al (Mcintosh, Job et al. 2004). Each subject was scanned on a 1.5 T GE MRI scanner (GE Medical Systems, Milwaukee, Wisconsin). Midline sagittal localization was followed by two further sequences to image the whole brain. The first sequence was a transverse spin-echo scan, which acquired both T2- and proton density–weighted images of the brain. A consultant in neuroradiology clinically reported these images. The third and final sequence was a coronal gradient echo sequence with magnetization preparation and produced 128 coronal high-resolution T1-weighted images, which were used for structural image analysis (time of inversion [TI] 600 msec, echo time 3.4 msec, flip

angle 15°s, field of view 22, slice thickness 1.7 mm, matrix 256 X 192).

Images were converted into ANALYZE 3-D file format for further processing. Each image was then viewed with SPM99 (Wellcome Department of Imaging Neuroscience, London, United Kingdom). Images were inspected for orientation and movement artifact, and the origin was set at the anterior commissure. Images were then transferred to a computer running SPM99 on the Red Hat Linux 8.0 platform.

In total 191 scans were available for image analysis, of which 70 were patients, 72 unaffected close family members and 49 control subjects.

6.2 Methods

6.2.1 Automatic Segmentation of Hippocampi

The automated hippocampal location and extraction methodology described in chapter 4 was used on each scan. In brief, for every scan, the algorithm creates four brain maps, a warp map, a white matter ridge map, an edge detection map and a threshold map. The threshold and warp maps are used to locate central hippocampal seeds and create initial manifolds. The edge detection and white matter ridge maps are used to deform the manifold. Once the manifold deformation reaches an equilibrium state, the algorithm moves on to the next step, correcting the manifolds using fuzzy inference in sagittal view. Finally, the hippocampal volumes are calculated and the traces and volume data are output.

6.2.2 Statistical Analysis

The data were analysed using the Statistical Program for Social Science (SPSS Inc., Chicago, Illinois) version 11.0 for Mac package. Group comparisons were calculated using a univariate general linear model. Sex, age and total hemisphere volumes were used as covariates to the statistical process. Bivariate correlations were calculated in order to look for correlations of left and right hippocampal volumes with age, sex, and cohort group.

6.3 Results

Automated hippocampal segmentation and volume extraction was performed on 182 of the 191 scans available. Ten scans were removed due to movement and artefacts in the scanning.

6.3.1 Group Comparisons

Using the automated hippocampal methodology, no differences were found between any of the controls, patient groups or relative groups, except for unaffected subjects from schizophrenic families and bipolar subjects from bipolar families, in the left hippocampal volume where there was a significance of $p<0.05$.

6.3.2 Correlations

The correlations table is represented in table 6.3. Using the volumes of 182 hippocampi shows a correlation between left and right hippocampus (correlation is significant at the 0.01 level). This shows that the volumes of both hippocampi are related to each other and is a measure of validation of the method.

Correlations

		volright	volleft	age
volright	Pearson Correlation	1	.546**	-.149*
	Sig. (2-tailed)		.000	.045
	N	182	182	182
volleft	Pearson Correlation	.546**	1	-.166*
	Sig. (2-tailed)	.000		.025
	N	182	182	182
age	Pearson Correlation	-.149*	-.166*	1
	Sig. (2-tailed)	.045	.025	
	N	182	182	182

**. Correlation is significant at the 0.01 level (2-tailed).

*. Correlation is significant at the 0.05 level (2-tailed).

Table 6.4: The correlations table

Figure 6.1 shows this strong correlation through a scatter graph of right vs. left volumes for each scan.

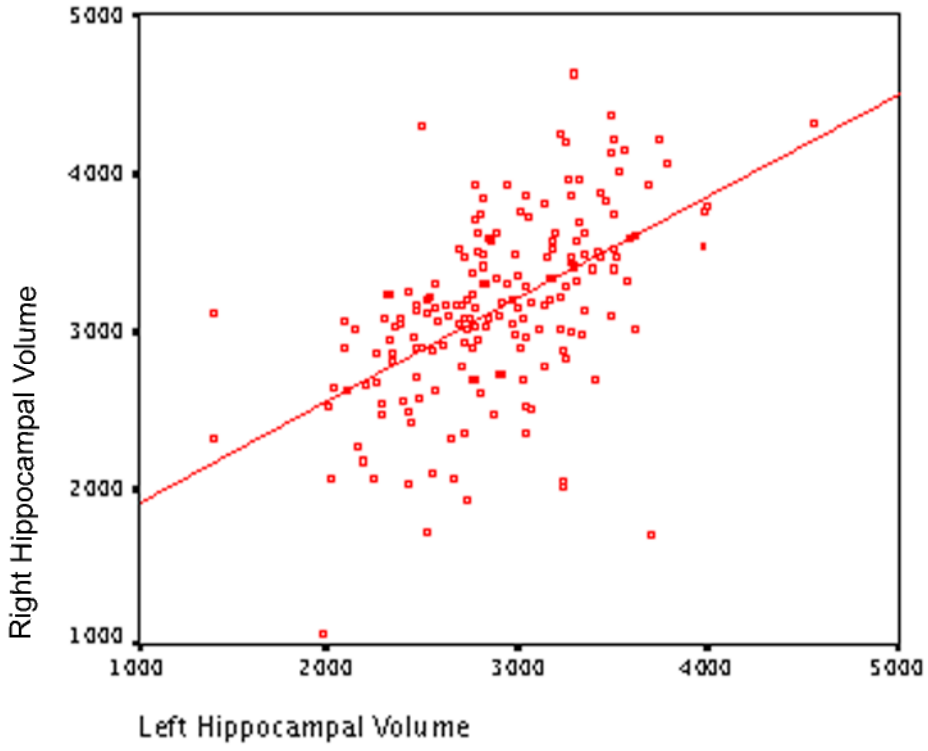

Figure 6.1: Right and left hippocampal volumes scatter graph shows strong correlation between the two volumes. Pearson correlation r = 0.546

A significant negative correlation of each hippocampus (left and right) is also observed with age (correlation is significant to the 0.05 level), and this can be seen in figures 6.2 and 6.3 for left and right hippocampal volumes respectively.

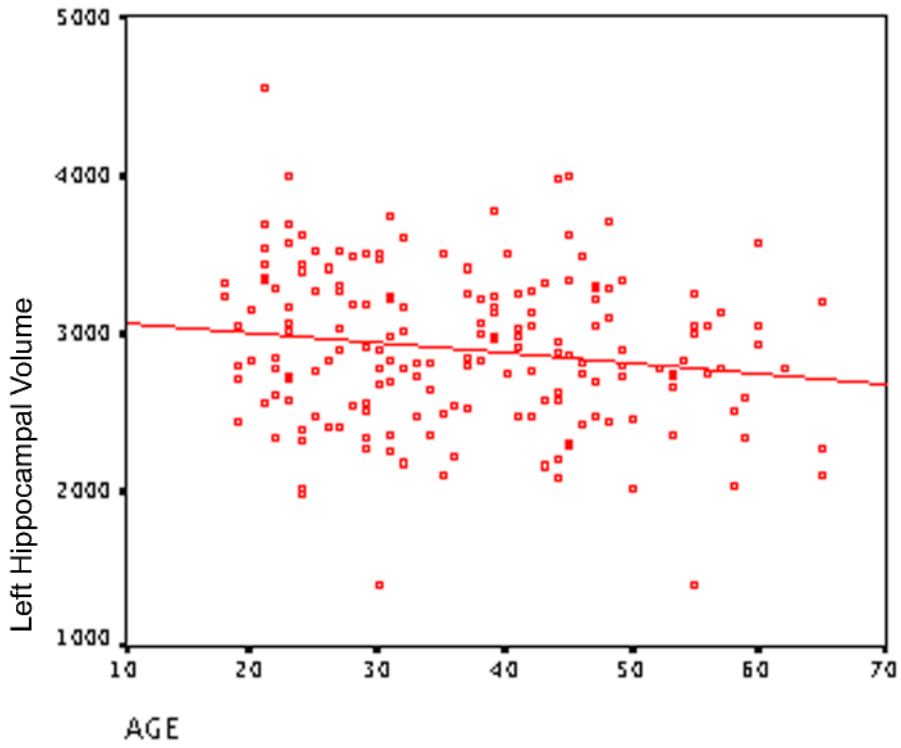

Figure 6.2: Left hippocampal scatter graph against age, showing a decrease of volume with age. Pearson correlation r = -0.166

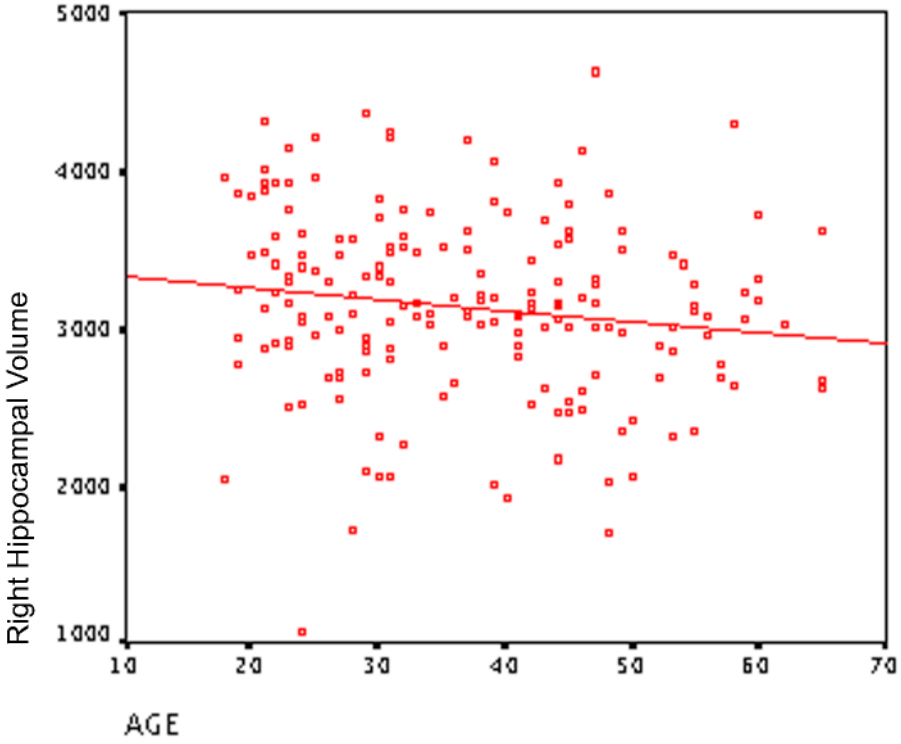

Figure 6.3: Right hippocampal scatter graph against age , showing a decrease of volume with age. Pearson correlation r = -0.149

Figures 6.4 and 6.5 show the same correlation of hippocampal volume against age, but depict the separate sex values, showing more a negative correlation for females than males in both hippocampi.

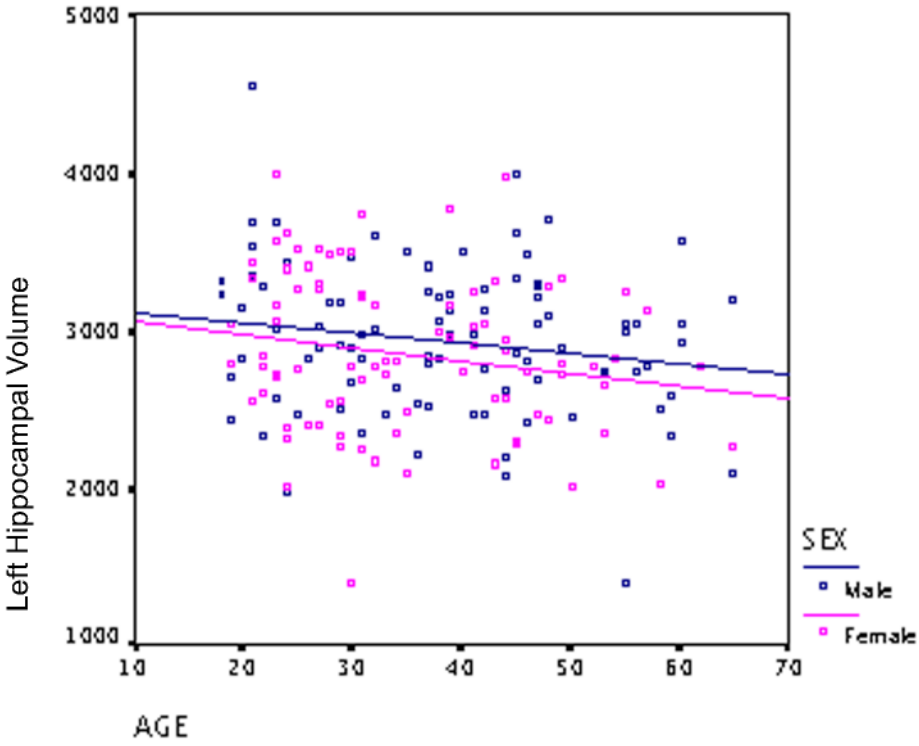

Figure 6.4: Left hippocampal scatter graph against age showing the different sex results

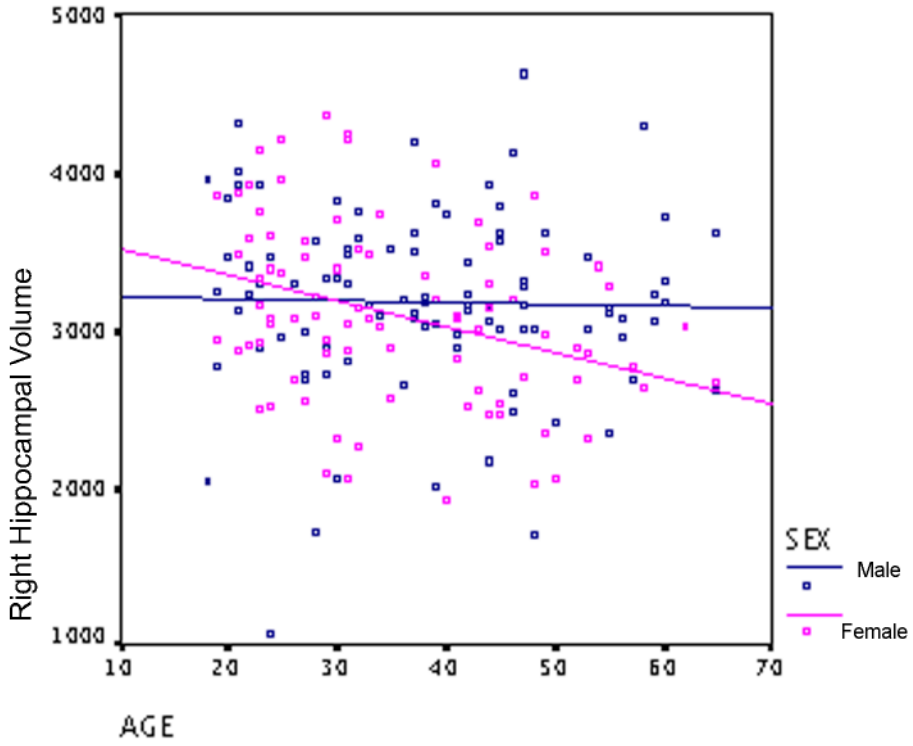

Figure 6.5: Right hippocampal scatter graph against age showing the different sex results

6.3.3 Sex Effects

Although no significant correlations between sexes were found, the hippocampal volume differences between males and females showed a trend. Bar graphs of right and left average hippocampal volumes separated for the sexes are depicted in figures 6.6 and 6.7 respectively.

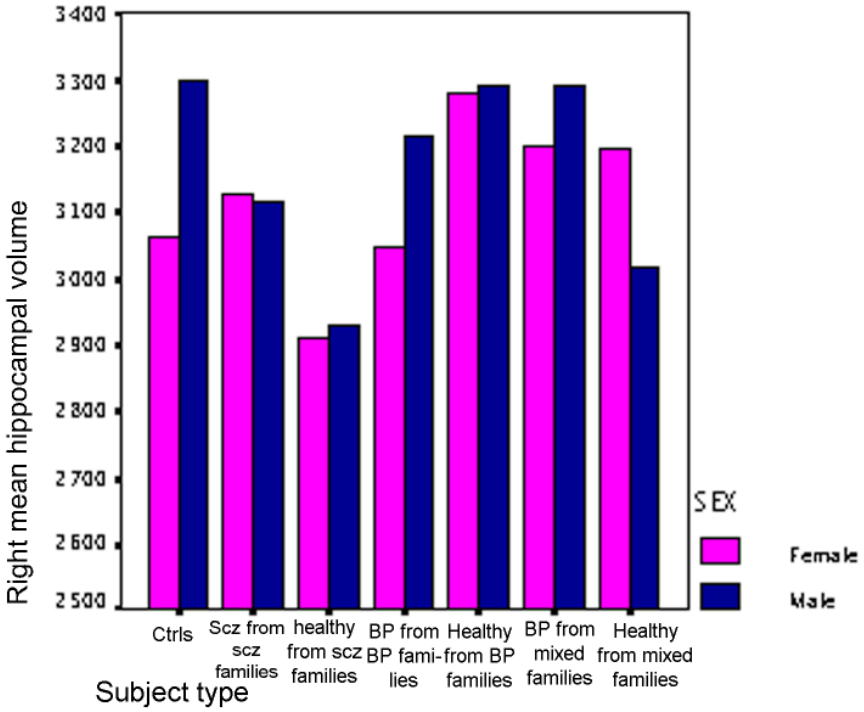

Figure 6.6: Male and female right average hippocampal volumes bar graph

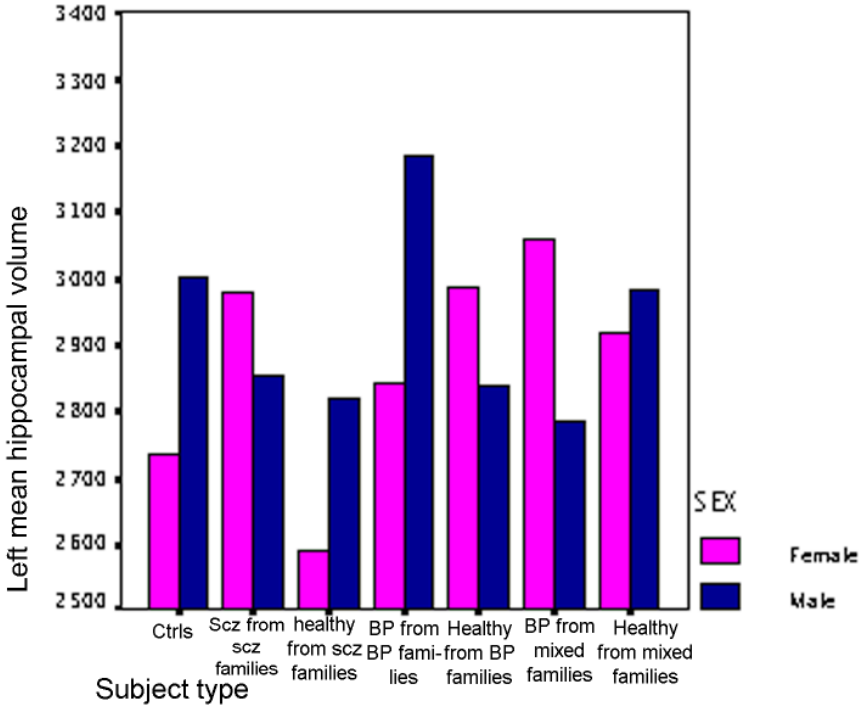

Figure 6.7: Male and female left average hippocampal volumes bar graph

Results suggest a trend where average right hippocampal volumes are greater for males than in females in all groups except for schizophrenic subjects from schizophrenic families and unaffected subjects from mixed families. The latter group provides the largest volume difference between the sexes. There is also a very large volume difference between the sexes for the control group, in which the males have a larger average hippocampal volume for the right hippocampus. This difference is also seen in the left average hippocampal volume for the control group. In this case, the largest variation between males and females is witnessed in the bipolar group. Schizophrenic subjects from schizophrenic families, unaffected subjects from bipolar families and bipolar subjects from mixed families all show larger volumes for females than males.

6.3.4 Right and Left Hippocampal Differences

In all groups, it is observed that the average right hippocampal volume is larger than the average left hippocampal volume, as can be seen in figure 6.8.

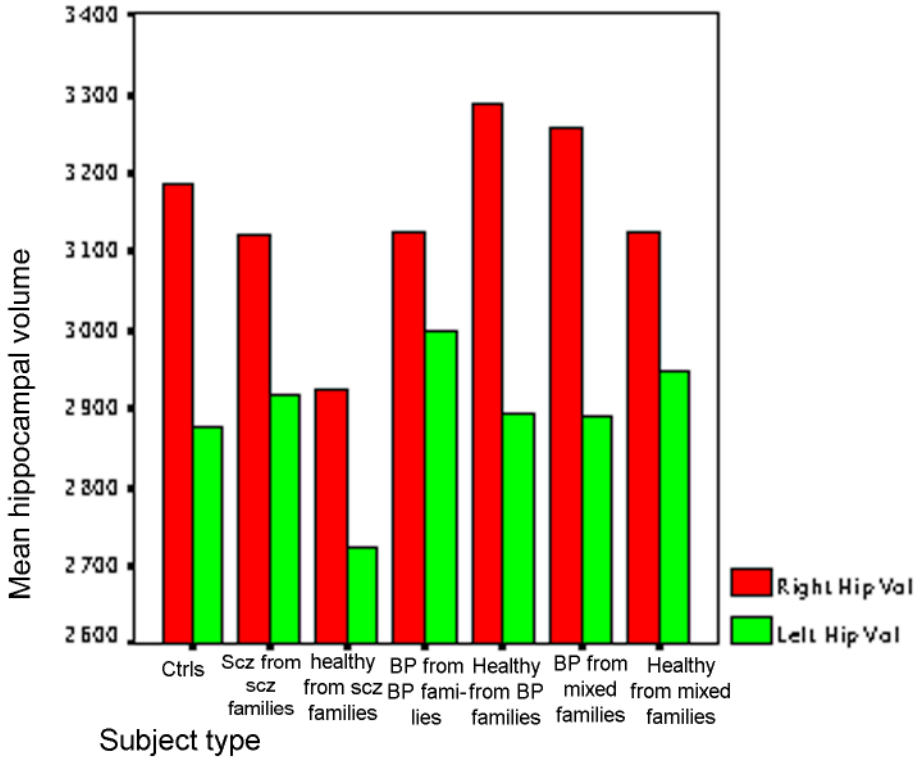

Figure 6.8: Right and left hippocampal volumes bar chart showing volume differences between the two hippocampi

Figure 6.9 once again shows the difference in average hippocampal volumes between males and females, and shows the difference of left and right hippocampal volumes between the sexes, where in both cases there is a decrease in volume for females.

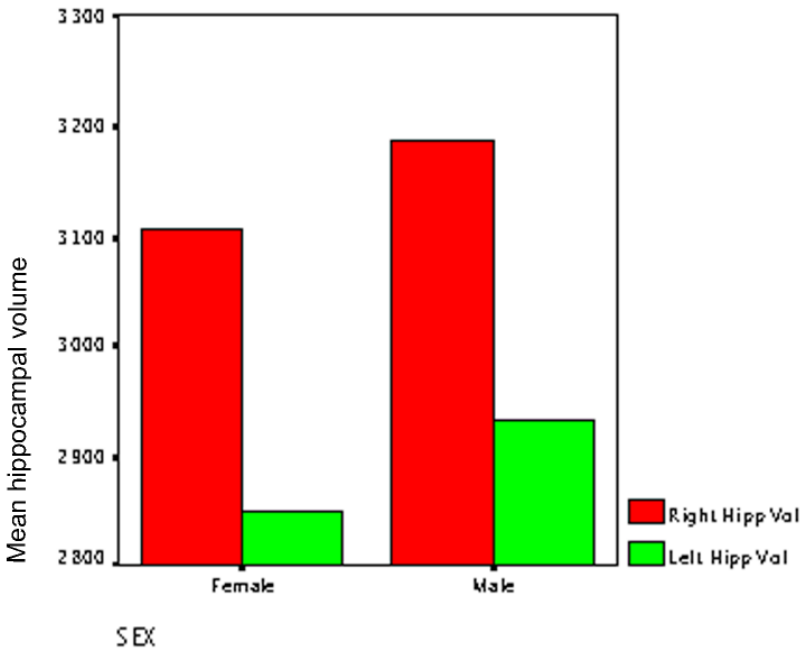

Figure 6.9: Right and left average hippocampal volumes for each sex

6.4 Discussion

6.4.1 Conclusion of Results

After using the Automated Hippocampal Location and Extraction methodology on 182 scans, no significant comparisons between groups were found for either hippocampus, except between unaffected subjects from schizophrenic families and bipolar subjects from bipolar families for the left hippocampus. The lack of hippocampal volume differences between groups is consistent with what is reported in a previous voxel based morphometry study of the same cohort, where no hippocampal volume differences were reported either (Mcintosh, Job et al. 2004). The difference between the unaffected subjects and bipolar subject from bipolar families in the left hippocampus was not found in this previous VBM study.

A negative correlation of each hippocampus (left and right) is observed with age. This gives strong evidence suggesting that, for all groups, the hippocampal volume does in fact reduce with age. This suggestion can only be strengthened through a longitudinal study observing volume change of the hippocampus over a period of time.

The control group results suggest that hippocampal volume between males and females is larger in males for both hippocampi. This result is noted even though the results are co varied for total brain volume. The result, however, is less defined for

the other groups in the study, except for the bipolar group, which is also strongly oriented to the male group possessing larger hippocampal volumes. The results seem to suggest larger volumes in both hippocampi for females in the schizophrenia group. The mean volumes across all groups show that males have larger hippocampus volumes for both left and right hippocampi (figure 6.9).

A result to note is the volume difference between left and right hippocampi, with the right hippocampal volume being larger than the left for all groups in the study, as well as for males and females alike, as can be seen in figure 6.9.

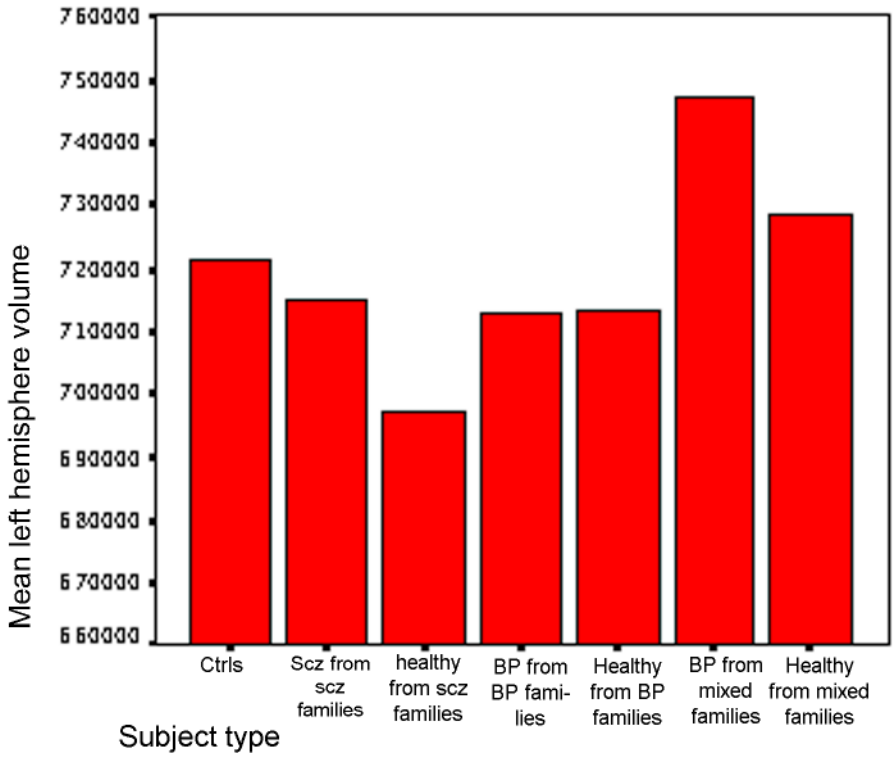

Figure 6.10: Mean volume of left hemisphere per group

The hippocampal volumes of the unaffected subjects from schizophrenic families group, are the smallest volumes in both hippocampi. This group also has the smallest total brain volumes for each hemisphere, as can be seen in figures 6.10 and 6.11.

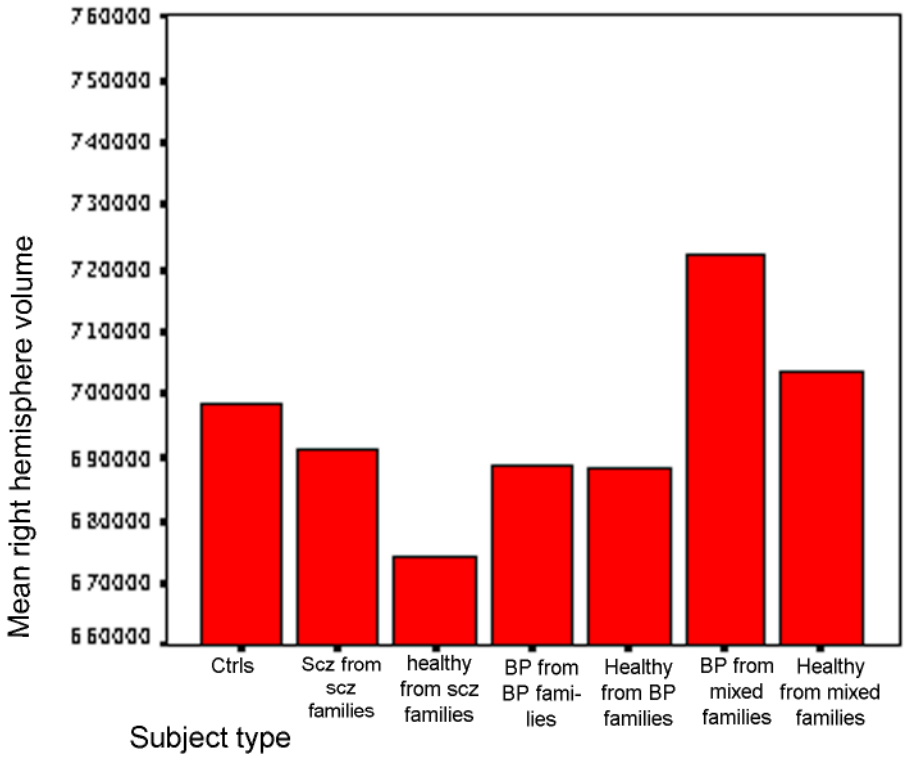

Figure 6.11: Mean volume of right hemisphere per group

6.4.2 Comparison to Other Studies

It is worth noting the male and female variations in hippocampal volume for schizophrenia subjects. For both hippocampi, the hippocampal volume is reduced for males and increased for females when comparing their volumes to the control group. The reason for this interest is that some recent studies ((Weiss, Dewitt et al. 2005),

(Chakos, Schobel et al. 2005), (Exner, Nehrkorn et al. 2008)) that all report bilateral hippocampal volume reductions only in males ((Weiss, Dewitt et al. 2005), (Chakos, Schobel et al. 2005)) and not females (Exner, Nehrkorn et al. 2008), results which fit the results found in this study.

As mentioned in the introduction, unlike schizophrenia, hippocampal volumes in bipolar disorder are a lot more inconsistent. From the studies discussed in the Introduction chapter, the general trend seems to be smaller hippocampal volumes for younger bipolar cohorts and enlarged hippocampi in older subjects. As can be seen in figure 6.12, the bipolar group (group 4) is the oldest group in the cohort. Beyer et al (Beyer, Kuchibhatla et al. 2004) report enlarged left hippocampi in older subjects, possibly due to medication exposure. Although not significant, this effect is also noted in this study.

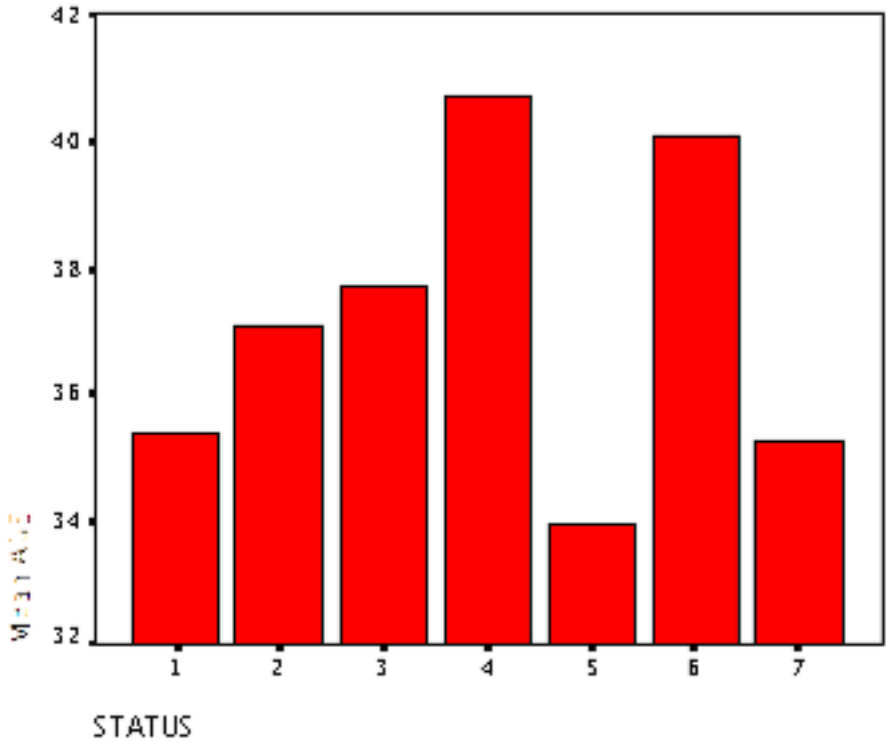

Figure 6.12: Average ages for each group in the cohort

Chapter 7 - Discussion

This thesis has introduced and described a new methodology for locating and extracting the hippocampus automatically from 1.5T T1 MRI scans. This final chapter discusses the advantages of this methodology as well as its limitations. Finally, possible improvements to the methodology are discussed in the future work section.

7.1 Performance and Result of Methodology

This thesis has described a fully automated hybrid methodology that is able to first locate and then extract hippocampal volumes in 3D MRI T1 brain scans. The hybrid algorithm uses brain maps and fuzzy inference to locate the hippocampal areas and create initial hippocampal boundaries, and then brain maps are used in a deformable manifold algorithm to help deform the manifolds until the correct boundaries are found. Finally, the boundaries are corrected for anomalies through fuzzy inference in a sagittal view.

Manual hippocampal segmentation ICC values reported range from 0.73 to 0.98. The ICC values of this methodology when compared to the manual segmentation of the same hippocampi result in a 0.73 for the left and 0.81 for the right hippocampi. These values both fall within range of manual reliability testing.

Comparing this methodology to other automated or semi-automated hippocampus segmentation extraction techniques. In this case, volume overlap error is taken into account (most of the time), and these values range from 6% to 15%. This methodology gives a volume overlap error rate of 15%, which falls at the higher error percentage end of the scale.

7.2 Performance on a Cohort of Bipolar and Schizophrenia Subjects

The methodology ran successfully on 182 scans in the cohort described in McIntosh et al. (Mcintosh, Job et al. 2004), yielding traces and volumes for each hippocampus in each scan. The lack of hippocampal volume differences between groups is consistent with what is reported in a previous voxel based morphometry study of the same cohort, where no hippocampal volume differences were reported either. This shows that the methodology's performance is consistent with previous findings, giving good comparison with voxel-based methodology.

The results produced by this methodology show that there is a trend towards age and sex effects on the hippocampus, where there is a trend of volume decrease with increase of age, and in the control groups males tended to have larger hippocampus volumes than females. Results also show differences in the volumes of left and right hippocampi, with the right hippocampus being larger than the left for all groups in this study.

7.3 Original Contributions, Strengths and Limitations

The unique ability of this methodology to extract information from the scans in both coronal and sagittal views is a technique that is original and novel to this methodology. It is a required step in successfully tracing hippocampal boundaries manually, and as such, mimics the procedure a hand tracer takes in tracing the boundaries manually. Another aspect that mimics the hand tracer's ability of manual tracing hippocampal boundaries is that of creating an initial boundary around the hippocampus and then adjusting it until the tracer is satisfied that the trace represents the true hippocampal boundary. This technique is also successfully adopted by this hybrid methodology.

Although the method that has been created has focused solely on the hippocampus, it is a generic process and can be applied to other MRI brain structure. Manifold initialization is the key, and some variables will need to be changed, such as which warp values to search for and the general location the structure is found in, but that essentially is all that is needed. as the manifolds are initialized close to the required boundaries, then the deformable manifold process will find the boundary required. The hippocampus was chosen for this study as it is a difficult boundary to locate, and successfully tracing it with this automated methodology shows the validity of the process.

The novel component of this methodology is that it is fully automated. In the process there is no human interaction, no need for human delineation of areas or initial

manually traced scans to help with imaging. This differs from other methodologies that have stated to be automated but actually require manual intervention with the input ((Ashton, Parker et al. 1997), (Fischl, Salat et al. 2002), (Zhou and Rajapakse 2005), Chupin (Chupin, Hammers et al. 2007; Chupin, Mukunabantumbakulu et al. 2007)). Using an automated methodology allows the whole process to be consistent on a scan-by-scan basis. Some criticism of manual segmentation is that the manual tracing can vary for each scan by the same tracer. Automated segmentation is a solution to assure that the scanning process is consistent and not variable.

Creating a hybrid algorithm by merging algorithms and procedures is another key feature of this methodology. This concept is not an original concept; it has been successfully applied to a couple of segmentation studies ((Yang and Duncan 2004), (Amini, Soltanian-Zadeh et al. 2004)). However, the combination of algorithms used is original in its own right, allowing the strengths of all the algorithms used to contribute to a positive result. This methodology is able to bring together SPM functions, image processing, edge detection, fuzzy inference and deformable modelling to achieve the result that is comparable to manual segmentation. This presents a novel approach to the methodology of automated hippocampus segmentation.

One limitation of this process is the sensitivity issue the algorithm seems to have with CSF voxel intensities. The algorithm errs when an abnormal amount of CSF is found around the hippocampus, sometimes including it as hippocampus, or else not being able to find the hippocampus at all. Some minor adjustments in the threshold

map creation and fuzzy inference would help to resolve this issue, thresholding for CSF so that the algorithms are able to distinguish the CSF in its own right, instead of having it confused with the grey matter of the hippocampus. Another limitation is the selection of the posterior extent of the hippocampus. As mentioned in Chapter 4 (page 80), this extent is standard across all scans, and does not take into account potential variability of different hippocampi.

7.4 Future Work

Further work can be carried out to assess methodology performance as well as possible optimization techniques to increase the reliability of the trace. This section is divided into two, the first section discussing possible future work to assess the methodology further, and the second section analyzing possible extensions to the current methodology to increase its reliability of results.

7.4.1 Assessing Methodology Performance

Two ways of continuing to assess the performance of the methodology are available. The first is to apply the same methodology to a different cohort, extracting hippocampi for a different group of subjects. The second is to apply the methodology to a different brain structure instead of the hippocampus and to analyze the results produced.

7.4.2 Applying the methodology to a different Cohort

Applying the methodology to a different set of MRI scans will allow further assessments of the performance of this methodology. The cohort that the methodology is applied to in this study is diverse, consisting of bipolar and schizophrenia patients as well as their ill and healthy relatives. This makes it likely

that this cohort consists of many variations of hippocampal size and shape. In order to compare this method to other automated segmentation techniques reliably, it would be of interest to test this methodology on a large control cohort, ideally the same cohort analyzed by other automated segmentation techniques.

7.4.3 Applying the methodology to a different brain structure

The hippocampal structure is a challenging structure to segment automatically, as the image is noisy and the hippocampal boundaries in particular are affected since they are already weak boundaries. This gave the methodology the additional challenge of segmenting a structure with weak information. As mentioned in the previous section, the methodology is general and can be applied to any other brain structure. By applying the methodology to a different, more well-defined brain structure (such as the corpus collosum) it would be possible to assess the performance of the hybrid algorithm more concretely. The results would be increasingly clear and less volatile for both automated segmentation as well as manual segmentation, making the reliability statistics more valid.

7.4.4 Increasing the reliability of the process: The Genetic Algorithm

As mentioned earlier, this methodology is a hybrid algorithm of different methods that come together to retrieve hippocampal volumes and traces successfully. The number of different processes, however, means that a large amount of variables exist, that can be adapted to produce a more accurate result. The use of genetic algorithms to automatically search for the best combination of variables would be an advantage to the methodology. This final section gives an overview of the theory of genetic algorithms, and a look at how it might be implemented for this particular situation, as a means of possible future work.

7.4.4.1 Overview

A Genetic Algorithm is a ‘search for solutions’ algorithm, specifically designed to find a solution in a large search space. This makes it an ideal algorithm to use for optimizing a solution. This section gives an overview of the theory behind these algorithms and proposes a variation of the algorithm that can be applied to the hybrid algorithm to optimize the hippocampus traces even further.

Genetic algorithms have already been used to some effect in image segmentation. Gudmundsson et al. (Gudmundsson, El-Kwae et al. 1998) developed an algorithm that produces edges in medical images that include optimizing the configurations

with a genetic algorithm. Brumby et al. (Brumby, Theiler et al. 1999) implemented a genetic algorithm named GENIE that is able to extract features from remote sensing applications. They use already traced images as fitness functions to help analyze the solutions created by the algorithm. The genes are various variables used for image segmentation, and the algorithm manipulates these values. The fitness functions described by Mishra et al. (Mishra, Dutta et al. 2006) are also based on manually segmented images. In this study a genetic algorithm was developed for pelvic computed tomography (CT) images, where the boundary was implemented as a level set function and evolved using a genetic algorithm.. A genetic algorithm was implemented to help select the optimal correction topology of cortical representations in Segonne et al (Segonne, Grimson et al. 2005). They calculated the fitness of their chromosomes by analyzing result's smoothness as well as by looking at the MRI intensity profile both inside and outside of the resulting surface.

A detailed explanation of the background and workings of genetic algorithms can be found in Mitchell et al. (Mitchell and Forrest 1994). In brief, genetic algorithms work by aiming to optimize a population of solutions using evolutionary functions. These functions include reproduction (using two solutions to create two new 'children' solutions) and selection of the best solutions – a case of nature's 'survival of the fittest'.

In genetic algorithm terms, a solution is known as a *chromosome*, and is made up of a set of *genes.* The chromosome can be considered to be an array, and each cell in the

array would be a gene. The gene values, which are usually binary, are what are manipulated during the algorithm processing, as can be seen in figure 7.1:

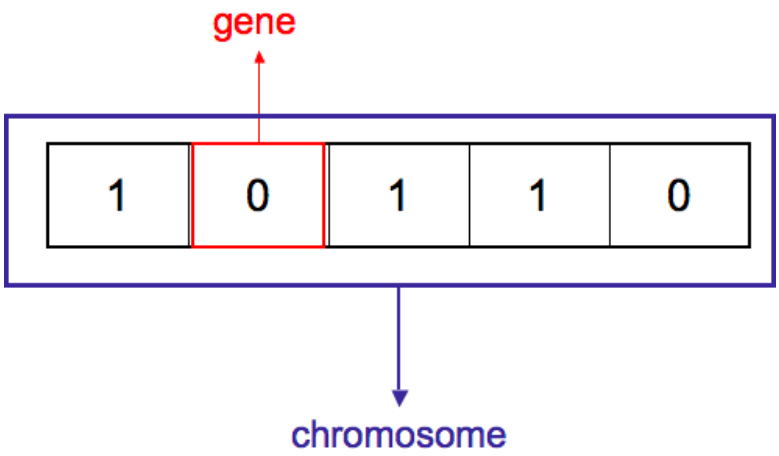

Figure 7.1: A graphic description of the chromosome and its genes

7.4.4.2 Generating the population

At the beginning of the algorithm, a chromosome population needs to be generated. In most genetic algorithm implementation, the population is generated randomly. In optimization, however, it is best to create the population from the result already obtained thus far. A number of copies of the result of the hybrid algorithm are therefore created, and random minor variations on each of the copies are done so that each chromosome is different to generate the population.

Evaluation

Each chromosome in the population needs to be evaluated in order to determine which of the chromosomes are the fittest in the population. This will be useful when deciding which of these chromosomes will be used as parents to produce a new generation of chromosomes. Evaluation is performed using a *fitness function.* This function must be able to decide how accurate the chromosome is to the solution. For the hippocampus boundary optimization problem, the function needs to calculate the smoothness of the boundary per slice (no breaks in the manifold) as well as how close the manifold is to the true boundary.

Parent selection

There are a number of possible methods to select the parents for reproduction. One of the most popular ones is known as Tournament Selection. This method is one of the ideal methods for choosing parents since it prevents premature convergence by not always selecting the fittest chromosomes in the population. The tournament method works by selecting two random chromosomes from the population. The fittest chromosome of the two has a 0.75 chance of getting selected whilst the unfit chromosome has a probability of 0.25. This is repeated for the selection of the second parent.

Reproduction

Reproduction functions are performed using the two parent chromosomes, creating two new ‘children’ chromosomes. Two functions are used to perform reproduction between the two parent chromosomes, mutation and crossover.

Mutation

Calculating a bitwise probability performs mutation. For every gene in the given chromosome, a probability of 0.05 is taken. If the probability succeeds then the bit is flipped, if its 0 it turns to 1 and vice versa.

Crossover

A random number is generated which selects a gene (bit) in the chromosome (string). The children of the two parents are then produced by copying the parents’ genes, parent 1 to child 1, and parent 2 to child 2. When the selected gene is reached, the parents swap and the rest of parent 2’s genes are copied to child 1, whilst child 2’s genes are copied from parent 1, as is seen in figure 7.2:

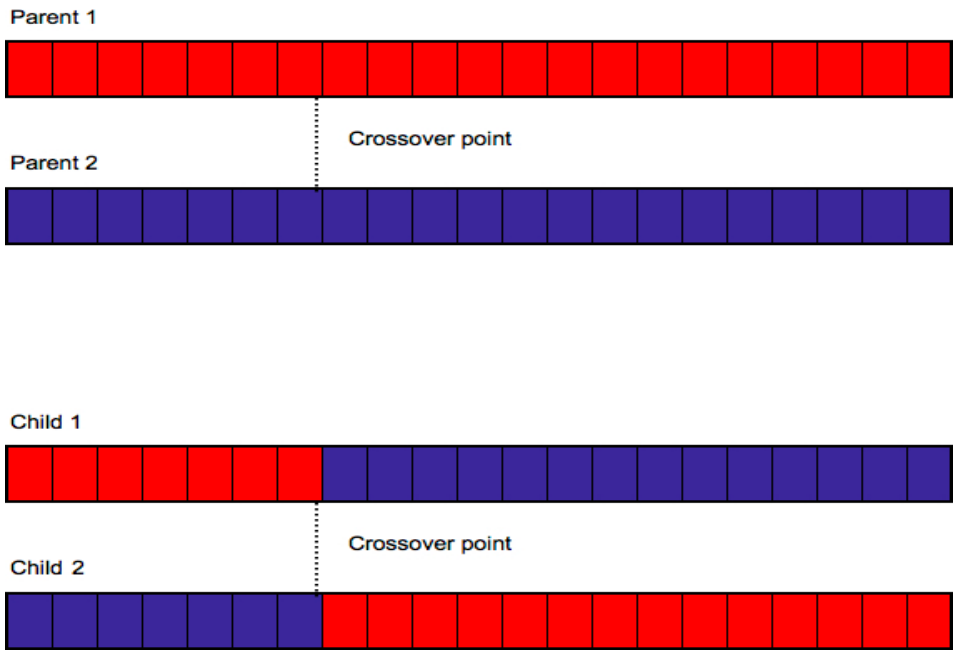

Figure 7.2: One-point crossover

A number of varieties exist for crossover. The type described above is known as the one-point crossover as it parents split at one given random point. However, parents can split up to any number of *N* points, to create children that are more varied. This form of crossover technique is known as *N*-point crossover. In most cases, one-point or two-point crossover is used. Two-point crossover is depicted in figure 7.3:

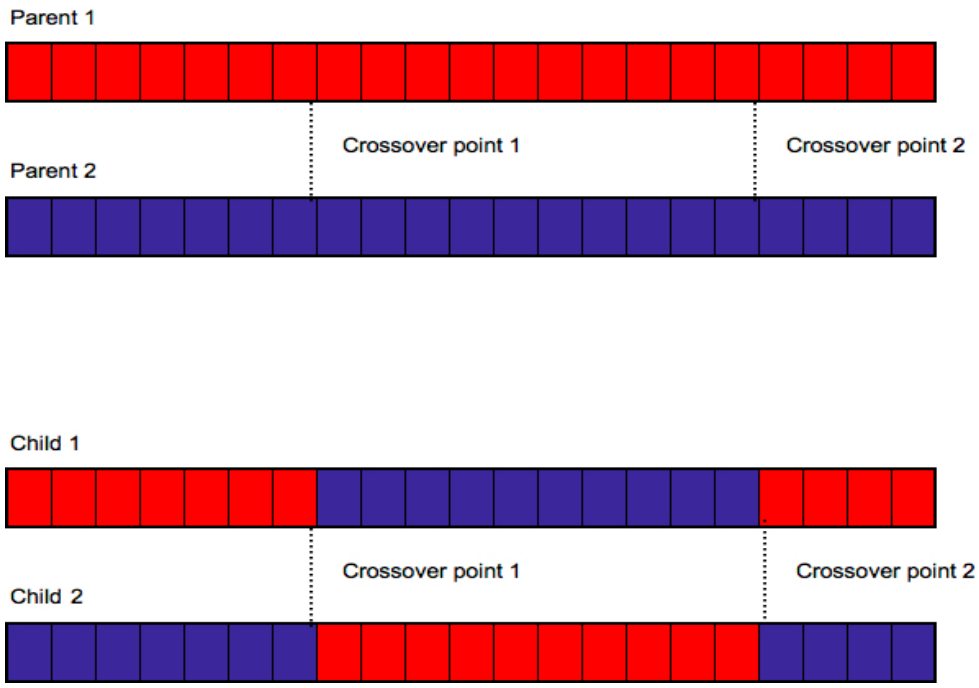

Figure 7.3: Two-point crossover

7.4.4.3 The Algorithm

Algorithm 14 The Genetic Algorithm

1. $i = 0$
2. Initialiaze population(i)
3. while $i < limit$
    4. Evaluate population(i)
    5. If optimum fitness reached then
        6. End algorithm and output fittest chromosome
    7. Else
        8. $parent1 <-$ tournamentSelect($population$)
        9. $parent2 <-$ tournamentSelect($population$)
        10. $child1, child2 <-$ crossover($parent1, parent2$)
        11. mutate($child1$)
        12. mutate($child2$)
        13. addToPopulation($child1$)
        14. addToPopulation($child2$)
        15. $i++$
    end If loop

end $While$ loop

7.4.4.4 Conclusion

Genetic Algorithms can provide an excellent optimization technique for improving the boundary traces of hippocampi as described in this thesis. This section provided an overview of the theory behind Genetic Algorithms and an example of how they might be applied to the hybrid algorithm, as an option for future work on optimizing this methodology.

Bibliography

Addis, D. R., M. Moscovitch, et al. (2004). "Recollective qualities modulate hippocampal activation during autobiographical memory retrieval." Hippocampus **14**(6): 752-62.

Amini, L., H. Soltanian-Zadeh, et al. (2004). "Automatic segmentation of thalamus from brain MRI integrating fuzzy clustering and dynamic contours." IEEE Trans Biomed Eng **51**(5): 800-11.

Ashburner, J., J. L. Andersson, et al. (2000). "Image registration using a symmetric prior--in three dimensions." Hum Brain Mapp **9**(4): 212-25.

Ashburner, J. and K. J. Friston (2000). "Voxel-based morphometry--the methods." NeuroImage **11**(6 Pt 1): 805-21.

Ashton, E., K. Parker, et al. (1997). "A novel volumetric feature extraction technique with applications to MR images." IEEE Trans Med Imaging **16**(4): 365-71.

Barnes, J., J. Foster, et al. (2008). "A comparison of methods for the automated calculation of volumes and atrophy rates in the hippocampus." NeuroImage **40**(4): 1655-1671.

Barnes, J., J. L. Whitwell, et al. (2006). "Measurements of the amygdala and hippocampus in pathologically confirmed Alzheimer disease and frontotemporal lobar degeneration." Arch Neurol **63**(10): 1434-9.

Barra, V. and J. Boire (2001). "Automatic segmentation of subcortical brain structures in MR images using information fusion." IEEE Trans Med Imaging **20**(7): 549-58.

Bearden, C., J. Soares, et al. (2008). "Three-Dimensional Mapping of Hippocampal Anatomy in Adolescents With Bipolar Disorder." Journal of the American Academy of Child & Adolescent Psychiatry **47**(5): 515-525.

Bearden, C., P. Thompson, et al. (2008). "Three-dimensional mapping of hippocampal anatomy in unmedicated and lithium-treated patients with bipolar disorder." Neuropsychopharmacology **33**(6): 1229-38.

Beyer, J., M. Kuchibhatla, et al. (2004). "Hippocampal volume measurement in older adults with bipolar disorder." Am J Geriatr Psychiatry **12**(6): 613-20.

Blumberg, H., J. Kaufman, et al. (2003). "Amygdala and hippocampal volumes in adolescents and adults with bipolar disorder." Arch Gen Psychiatry **60**(12): 1201-8.

Bogerts, B., E. Meertz, et al. (1985). "Basal ganglia and limbic system pathology in schizophrenia. A morphometric study of brain volume and shrinkage." Arch Gen Psychiatry **42**(8): 784-91.

Bonnici, H., T. William, et al. (2007). "Pre-frontal lobe gyrification index in schizophrenia, mental retardation and comorbid groups: An automated study." NeuroImage **35**(2): 648-654.

Bresenham, J. E. (1965). "Algorithm for computer control of a digital plotter." IBM Systems Journal **4**(1): 25-30.

Brumby, S. P., J. Theiler, et al. (1999). Investigation of image feature extraction by a genetic algorithm. in Proc. SPIE 3812**:** 24--31.

Canny, J. (1986). "A Computational Approach To Edge Detection." IEEE Transactions on Pattern Analysis and Machine Intelligence **8**(6): 679 - 698

Caselles, V., R. Kimmel, et al. (1997). "Geodesic Active Contours." International Journal of Computer Vision.

Chakos, M., S. Schobel, et al. (2005). "Duration of illness and treatment effects on hippocampal volume in male patients with schizophrenia." Br J Psychiatry **186**: 26-31.

Chupin, M., A. Hammers, et al. (2007). "Fully automatic segmentation of the hippocampus and the amygdala from MRI using hybrid prior knowledge." Med Image Comput Comput Assist Interv Int Conf Med Image Comput Comput Assist Interv **10**(Pt 1): 875-82.

Chupin, M., A. Mukuna-Bantumbakulu, et al. (2007). "Anatomically constrained region deformation for the automated segmentation of the hippocampus and the amygdala: Method and validation on controls and patients with Alzheimer's disease." Neuroimage **34**(3): 996-1019.

Chupin, M., A. Mukunabantumbakulu, et al. (2007). "Anatomically constrained region deformation for the automated segmentation of the hippocampus and the amygdala: Method and validation on controls and patients with Alzheimer's disease." NeuroImage **34**(3): 996-1019.

Cohen, I. and L. D. Cohen (1993). "Using Deformable Surfaces to Segment 3-D Images and Infer Differential Structures." IMAGE UNDERSTANDING **56**(2): 242--263.

Duvernoy, H. M. (2004). The Human Hippocampus: Functional Anatomy, Vascularization and Serial Sections with MRI, Springer; 3rd edition.

Eichenbaum, H. (1999). "Conscious awareness, memory and the hippocampus." Nat Neurosci **2**(9): 775-6.

Eichenbaum, H. (1999). "The hippocampus and mechanisms of declarative memory." Behav Brain Res **103**(2): 123-33.

Exner, C., B. Nehrkorn, et al. (2008). "Sex-dependent hippocampal volume reductions in schizophrenia relate to episodic memory deficits." J Neuropsychiatry Clin Neurosci **20**(2): 227-30.

Fischl, B., D. Salat, et al. (2002). "Whole brain segmentation: automated labeling of neuroanatomical structures in the human brain." Neuron **33**(3): 341-55.

Foland, L., L. Altshuler, et al. (2008). "Increased volume of the amygdala and hippocampus in bipolar patients treated with lithium." Neuroreport **19**(2): 221-4.

Frazier, J., S. Chiu, et al. (2005). "Structural brain magnetic resonance imaging of limbic and thalamic volumes in pediatric bipolar disorder." Am J Psychiatry **162**(7): 1256-65.

Frazier, J., S. Hodge, et al. (2008). "Diagnostic and sex effects on limbic volumes in early-onset bipolar disorder and schizophrenia." Schizophr Bull **34**(1): 37-46.

Frey, B., A. Andreazza, et al. (2007). "The role of hippocampus in the pathophysiology of bipolar disorder." Behav Pharmacol **18**(5-6): 419-30.

Gudmundsson, M., E. A. El-Kwae, et al. (1998). "Edge detection in medical images using a genetic algorithm." IEEE Trans Med Imaging **17**(3): 469-74.

Hasselmo, M. E. and J. L. McClelland (1999). "Neural models of memory." Curr Opin Neurobiol **9**(2): 184-8.

Hauser, P., J. Matochik, et al. (2000). "MRI-based measurements of temporal lobe and ventricular structures in patients with bipolar I and bipolar II disorders." J Affect Disord **60**(1): 25-32.

He, L., Z. Peng, et al. (2008). "A comparative study of deformable contour methods on medical image segmentation." Image and Vision Computing **26**(2): 141-163.

Heath, M., S. Sarkar, et al. (1997). "A Robust Visual Method for Assessing the Relative Performance of Edge-Detection Algorithms." IEEE Transactions on Pattern Analysis and Machine Intelligence **19**(12): 1338-1359.

Heckers, S. (2001). "Neuroimaging studies of the hippocampus in schizophrenia." Hippocampus **11**(5): 520-8.

Honea, R. (2008). "Is Gray Matter Volume an Intermediate Phenotype for Schizophrenia A Voxel-Based Morphometry Study of Patients with Schizophrenia and Their Healthy Siblings." Biological Psychiatry **63**(5): 465-474.

Job, D., H. Whalley, et al. (2005). "Grey matter changes over time in high risk subjects developing schizophrenia." Neuroimage **25**(4): 1023-30.

Job, D. E., H. C. Whalley, et al. (2002). "Structural gray matter differences between first-episode schizophrenics and normal controls using voxel-based morphometry." NeuroImage **17**(2): 880-9.

Kass, M., A. Witkin, et al. (1988). "Snakes: Active contour models." International Journal of Computer Vision.

Kelemen, A., G. Szekely, et al. (1999). "Elastic model-based segmentation of 3-D neuroradiological data sets." IEEE Trans Med Imaging **18**(10): 828-39.

Kubicki, M. (2002). "Voxel-Based Morphometric Analysis of Gray Matter in First Episode Schizophrenia." NeuroImage **17**(4): 1711-1719.

Lavenex, P. B., D. G. Amaral, et al. (2006). "Hippocampal lesion prevents spatial relational learning in adult macaque monkeys." J Neurosci **26**(17): 4546-58.

Lawrie, S., H. Whalley, et al. (2002). "Temporal lobe volume changes in people at high risk of schizophrenia with psychotic symptoms." Br J Psychiatry **181**: 138-43.

Lee, J., S. Kim, et al. (2004). "Deformable model with surface registration for hippocampal shape deformity analysis in schizophrenia." NeuroImage **22**(2): 831-840.

Lopez-Garcia, P., H. Aizenstein, et al. (2006). "Automated ROI-based brain parcellation analysis of frontal and temporal brain volumes in schizophrenia." Psychiatry Res **147**(2-3): 153-61.

Maguire, E. A., N. Burgess, et al. (1998). "Knowing where and getting there: a human navigation network." Science **280**(5365): 921-4.

Maguire, E. A., D. G. Gadian, et al. (2000). "Navigation-related structural change in the hippocampi of taxi drivers." Proc Natl Acad Sci U S A **97**(8): 4398-403.

Maguire, E. A., H. J. Spiers, et al. (2003). "Navigation expertise and the human hippocampus: a structural brain imaging analysis." Hippocampus **13**(2): 250-9.

Maguire, E. A., E. R. Valentine, et al. (2003). "Routes to remembering: the brains behind superior memory." Nat Neurosci **6**(1): 90-5.

Malladi, R. and J. A. Sethian (1995). "Image processing via level set curvature flow." Proc Natl Acad Sci U S A **92**(15): 7046-50.

Mangin, J., D. Riviere, et al. (2004). "Coordinate-based versus structural approaches to brain image analysis." Artificial Intelligence in Medicine **30**(2): 177-197.

McCarley, R., C. Wible, et al. (1999). "MRI anatomy of schizophrenia." Biol Psychiatry **45**(9): 1099-119.

McInerney, T. and D. Terzopoulos (2000). "T-snakes: Topology adaptive snakes." Medical Image Analysis **4**(2): 73-91.

Mcintosh, A., D. Job, et al. (2004). "Voxel-based morphometry of patients with schizophrenia or bipolar disorder and their unaffected relatives." Biological Psychiatry **56**(8): 544-552.

McNaughton, B. L., C. A. Barnes, et al. (1989). "Hippocampal granule cells are necessary for normal spatial learning but not for spatially-selective pyramidal cell discharge." Exp Brain Res **76**(3): 485-96.

Mishra, A., P. Dutta, et al. (2006). "Fuzzy shape based motion evaluation of left ventricle using genetic algorithm." Image and Vision Computing **24**(5): 436-446.

Mitchell, M. and S. Forrest (1994). "Genetic algorithms and artificial life." Artificial Life(1): 267--289.

Moorhead, T., J. Harris, et al. (2006). "Automated computation of the Gyrification Index in prefrontal lobes: Methods and comparison with manual implementation." NeuroImage **31**(4): 1560-1566.

Moorhead, T. W., D. E. Job, et al. (2004). "Voxel-based morphometry of comorbid schizophrenia and learning disability: analyses in normalized and native spaces using parametric and nonparametric statistical methods." NeuroImage **22**(1): 188-202.

Morey, R. A., C. M. Petty, et al. (2009). "A comparison of automated segmentation and manual tracing for quantifying hippocampal and amygdala volumes." NeuroImage **45**(3): 855-66.

Morra, J. H., Z. Tu, et al. (2008). "Validation of a fully automated 3D hippocampal segmentation method using subjects with Alzheimer's disease mild cognitive impairment, and elderly controls." NeuroImage **43**(1): 59-68.

Narr, K., P. Thompson, et al. (2004). "Regional specificity of hippocampal volume reductions in first-episode schizophrenia." NeuroImage **21**(4): 1563-1575.

Pantel, J., D. S. O'Leary, et al. (2000). "A new method for the in vivo volumetric measurement of the human hippocampus with high neuroanatomical accuracy." Hippocampus **10**(6): 752-8.

Parker, J. R. (1997). Algorithms for Image Processing and Computer Vision. Professional, Reference and Trade Group, United States of America, Wiley Computer Publishing, John Wiley & Sons, Inc.

Prince, J. L. (1997). "Gradient Vector Flow: A New External Force for Snakes."

Prince, J. L. and C. Xu (1996). A new external force model for snakes. In 1996 Image and Multidimensional Signal Processing Workshop**:** 30--31.

Pruessner, J. C., L. M. Li, et al. (2000). "Volumetry of hippocampus and amygdala with high-resolution MRI and three-dimensional analysis software: minimizing the discrepancies between laboratories." Cereb Cortex **10**(4): 433-42.

Rametti, G., N. Segarra, et al. (2007). "Left posterior hippocampal density reduction using VBM and stereological MRI procedures in schizophrenia." Schizophrenia Research **96**(1-3): 62-71.

Scoville WB, M. B. (1957). "Loss of recent memory after bilateral hippocampal lesions." J Neurol Neurosurg Psychiatry **20**(1): 11-21.

Segonne, F., E. Grimson, et al. (2005). "A genetic algorithm for the topology correction of cortical surfaces." Inf Process Med Imaging **19**: 393-405.

Shenton, M., G. Gerig, et al. (2002). "Amygdala-hippocampal shape differences in schizophrenia: the application of 3D shape models to volumetric MR data." Psychiatry Res **115**(1-2): 15-35.

Siddiqi, K., Y. B. Lauziere, et al. (1998). "Area and length minimizing flows for shape segmentation." Image Processing.

Strasser, H., J. Lilyestrom, et al. (2005). "Hippocampal and ventricular volumes in psychotic and nonpsychotic bipolar patients compared with schizophrenia patients and community control subjects: A pilot study." Biological Psychiatry **57**(6): 633-639.

Tanskanen, P., J. Veijola, et al. (2005). "Hippocampus and amygdala volumes in schizophrenia and other psychoses in the Northern Finland 1966 birth cohort." Schizophrenia Research **75**(2-3): 283-294.

Terzopoulos, D. and T. McInerney (1997). "Deformable models and the analysis of medical images." Stud Health Technol Inform **39**: 369-78.

Tisserand, D., P. Visser, et al. (2000). "The relation between global and limbic brain volumes on MRI and cognitive performance in healthy individuals across the age range." Neurobiol Aging **21**(4): 569-76.

Velakoulis, D., C. Pantelis, et al. (1999). "Hippocampal volume in first-episode psychoses and chronic schizophrenia: a high-resolution magnetic resonance imaging study." Arch Gen Psychiatry **56**(2): 133-41.

Velakoulis, D., S. Wood, et al. (2006). "Hippocampal and amygdala volumes according to psychosis stage and diagnosis: a magnetic resonance imaging study of chronic schizophrenia, first-episode psychosis, and ultra-high-risk individuals." Arch Gen Psychiatry **63**(2): 139-49.

Weiss, A., I. Dewitt, et al. (2005). "Anterior and posterior hippocampal volumes in schizophrenia." Schizophrenia Research **73**(1): 103-112.

Whalley, H. C. and J. M. Wardlaw (2001). "Accuracy and reproducibility of simple cross-sectional linear and area measurements of brain structures and their comparison with volume measurements." Neuroradiology **43**(4): 263-71.

Xu, C. (2000). Gradient vector flow deformable models. In Handbook of Medical Imaging, Academic Press**:** 159--170.

Xu, Y., D. Valentino, et al. (2008). "Age effects on hippocampal structural changes in old men: The HAAS." NeuroImage **40**(3): 1003-1015.

Yang, J. and J. S. Duncan (2004). "3D image segmentation of deformable objects with joint shape-intensity prior models using level sets." Med Image Anal **8**(3): 285-94.

Yucel, K., M. McKinnon, et al. (2007). "Bilateral hippocampal volume increases after long-term lithium treatment in patients with bipolar disorder: a longitudinal MRI study." Psychopharmacology (Berl) **195**(3): 357-67.

Yucel, K., V. Taylor, et al. (2008). "Bilateral Hippocampal Volume Increase in Patients with Bipolar Disorder and Short-term Lithium Treatment." Neuropsychopharmacology **33**(2): 361-367.

Zadeh, L. A. (1965). "Fuzzy Sets." Information and Control(8).

Zhou, J. and J. Rajapakse (2005). "Segmentation of subcortical brain structures using fuzzy templates." NeuroImage **28**(4): 915-924.